Effects of Heat Treatment on the Microstructure and Mechanical Properties of Electron Beam Additively Manufactured Ti6Al4V with Powder Reuse

Taehoon Kim

A thesis

submitted in partial fulfillment of the

requirements for the degree of

Master of Science

University of Washington

2020

Committee:

Dwayne Arola

Ramulu Mamidala

Program Authorized to Offer Degree:

Materials Science and Engineering

University of Washington

Abstract

Effects of Heat Treatment on the Microstructure and Mechanical Properties of Electron Beam Additively Manufactured Ti6Al4V with Powder Reuse

Taehoon Kim

Chair of the Supervisory Committee:

Dwayne Arola

Department of Materials Science and Engineering

Metal additive manufacturing has many advantages such as low material waste, unlimited design complexity, and its cost-effectiveness as a near-net-shape process. It has been applied to many materials, but especially for the fabrication of Ti6Al4V components due to its excellent corrosion resistance, high strength to weight ratio, and biocompatibility. Among a variety of additive manufacturing (AM) techniques, especially powder bed fusion systems, electron beam melting (EBM) has been extensively investigated because of its lower thermal stress in parts compared to Selective Laser Melting (SLM), and high density of parts produced. However, there are limited investigations related to heat treatment as a post-processing technique with

powder reuse in EBM AM of Ti6Al4V over consecutive builds for the comparison of microstructure and mechanical properties. Therefore, this research analyzed the effects of heat treatment with powder reuse over 30 build cycles to identify the changes in microstructures and mechanical properties of Grade 5 Ti6Al4V. EBM printed samples were analyzed by tensile testing and scanning electron microscopy. Heat treatment was conducted with sub (710°C), near (950°C) and super (1050°C) β-transus temperature. As a result of these heat treatments, the α lath thickness increased, which caused a reduction in strength and an increase in ductility. Metal subjected to the near β-transus temperature heat treatment (950°C/1hr) exhibited the best ductility among other heat treatments. The sub β-transus temperature did not show any difference when compared to the as-built samples, whereas the super β-transus heat treatment caused a decrease in both the strength and ductility. Through microstructural analysis, sub β-transus heat treatment showed the same microstructure as as-built samples (prior beta columnar grains with alpha lath). The near β-transus heat treatment caused coarsening of the α lath, whereas the super β-transus heat treatment caused recrystallization to uniform equiaxed structure with alpha grain boundaries. The super β-transus heat treatment and corresponding equiaxed grain microstructure caused a change in fracture mode from transcrystalline to intercrystalline. In addition to the use of the near β-transus heat treatment, the controlling cooling rate is an important factor in obtaining the optimum tensile properties. Regarding powder reuse, there was an increase in the oxygen content, which contributed to the α lath thickness and the tensile properties. Lastly, heat treatment and post-build machining the samples appeared to improve the reliability of the Ti6Al4V produced by EBM AM.

Table of Contents

Lists of Figures

Lists of Tables

Chapter 1. Introduction

Additive manufacturing (AM), which is also called 3D printing, refers to the process of joining materials to make objects from three-dimensional (3D) models of computer-aided design (CAD), usually layer upon layer, as opposed to subtractive manufacturing methodologies [1]. Rapid prototyping (RP), which fabricates complex polymer prototypes has been used over the past several decades. However, due to its promising potentials and possibilities for industrial applications such as aerospace, automobiles, and military defense, a variety of industries have been trying to develop and optimize the mass production of components with various materials including plastics and metals.

Additive manufacturing has lots of advantages over conventional manufacturing techniques such as forging, machining, and casting. First of all, AM has a freeform production capability of complex designed parts from feedstock powder materials without any conventional manufacturing methods. Furthermore, it is a near-net-shape process, which is cost-effective because it minimizes material waste. For instance, when it comes to titanium products, the buy-to-fly ratio, the weight ratio between the raw material used for a component and the weight of the component itself, is 3-12:1 for the titanium components produced by AM [2,3] whereas it is 12-25:1 for the same products fabricated by conventional methods [4]. Not only that, but AM also has high flexibility on feedstock material types [5] and recyclability of unused powders, which makes it more cost-effective.

AM processes have a wide range of methods for metal components fabrication, as seen in **Figure 1**, based on ASTM standards categorizing seven types of manufacturing [81]. Powder bed fusion techniques, commonly used in metal additive

manufacturing [6,7], are used to selectively melt and fuse metal powders layer by layer with a heat source like a laser beam or electron beam. It has several kinds of systems categorized processes using metal powder such as Direct energy deposition (DED), selective laser melting (SLM), Sheet lamination, and electron beam melting (EBM).

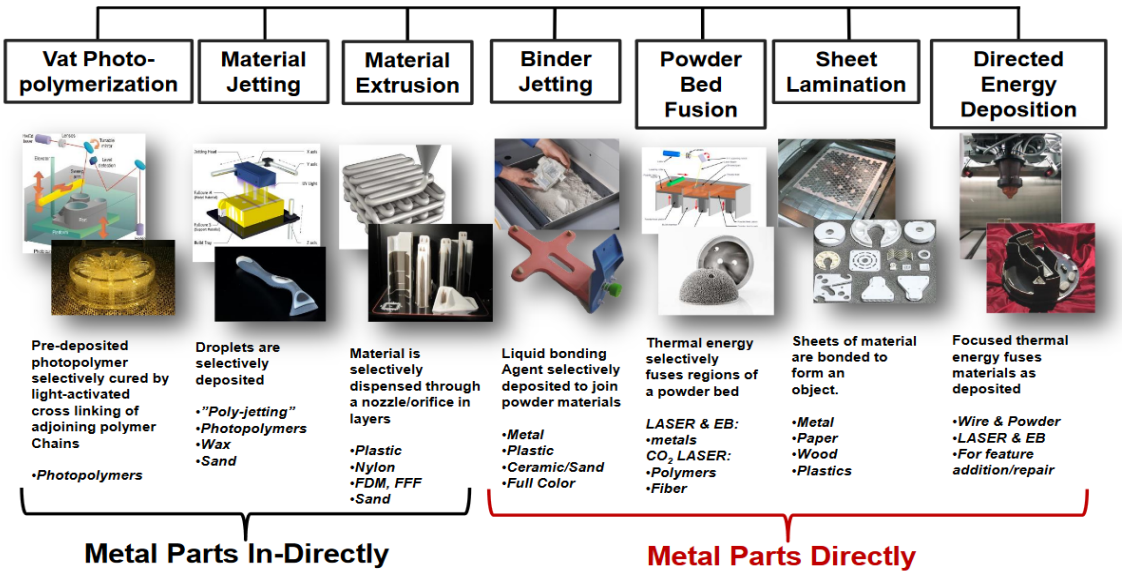

Figure 1. Seven types of additive manufacturing (AM) processes in terms of metal additive manufacturing [81]. Available source from Boeing company and ASTM committee F42. 3 types of additive manufacturing processes starting left side use plastics or binder, and then sinter or cast the metal part. The rest of processes use metal powder for building parts.

They have advantages and limitations in terms of defects and process features, as shown in **Figure 2**. Amongst these techniques, because of the special working nature of electron beam, EBM builds parts in a high-vacuum environment of 10^{-4} mbar or greater, providing an ideal contamination-free environment for the manufacturing of reactive materials that have a high affinity to oxygen and nitrogen, such as Ti6Al4V [8].

Defect or feature	LM	EBM	DED – powder fed	DED – wire fed	Binder jetting	Sheet lamination
Feedstock	Powder	Powder	Powder	Wire	Powder	Sheets
Heat source	Laser	E-beam	Laser	Laser/E-beam	N/A; kiln	N/A; ultrasound
Atmosphere	Inert	Vacuum	Inert	Inert/vacuum	Open air	Open air
Part repair	No	No	Yes	Yes	No	No
New parts	Yes	Yes	Yes	Yes	Yes	Yes
Multi-material	No	No	Possible	Possible	Infiltration	Yes
Porosity	Low	Low	Low	Low	High	At sheet interfaces
Residual stress	Yes	Low	Yes	Yes	Unknown	Unknown
Substrate adherence	Yes	Material dependent	Yes	Yes	N/A	Yes
Cracking	Yes	Not typical	Yes	Yes	Fragile green bodies	No
Delamination	Yes	Yes	Yes	Yes	No	Yes
Rapid solidification	Yes	Yes	Yes	Yes	No	No
In situ aging	No	Yes	No	No	No	No
Overhangs	Yes	Yes	Limited	Limited	Yes	Limited
Mesh structures	Yes	Yes	No	No	Limited	No
Surface finish	Medium-rough	Rough	Medium-poor	Poor but smooth	Medium-rough	Machined
Build clean-up from process	Loose powder	Sintered powder	Some loose powder	N/A	Loose powder	Metal shavings

Figure 2. Comparison of process features, capabilities, and defects among metal additive manufacturing processes. Source from Oak Ridge National Laboratory (ORNL)

Ti6Al4V is an α +β titanium alloy which accounts for about half of the market share of titanium products in the world. Due to its attractive properties such as great corrosion resistance, biocompatibility, high strength, low density, and high fracture toughness, various industries including aerospace, marine, chemical, automobile, and energy fields have shown high Ti6Al4V demands. Especially, demands for Ti6Al4V from aerospace industries account for the most part of applications of this material in demand because of its excellent strength-to-weight ratio and good compatibility of applied composite materials [82,83] in **Figure 3**. Ti6Al4V can be used for military defense applications as well. AM techniques can produce metal components economically of aluminum steel, maraging steel, stainless steel, and titanium alloys. With these techniques, replacing components with reasonable prices is possible and results in an improvement in the reliability of military equipment. In this study, Ti6Al4V was studied since conducting experiments with EBM printed Ti6Al4V was available.

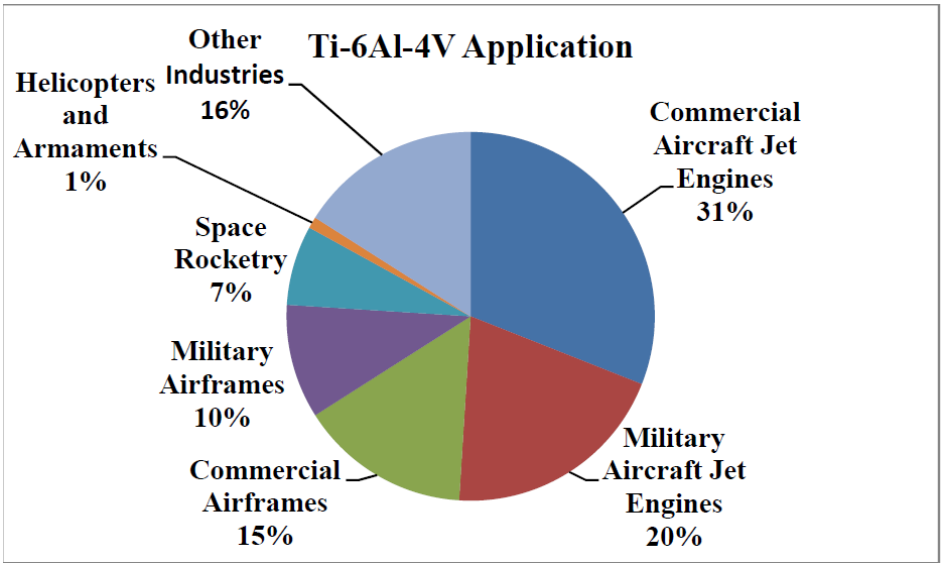

Figure 3. Ti6Al4V applications. Aerospace industries show the largest demand for Ti6Al4V [82,83].

However, as other additive manufacturing techniques have their limitations, EBM has challenges for Ti6Al4V fabrication. First of all, Ti6Al4V powder itself is expensive to manufacture, which is why a recycling process is necessary. Furthermore, even though EBM can produce titanium products with reused powder by using a powder recovery system, the quality and properties of products do not remain constant between new powder and recycled powder. There have been several works of literature concerning powder reuse study for establishing knowledge about powder properties and their effect on the performance [9,10,11]. These papers showed that the more recycled powder used for the fabrication, the worse mechanical properties of the products observed. Due to the price of Ti6Al4V powder and issues from the manufacturing process itself, post-processing techniques and powder reuse have been studied by many researchers to improve the mechanical properties of the Ti6Al4V products.

1.1 Motivation

There has been limited investigation [12] of utilizing post-processing heat treatment of EBM printed Ti6Al4V built with reused powder to improve the mechanical properties. Most studies analyze the effect of heat treatment of only Ti6Al4V ELI (Grade 23) or Ti6Al4V Grade 5 samples printed by SLM or EBM [12,13,14,15,16], but not with reused powder to see the changes of microstructure and mechanical properties. The properties they focused on vary depending on the potential applications, such as micro-hardness and tensile strength, fatigue strength, surface roughness, ductility, and strength or corrosion resistance. Galarraga et al. [17] covered the relation between tensile strength and ductility [17] with recycled powder. However, they did not mention the correlation between microstructure and these two properties depending on each reused powder sample. Since Hot isostatic pressing (HIP) can close the pores inside the specimens and improve mechanical properties, many researchers used this process [18,19]. However, a more detailed study on heat treatment as post-processing for improvement of mechanical properties of reused powder samples is necessary. Therefore, heat treatments in this study were performed based on the β-transus temperature that affects the microstructure of Ti6Al4V parts with consecutive 31 builds, as shown in **Figure 4**. For microstructural analysis, prior β grain width and α lath thickness, in **Figure 5**, were measured to see changes in the microstructure from heat treatments.

1.2 Objectives

The overall goal of this study is to investigate the effects of heat treatment on the microstructure and mechanical properties of Ti6Al4V through 31 powder reuses. The specific objectives include:

1) Heat treatment with 3 conditions based on β-transus temperature(sub/near/super).

2) Machining the surface of heat-treated samples and performing tensile testing to compare the mechanical properties between as-built and heat-treated specimens

3) Microstructural analysis with SEM images. Observation of changes in the microstructure such as measuring of prior β grain width and α lath thickness.

4) Plotting the graph of microstructure and mechanical properties of heat-treated Ti6Al4V to observe the trend and to identify correlations.

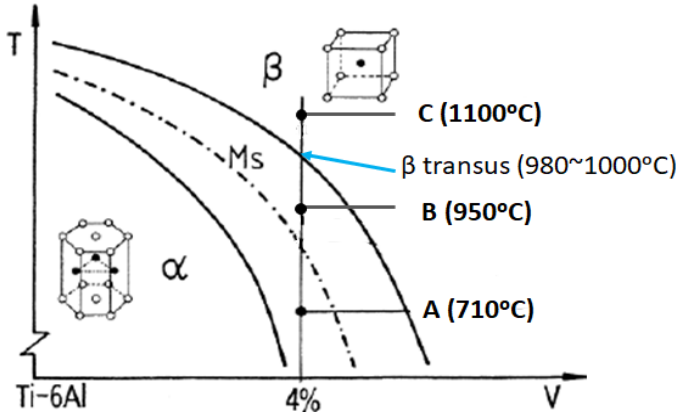

Figure 4. A schematic phase diagram of Ti6Al4V from Heat treater's guide (Harry Chandler, 1994). The three heat treatment conditions based on β transus temperature in this study marked with A(sub, 710°C, 2hrs), B(near, 950°C, 1hr), and C(super, 1050°C, 1hr).

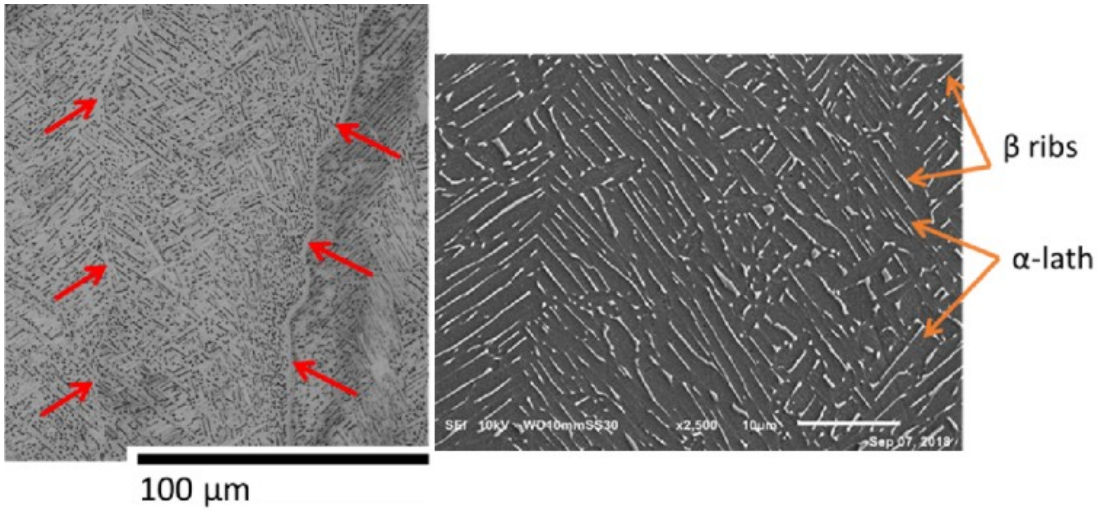

(a) (b)

Figure 5. The microstructure of as-built Ti6Al4V [85]; (a) Red arrows indicate prior β grains with boundaries and (b) SEM images with β grains ribs (light, white color) and α laths (dark color).

Chapter 2. Literature Review

Ti6Al4V is an α+β titanium alloy with a high strength to weight ratio, biocompatibility, high fracture toughness, and excellent corrosion resistance, which is why a wide range of industries, such as aerospace, biomedical, military defense, automobile, energy, and chemical, need this material for industrial applications. Despite the high demand for Ti6Al4V products, conventional production of Ti6Al4V has some challenging issues due to its high chemical reactivity [20], low thermal conductivity [20], and the tendency of strain hardening [14]. Furthermore, traditional manufacturing of Ti6Al4V is dependent on several processes such as forging, rolling, and casting of feedstock materials, which need machining for final shapes and leads to quite a large amount of material waste, time, and money for production [21].

Additive manufacturing (AM), which fabricates Ti6Al4V products from 3D model design directly layer by layer, has several advantages over conventional manufacturing such as freedom of complex shapes and geometries, inert gas atmosphere or high vacuum status for anti-oxidation, the near-net-shape process leading to less material waste and recycling of feedstock materials for cost-effective processing. In **Table 1**, other advantages of AM over traditional manufacturing in terms of applications are listed [80].

Table 1. Advantages of AM over conventional manufacturing [80].

Areas of Application	**Advantages**
Rapid Prototyping	Reduce time to market by accelerating prototyping Reduce the cost involved in product development Making companies more efficient and competitive at innovation
Production of Spare Parts	Reduce repair times Reduce labor cost Avoid costly warehousing

Small Volume Manufacturing	Small batches can be produced cost-efficiently Eliminate the investment in tooling
Customized Unique Items	Enable mass customization at low-cost Quick production of exact and customized replacement parts on-site Eliminate penalty for redesign
Very Complex Work Pieces	Produce very complex workpieces at low cost
Machine Tool Manufacturing	Reduce labor cost Avoid costly warehousing Enables mass customization at low cost
Rapid Manufacturing	Directly manufacturing finished components Relatively inexpensive production of small numbers of parts
Component Manufacturing	Enable mass customization at low cost Improve quality Shorten supply chain Reduce the cost involved in development Help eliminate excess parts
On-Site and On-Demand Manufacturing of Customized Replacement Parts	Eliminate storage and transportation costs Save money by preventing downtimes Reduces repair costs considerably Shorten supply chain The need for large inventory is reduced Allow product lifecycle leverage
Rapid Repair	Significant reduction in repair time Opportunity to modify repaired components to the latest design

When it comes to metal additive manufacturing including, powder bed fusion systems and directed energy deposition can be for industrial applications of Ti6Al4V. The mechanism of powder bed fusion systems, especially SLM and EBM, is using the 3D design file and is cut into layers with a specified thickness. A certain amount of powder materials is deposited layer by layer with the computer-aided design (CAD) file and software built-in 3D printers that decide process parameters. Then, the layer is selectively melted on the build plate by using a focused heat source such as a laser or electron beam for scanning the surface. After the powder is spread over the build plate and partially fused, the build plate goes down, and then another new layer is raked on the top of the build plate. The process repeats until the products are made completely.

Electron beam melting (EBM) has multiple advantages over other laser melting systems. First of all, since the heating source is an electron beam that has higher energy

and a faster scan speed than other laser beams, EBM has a faster build rate than other laser systems [22]. On top of that, the EBM process performs with elevated temperature and high vacuum status, which relieves residual stress and makes reactive metal powders that have a very high affinity to gases such as oxygen, hydrogen, and nitrogen possible to be produced without contamination [23]. This environment makes α' martensite decompose to α+β lamellar microstructure. The lamellar structure is more ductile than the fine needle-shaped α' martensite structure that selective laser melting (SLM) and directed energy deposition (DED) usually produce [12,24,25,26,27]. The microstructure of Ti6Al4V manufactured by EBM has higher ductility and lower tensile strength compared to Ti6Al4V products made by SLM and DED.

However, despite these advantages, all of the additive manufacturing (AM) processes, including EBM, have some challenging issues and intrinsic limitations. To begin, inherent defects made by AM processes unavoidably can seriously deteriorate Ti6Al4V product's fatigue and mechanical properties [28,29,30]. For example, as-built parts produced by AM have a high surface roughness that causes the necessity of the machining process as post-processing [31]. According to Li et al. [22], three things can cause an increase in surface roughness. 1) the staircase effect concerning deposited layers increasingly, 2) powder particles partially melted and stick to the surface, and 3) the existence of unmelted areas and porosity, which is related to layer thickness deposited, powder size, and processing parameters depending on AM methods. To figure out this issue, post-processing for machining and polishing the surface could be one of the effective methods that could get rid of detrimental defects that cause stress concentration and also function as crack initiators on the surface [15]. Also, inherent residual stresses are one of the main issues to be addressed for laser-based AM systems

in particular due to a high thermal gradient [32,33,34,35]. These residual stresses cause the formation of crack and warping in final components [36,37], which is why laser-based AM processes like SLM and EBM need supporting structures to prevent distortion during manufacturing procedures. [38,39]. One good way to run temperature gradients down is conducting stress relief heat treatment with high temperature. Vastola et al. [33] found that pre-heating temperature on the bed had a huge influence on residual stress. This phenomenon can explain why residual stresses are relatively not much significant in the EBM process with a continuous high build temperature (600-750°C) during the deposition process [25,40,41], compared to SLM and DED.

The principal drawback of AM is the unmanageable porosities in Ti6Al4V parts that worsen the mechanical properties. Vilaro et al. [42] found that the shape and orientation of pores adversely affected ductility. Biswas et al. [29] suggested that porosities could be the main factor of failure mechanism since pores can be the nucleation sites leading to the formation of adiabatic shear bands and following failure. Galarraga et al. [12] concluded that porosity is the critical factor that controls mechanical properties with regards to other parameters. Pores are common in AM. Leuders et al. [43] offered that pores of Ti6Al4V by SLM originate from defects that are induced by the process and come from initial powder contaminations, evaporation, or regional voids after powder-layer deposition. Ackelid and Svensson et al. [44] found pores in as-built EBM specimens. Li et al. [45] showed two common types of pores in AM Ti6Al4V: 1) lack of fusion voids and 2) gas pores made by entrapped gas within the gas atomized powder particles during the process in the molten pool, as shown in **Figure 6** [12]. Both of them are related to deviation from optimized conditions for melting and not enough laser energy that causes inappropriate melting [15,42,46,47].

These many pores in the EBM produced as-built Ti6Al4V parts lead to the low fatigue life of Ti6Al4V products [13]. Since these three main limitations: 1) surface roughness, 2) residual stress, and 3) porosity have a negative influence on the mechanical performances of as-built specimens by acting as a crack initiator [8], AM processes have been a difficulty manufacturing good enough quality products. The mechanical properties of EBM printed Ti6Al4V are mainly related to process parameters that control the porosity and microstructure [48,49]. So the as-built Ti6Al4V components have been subjected to post-processing such as machining, heat treatment, or hot isostatic pressing (HIP) to remove numerous pores in the parts and debilitate the crack initiation for improvement of the properties.

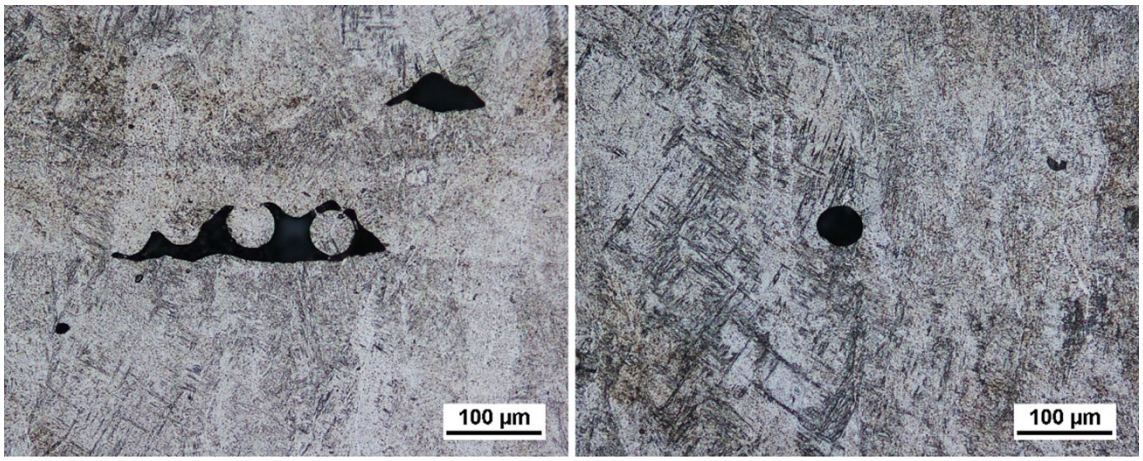

(a) (b)

Figure 6. Defects in EBM of Ti6Al4V; (a) lack-of-fusion pore and (b) gas pore [12].

There is quite a few literatures with regards to the tensile properties of as-built and post-processed AM Ti6Al4V, as shown in **Table 2**. The strength of most of the AM Ti6Al4V parts satisfies ASTM F136 [50], even though Ti6Al4V components that are

produced by wire arc additive manufacturing (WAAM) and directed energy deposition (DED) partially does not meet the requirement [50]. It is hard to compare the properties to see the effects of heat treatment and other post-processing directly in the same way since the result came from different powder material used and processing parameters such as manufacturing machine and post-processing conditions. Above all, the processing parameters affect the microstructure and the porosity, which could lead to an influence on the mechanical properties since the microstructure is closely related to the material properties of final components and the manufacturing process used by controlling the processing parameters [8].

Table 2. Reported tensile properties of heat-treated and machined Ti6Al4V parts produced by electron beam melting (EBM), selective laser melting (SLM) and directed energy deposition (DED). The properties of as-built, wrought, HIPed (Hot Isostatic Pressing), forged and cast Ti6Al4V are also shown for comparison.

eu : uniform engineering strain / σm : True UTS

WQ : Water quenched / AC : Air cooled

STA : Solution heat Treated and Aged

Type	Condition	Build direction	Ultimate tensile strength (MPa)	Yield strength (MPa)	Elongation (%)	Source
Conventional	Wrought	-	1050	875	10	[14]
EBM (Arcam AB A2)	Annealed(850°C), WQ , machined	-	1106±3.3, σm	688±18.2	8.8±2.1, eu	[14]
	Annealed(900°C), WQ, machined	-	1161±17.2, σm	745±12.1	11.4±1.0, eu	[14]
	Annealed(950°C), WQ, machined	-	1210±1.8, σm	926±9.2	6.2±1.3, eu	[14]
	HIP, machined	-	1056±33.5, σm	914±20.1	8.8±2.1, eu	[14]
EBM	As-built	-	~1000	910±10	15±0.5	[13]

(Arcam A2X)	STA (1050°C,2h→700°C,3h,AC)	-	950±30	840±50	14.2±0.3	[13]
	STA (1050°C,2h→500°C,10h,AC)	-	~980	850	16.2±1	[13]
EBM (Arcam A2)	As-built	-	~990	~910	4	[51]
	Annealed(920°C,2h), AC	-	~920	~850	5	[51]
	Annealed(1030°C,2h,AC)	-	~840	~820	9	[51]
SLM (Trumpf LF250)	As-built	Vertical	1166±25	962±47	1.7±0.3	[42]
	Annealed(730°C, 2h,AC), machined	Vertical	1000±53	900±101	1.9±0.8	[42]
	Annealed (950°C,1h,WQ), machined	Vertical	1040±4	925±14	7.5±2	[42]
	Annealed (1050°C,1h,WQ), machined	Vertical	951±55	836±64	7.9±2	[42]
	As-built	Horizontal	1206±8	1137±20	7.6±2	[42]
	Annealed(730°C,2h) AC, machined	Horizontal	1046±6	965±16	9.5±1	[42]
	Annealed(950°C,1h), WQ, machined	Horizontal	1036±30	944±8	8.5±1	[42]
	Annealed(1050°C,1h), WQ, machined	Horizontal	1019±11	913±7	8.9±1	[42]
SLM (250HL machine)	As-built machined	-	1080±30	1008±30	1.6±2	[43]
	Annealed(800°C) machined	-	1040±30	962±30	5±2	[43]
	Annealed(1000°C), machined	-	945±30	798±30	11.6±2	[43]
	HIPed,machined	-	1005±30	912±30	8.3±2	[43]
DED (Triton Systems)	As-built, machined	Horizontal	902-923	881-906	~6.4	[52]
	As-built, not-machined	Horizontal	1033-1109	941-1029	~6.8	[52]
	Annealed, machined	Horizontal	751-766	620-708	~4.8	[52]
	Annealed, not machined	Horizontal	907-967	854-889	~11.9	[52]
Wire Arc AM (EWM Tetrix350)	As-built	-	820±6.23	710±4.00	7.18±0.9	[53]
	STA (967°C,1h,WQ→595°C, 2h,AC)	-	918±30.4	858±39.2	5.85±1.1	[53]
	Heat-treated	-	801±9	721±16.4	11.5±4.2	[53]

	(vacuum) (927°C,2h,FC)					
	HIPed	-	800±11.6	712±11.5	11.0±1.7	[53]
Wrought	-	Vertical	942±8	836±9	12.5±1.2	[24]
		Horizontal	933±7	832±10	13.0±1.5	[24]
Cast	-	-	980	865	13.5	[42]
Forged	Mill-annealed	-	1030	970	16	[25]
ASTM F136	-	-	>860	>795	>10	[50]

Murr et al. [48] measured micro-hardness values and other tensile properties to compare between as-built and wrought Ti6Al4V components. They found that the mechanical properties can vary much depending on the process parameters that manage the microstructure and porosity. Tan et al. [49] applied the Hall-Petch relation that refers to the correlation between the properties and the microstructures by observing the morphology of as-built EBM Ti6Al4V and tensile properties with a different build height. They also indicated that properties were related to how people set up the processing parameters to control the microstructure. Gong et al. [54] found that the variation of processing parameters such as input energy density, line and focus offset, gas flow on the surface, and unprocessed material could cause the creation of porosity.

Not only the processing parameters but also the shape of tensile specimens and chemical compositions of the powder vary in the literature in Table 1. Raghavan et al. [13] used Ti6Al4V Grade 5 powders for the rectangular block. Syed et al. [51] used the Grade 5 powder for the dogbone shaped plates. On the other hand, Galarraga et al. [17] used Ti6Al4V Grade 23 powders that are called extra-low interstitial (ELI) for round bar tensile samples. Even though these two types of Ti6Al4V powders meet the ASTM F1472 requirement, Parry et al. [32] and Hao, Yu-Lin et al. [55] used ELI Ti6Al4V that included a lower amount of oxygen, carbon, iron, and nitrogen to increase the ductility.

The chemical compositions of Ti6Al4V with Grade 5 and Grade 23 powders in **Table 3** with the ASTM F2924 requirement [56]. The amount of oxygen content in Ti6Al4V powder is especially crucial since it can significantly affect the tensile properties [57,58].

Table 3. Nominal chemical compositions of Ti6Al4V(wt.%).

Type	**Ti**	**Al**	**V**	**Fe**	**C**	**O**	**N**	**H**
Grade 5	balanced.	6.0	4.0	<0.2	<0.25	<0.2	-	-
Grade 23 (ELI)	balanced.	5.5-6.5	3.5-4.5	0.25 max	0.08 max	0.13 max	0.05 max	0.13 max
ASTM F2924	balanced.	5.5-6.75	3.5-4.5	0.30 max	0.10 max	0.20 max	0.05 max	0.015 max

Tensile properties also differ depending on the orientation of the tensile specimens in Table 1. There are inconsistencies in the result of tensile properties between vertical and horizontal Ti6Al4V samples. Hrabe et al. [57] found that % the elongation of the horizontal Ti6Al4V samples is higher than that of vertical specimens due to the microstructure texture. On the other hand, Zhao et al. [18] concluded that Both vertical oriented Ti6Al4V components printed by EBM and SLM showed higher tensile properties than horizontal samples by EBM and SLM.

Galarraga et al. [12] mentioned anisotropy of mechanical properties resulted from the difference in the amount of porosity depending on the locations. Not only previous variables but also the way of post-processing is different among the literature. One of the main reasons is that the microstructure of Ti6Al4V components is different. For instance, Ti6Al4V produced by selective laser melting (SLM) usually has α' martensite structure while EBM printed Ti6Al4V has an α+β lamellar structure due to a different cooling rate [18], as shown in **Figure 7** [55]. Since the microstructure plays an

important role in tensile behavior, the post-processing that changes the microstructure for improvement on the mechanical performances should be applied differently. There are diverse post-processing methods that many researchers performed with SLM and EBM printed Ti6Al4V products to find the correlation between the microstructure and a variety of properties. Fousová et al. [59] compared the microstructure and the mechanical properties with heat-treated SLM Ti6Al4V and as-built EBM Ti6Al4V because they wanted to see comparable microstructure with a similar state. Both of the samples were not machined. SLM printed Ti6Al4V specimens were annealed at 820°C for 90 minutes. The result of this paper is the values of tensile properties are not much different contrary to the fatigue strength of Ti6Al4V by SLM is higher than that of Ti6Al4V by EBM.

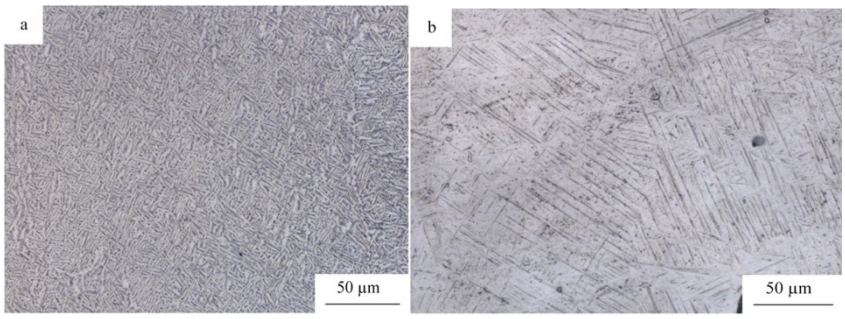

Figure 7. Microstructure images using optical microscopy [55]; (a) α+β lamellar structure by EBM and (b) α' martensite structure from SLM printed Ti6Al4V parts.

Raghavan et al. [13] found the correlation between the hardness value and the microstructure (α lath width) by conducting heat treatment based on β-transus temperature (996°C-1000°C for EBM Ti6Al4V Grade 5 powders). Four kinds of heat treatments were carried out; sub-β transus from 930°C to 980°C, near-β transus from 990 to 1000°C, super β-transus from 1000°C to 1050°C, and solution air-cooled following the aging process at 1050 for 1 to 3 hours each. They concluded that the most

optimized heat treatment they performed was a solution heat treatment (1020°C for 1 to 2 hours and then air cooled) with an aging process (500°C for 10 hours) based on the result of the elongation percentage even though tensile strength reduced. When it comes to the correlation between the property and the microstructure, they mentioned that coarsening of α lath cause a decrease of hardness. Syed et al. [51] found that super β-transus heat treatment (1030°C, 2hrs, air-cooled) improved the ductility by 125% compared to as-built EBM printed Ti6Al4V that consists of grade 5 powder. Sub β-transus heat treatment (920°C, 2hrs, aircooled) also led to a 25% increase in ductility. They concluded the improvement of ductility after these two kinds of heat treatment was because of the increase of α lath width causing an increase of effective slip length. The work-hardening process was performed to improve ductility by Formanoir et al. [14]. They did sub β-transus heat treatment (from 850°C to 980°C for 2 hours) and then water quenched. The improvement of ductility and strength was attributed to heterogeneous multiphase microstructure affected by the work-hardening effect from heat treatment and water quenching.

Tao et al. [16] focused on compression and fretting wear properties by conducting three kinds of heat treatments. They found that sub β-transus heat treatment (950°C for an hour, air-cooled and then aging at 650°C for an hour, air-cooled) showed better ductility than super β-transus heat treatment (1050°C, 30 minutes with air cooling and subsequent aging at 730°C for 2 hours with air cooling) due to thin spacing between α lath that caused a decrease of effective slip length and reduced nanoscale dispersoids observed in β phase. Formanoir et al. [15] made an emphasis on the importance of the machining process. The mechanical properties of the ELI Ti6Al4V samples with sub β-transus heat treatment (950°C for an hour, furnace cooled) and super-β transus heat

treatment (1040°C, for 30 minutes, furnace cooled) did not show significant improvement because they thought they could not control key processing parameters to tailor the microstructure. Pushilina et al. [60] connected with the effect of heat treatment and hydrogen absorption rates by comparing the microhardness and rate of as-built and heat-treated Ti6Al4V samples. Galarraga et al. [17] found three parameters (cooling rates, span, and temperature of heat treatment) for the optimization of heat treatment depending on the applications of products. They stated that the coarsening of α lath width harms mechanical properties including tensile strength and ductility. Galarraga et al. [12] carried out annealing processes (600°C, 700°C and 800°C each for 10 to 120 hours and then samples were air-cooled) and found that the longer the samples dwell in the chamber and the higher temperature, coarser microstructure happened, which means alpha lath thickness in Ti6Al4V increase as well. Sun et al. [61] performed machining and chemical etching with Kroll reagent (3mL 48% HF, 6mL 70% HNO3, 100mL water) for two hours. The authors found that the surface modification of Ti6Al4V ELI alloy that they did worked for improving tensile strength, ductility, and surface roughness even though these post-processings could not be effective for removing internal pores in the samples.

Also, many researchers have been taking advantage of hot isostatic pressing (HIP) for reducing the porosity of metals and increasing the density of metals. Zhao et al. [18] found that the HIP process closed the pores in the SLM and EBM printed samples with improved fatigue strength. Leuders et al. and Cain et al. [43,62] concluded that HIP processing could increase the ductility at the expense of tensile strength. Galarraga et al. [12] mentioned that HIP-treated ELI alloys showed an improvement of ductility despite insignificant changes in the strength because HIP could lead to a

coarsening of the microstructure.

Despite all benefits of EBM processes and post-processing for the improvement of mechanical properties, manufacturing Ti6Al4V is still pricey without a powder recycling process. The reason is that Ti6Al4V powder is necessary to meet strict requirements such as flowability, the size distribution of particles, and chemical composition. To figure out this issue, reusing unmelted powders in the chamber could be a method. For instance, Arcam company from Sweden made an EBM machine with Powder Recovery System (PRS) possible for Ti6Al4V powder to take apart sintered powder so that sieved unmelted powder can reuse.

However, as the powder is recycled over again, the oxygen content that could deteriorate mechanical properties in the powder increases [15] because oxygen contamination can happen during the stocking and the recycling of the powder. Formanoir et al. [13] also suggested that the recycling process should be restricted to keep away from oxygen contamination. There is another study that increasing reused powder could influence the microstructure and mechanical properties [63]. This issue raises the questions of whether there is a way to use heat treatment as post-processing to improve the properties of Ti6Al4V products with reused powders. Besides, what conditions of heat treatment are the optimizations for getting the best mechanical properties?

Unfortunately, only limited investigations are available on the effect of heat treatment of Ti6Al4V components with recycled powder even though there are several powder reuse studies not covering the heat treatment as post-processing [11,64,65]. Galarraga et al. [12] used ELI Ti6Al4V alloys with 50% fresh and 50% reused powder. However, they did not state how many times they recycled the powder. The literature

above covering the effect of heat treatment to see the correlation between the microstructure and the mechanical properties did not put together a relationship between powder reuse and heat treatment.

There are quite a few literatures about the relationship between the microstructure and tensile properties of Ti6Al4V produced by SLM and EBM to observe the effects of post-processing heat treatment and HIP process [13]. The microstructure of heat-treated samples with three conditions in this study could be expected from the papers above [13], as shown in **Figure 8**. Therefore, this study will focus on observing the trend of as-built and heat-treated EBM printed Ti6Al4V samples with vertical and horizontal orientation to find the relationship between the effects of heat treatment and powder reuse. Also, optimal heat treatment conditions will discuss by analyzing the changes in the microstructure and tensile properties considering the trend of properties with consecutive 31 builds. In particular, the measurement of α lath and prior β grains was performed to compare these values among heat-treated samples. Wrought titanium samples were used as well for the reference.

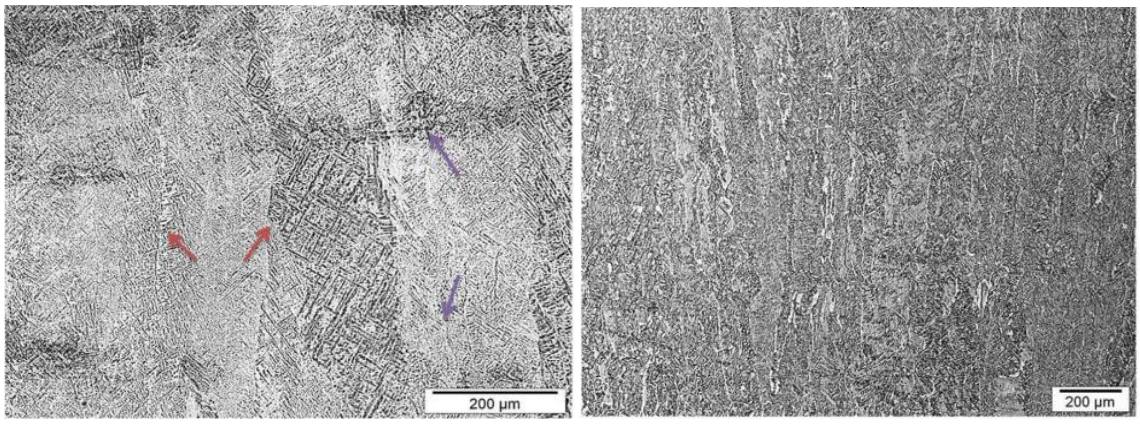

(a) (b)

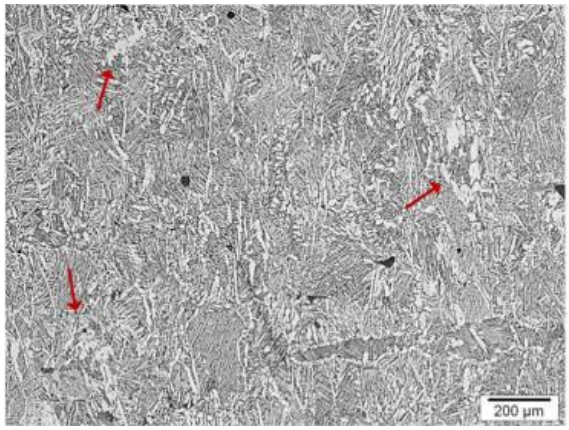

(c)

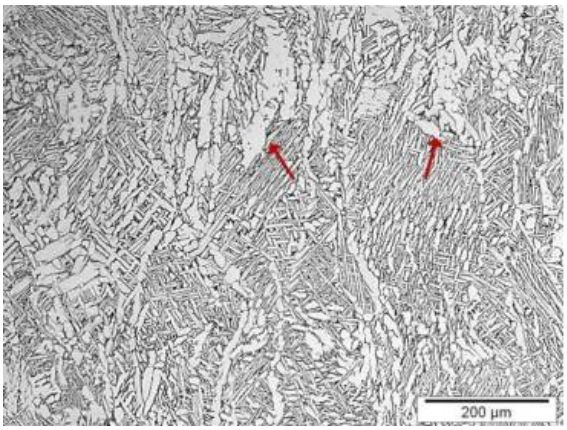

(d)

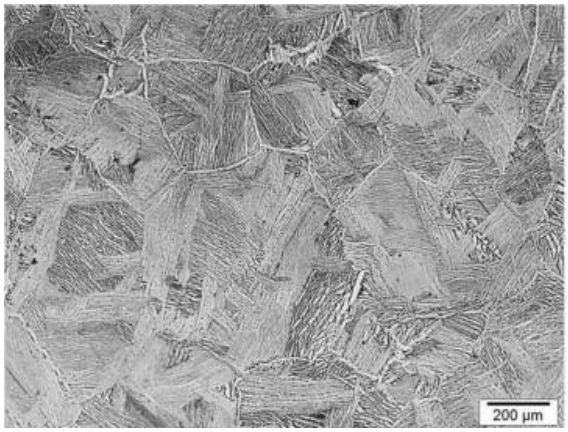

(e)

Figure 8. The microstructure of EBM printed Ti6Al4V parts with optical microscopy; (a) as-built with red arrows (light α phase) and blue arrows (dark β phase), (b) heat-treated (sub β, 930°C for 3 hours), (c) heat-treated (near β, 990°C for 2 hours) with red arrows (large α precipitates), (d) heat-treated (near β, 990°C for 3 hours) with red arrows (large α precipitates) and (e) heat-treated(super β, 1050°C for 2 hours) samples [13].

Chapter 3. Experimental Procedures and Methods

An evaluation of the effects of heat treatment with recycled powder on mechanical properties and microstructure of additively manufactured Ti6Al4V parts is important. Improvement of mechanical properties obtained from heat treatment could increase the possibility of continuous powder reuse for industrial applications. In this section, experimental procedures and the methods for the questions posed above are discussed.

3.1 Materials and Methods

3.1.1 Arcam A2X Printer

In this study, the Arcam A2X Electron Beam Melting machine (Arcam, Mölnlycke, Sweden) was used, which is one of the powder bed fusion systems with an electron beam as a heating source instead of a laser beam. The build chamber is controlled by the vacuum system to prevent any contamination so that the chemical specification of the build material can be maintained. A schematic of the exterior and interior of the system is seen in **Figure 9.**

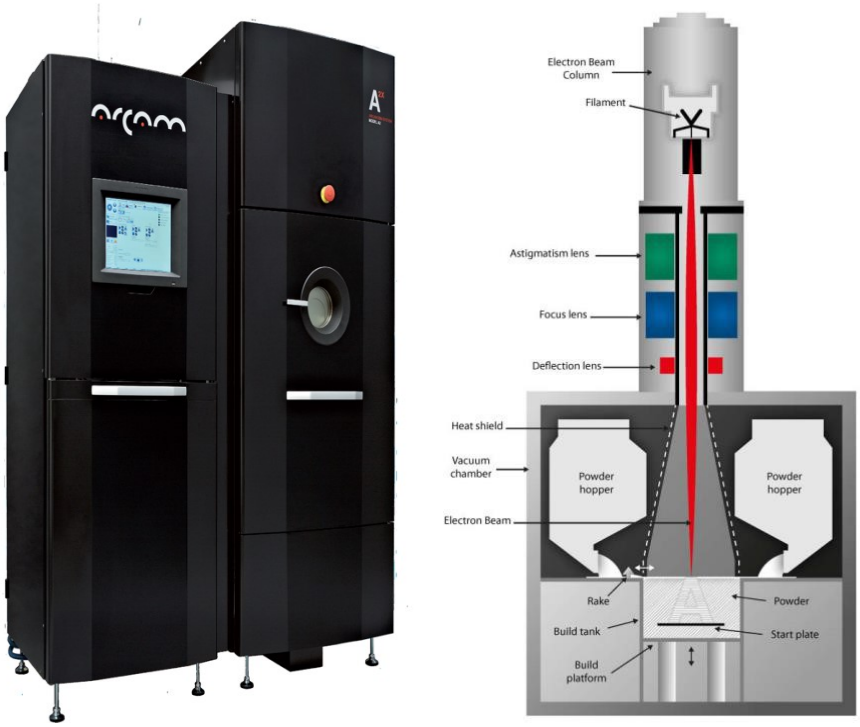

(a) (b)

Figure 9. Schematic diagrams of exterior (a) and interior (b) of Arcam A2X EBM system from Arcam EBM Technology brochure. The machine works with five steps of the whole process flow: file preparation, build preparation, build process, powder recovery, and build extraction. These steps encapsulate below.

3.1.1.1 File preparation

Three-dimensional(3D) models are necessary to make objects for printing. With computer-aided design(CAD) model made by CAD software such as Solidworks, Magics, and AutoCAD, the file which has a file extension 'STL' is generated for build model generation by including build distribution, support generation, and slicing layer by layer. The file going through these procedures are then exported as ABF(Arcam Build File) interface with the controller.

3.1.1.2 Build preparation

ABF file in the controller is loaded to generate ABP(Arcam Build Processor) file. Several factors such as process parameters, build plate, and melt themes are set up with the ABP file. Checking the parts inside the chamber such as heat shields, windowpane, rake shorts, filament, and then cleaning the chamber to get rid of metalized parts and then sandblast proceeds. The build plate is cleaned with isopropyl alcohol (IPA), locating and marking the center. The powder is then filled in hoppers with a build chamber open after depressurization to set up the build. After this step, the following occurs: setting up and checking a thermocouple, filling with powder, scooping out the thermocouple, and loading the build plate resting on the thermocouple. For even powder distribution, calibration of table height is necessary. After installing the heat shield and pumping down to chamber pressure up to 10^7 mBar, beam focus and center alignment are calibrated right before the build process.

3.1.1.3 Build process

The build plate is preheated up to 700°C while outgassing happens. Because of the build temperature, the EBM process can eliminate the thermal stresses and decomposes α' martensite phase into α+ß lamellar microstructure [8]. A stress relief heat treatment is not necessary for EBM due to high build temperature while laser melt systems such as selective laser melting (SLM) do. This process is conducted under the vacuum conditions to prevent the dissipation of an electron beam. After this preheating step, powder material in the chamber is spread onto the build platform in an even layer, which is called powder raking. The powder is then sintered, selectively melted, and fused by the electron beam rastered across the surface of the powder following the data

that makes the whole shape of the CAD model sliced into multiple layers. When the melting of a layer is finished, the build plate is moved downward and a new layer of powder is spread. The electron beam detects the cross-section of the layer and selectively melt the powder, followed by outlining regions and rastering based on hatching patterns. Support structures are also melted during the melting step. Procedures from the raking step to the melting step repeat until the printing is finished. This build process is carried out by many processing parameters. Detailed settings of the Arcam A2X printer and processing parameters used for the experiment include in **Appendix A**.

3.1.1.4 Powder recovery

The chamber is vented and heat shields are removed to prepare taking out components. Then the printing is finished and cooled down for 4 to 5 hours under the helium in the chamber. The build block of sintered powder including the parts is detached and moved to the powder recovery system (PRS) which was used in this study , as shown in **Appendix A**. The PRS impinges on the build to take apart the sintered powder and then get the parts by using titanium powder and compressed air inside the glove box. The powder is sifted and sieved to get rid of big particles, followed by the recovery of the powder with a vacuum cleaner. The final parts detach with the sintered powder that will reuse in the printer and are extracted by removing support structures. In these experiments, the powder was reused for a total 30 of prints.

3.1.2 Raw material

Ti6Al4V, which is commonly used for aerospace applications due to its properties such as excellent biocompatibility, high corrosion resistance, and high strength to weight ratio, was used in these experiments.

Ti6Al4V powder for the experiments was acquired from Arcam company (Batch P1303, Part #430944) [67] with plasma atomization that is one of the most common methods in terms of metal powder production. The plasma atomization uses plasma torches to melt and atomize the Ti6Al4V wire feedstock, as seen in **Figure 10** [73]. The chamber is under the low vacuum condition by purging the gas with a high purity of argon gas for the powder to be atomized. After the process superheats the metal, fast cooling stage solidifies the molten metal into spherical powder.

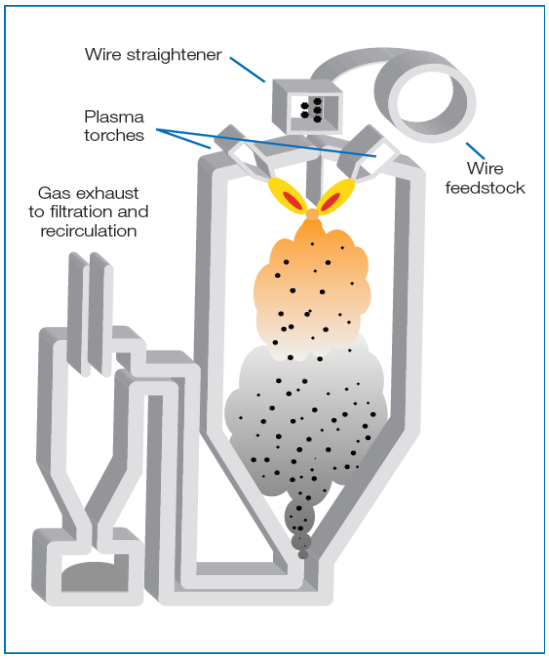

Figure 10. A schematic of plasma atomization [73].

Arcam company certified the chemical composition and particle size distribution of the Ti6Al4V Grade 5 powder made by the plasma atomization [66]. In these experiments, wrought form Ti6Al4V as reference material and Arcam AM

Ti6Al4V were used. The wrought form Ti6Al4V in these experiments was solution treated and aged condition (STA) Grade 5. Detailed mechanical properties are shown in **Table 4**, which indicates that the properties of the powder made by Arcam meet ASTM F2924 and ASTM F1472 requirements. Specific chemical composition and particle distribution are seen in **Appendix B**.

Table 4. Mechanical properties of Arcam AM [66], wrought form [56], ASTM F2924 requirement [56] and wrought form Ti6Al4V used in these experiments.

	Elongation (%)	**Ultimate Tensile Strength (MPa)**	**Yield Strength (MPa)**	**Elastic Modulus (GPa)**
Arcam	14	1020	950	120
ASTM Wrought Form(F 1472)	10	930	860	-
ASTM F2924	10	895	825	120
Wrought form (STA,Grade5)	10	1284	1184	-

3.1.3 Standard Build

30 builds from build 1 made of 50kg of virgin powder to build 30 made of 30 times recycled powder were printed, as shown in **Figure 11** [67]. New powder was not added in subsequent builds. The number of specimens was 16, containing six vertical and horizontal tensile specimens followed by ASTM E08, two staircases, a cylindrical pyramid, and a cylinder shape micro CT specimen which were used for porosity assessment. The staircases and cylindrical pyramid were used for microstructure analysis. In these experiments, only vertical and horizontal tensile specimens were heat

treated and used for tensile testing and SEM analysis. The tensile specimens followed sub size rectangular specimen specifications [68]. The dimensions of the specimens are seen in **Figure 12** [69]. For the vertical design of experiments (DOE) samples, schematic and dimensions of the samples are seen in **Figure 13(a)** and **(b)**. Compared to horizontal build 31 and other vertical samples used three as-built samples per build, six as-built samples were used in terms of vertical DOE samples to compare the microstructure and tensile properties for accuracy as an exception.

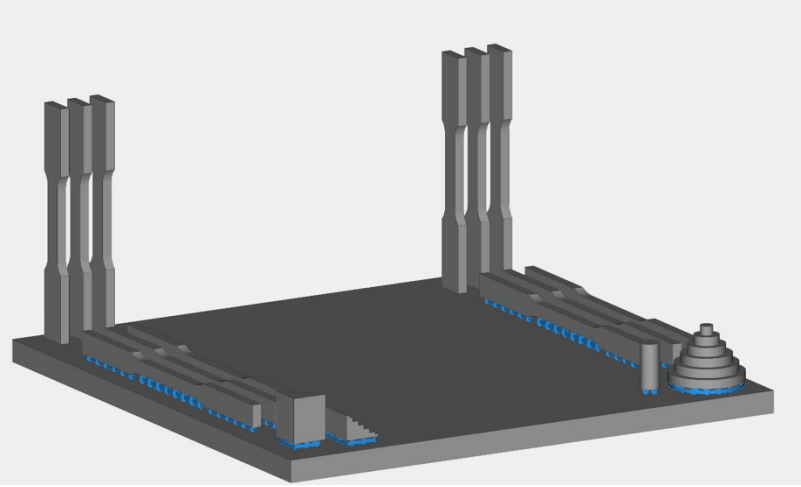

Figure 11. A schematic of standard build printed by the Arcam A2X EBM printer, including horizontal and vertical tensile specimens, staircase shape and a cylindrical pyramid shape specimens [67]. In these experiments, only vertical and horizontal specimens were used.

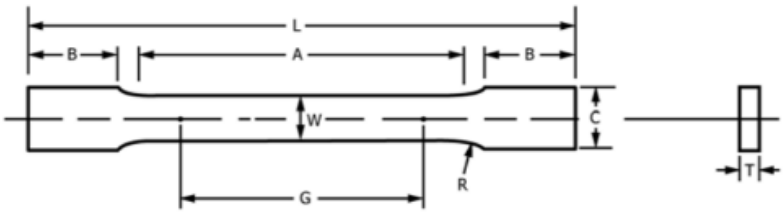

Figure 12. Tensile specimen dimensions, which include L = 104 mm, W = 6 mm, G = 25 mm, C = 10 mm, T = 3 mm [69].

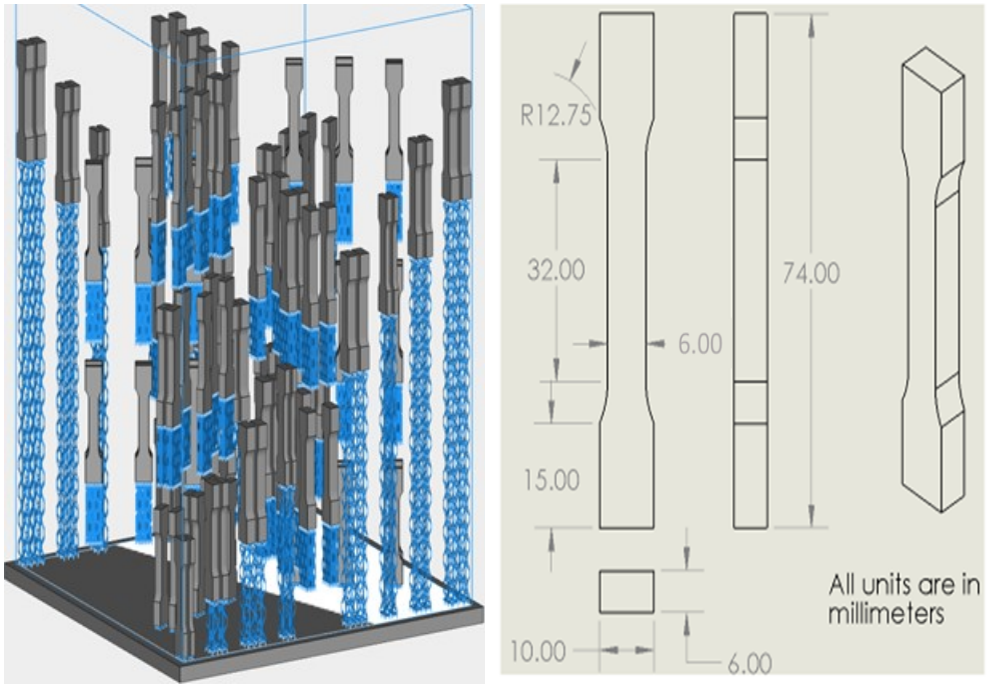

(a) (b)

Figure 13. (a) A schematic of vertical DOE (design of experiments) samples printed by the Arcam A2X EBM printer, (b) Vertical DOE tensile specimen dimensions, which include L = 104 mm, W = 6 mm, G = 25 mm, C = 10 mm, T = 3 mm

3.1.4 Heat treatment

After the tensile testings, heat treatment was carried out with three conditions based on the β-transus temperature of Ti6Al4V from 980°C to 1000°C which could be affected by several factors such as composition homogeneity, impurities, and initial microstructure [8]. Phase diagram of Ti6Al4V and phase transformation diagram in terms of cooling rates in **Figure 14**. Ms refers to the martensite start temperature and Mf means the martensite final temperature. Ti6Al4V goes through a variety of transformations from α + β, β, liquid, β, and α + β/α' phase during the whole melting and solidification process. Below the β-transus temperature, a hexagonal close-packed

(HCP) structure with α-titanium exists. A body-centered cubic (BCC) structure with β-titanium exists above the β-transus temperature. At room temperature, α + β phase exists because of aluminum atoms as an α stabilizer and vanadium atoms as a β stabilizer. However, this phase maintains only if cooling rates are slow. For instance, due to fast cooling rates in SLM, non-equilibrium α' martensite microstructure is formed at room temperature while equilibrium α + β lamellar microstructure is formed in EBM because of the high build temperature that results in relatively slow cooling rates. The range of cooling rates which make Ti6Al4V form α' martensite structure is from 20°C/s to 410°C/s in **Figure 14.(b)** [71].

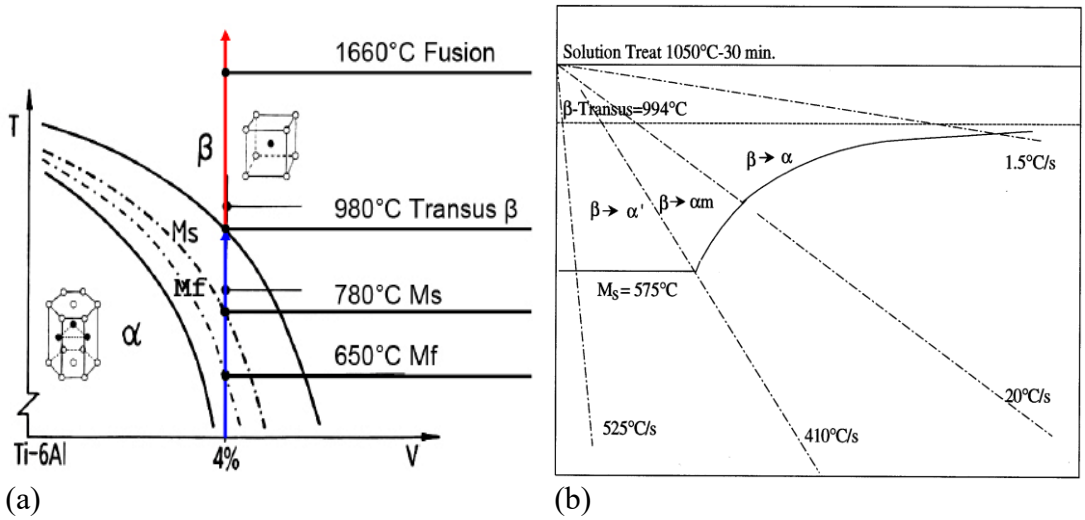

(a) (b)

Figure 14. (a) Phase diagram of Ti6Al4V [70]. (b) Phase transformation diagram in terms of cooling rates [71].

Specific heat treatment conditions used in these experiments are demonstrated in **Table 5**. All samples were machined and went through the same mounting, polishing, and etching process. Based on the β-transus temperature of Ti6Al4V, sub β-transus temperature (710°C for 2 hours), near β-transus temperature (950°C for 1 hour), and

super β-transus temperature heat treatment (1050°C for 1 hour) were performed. In particular, the sub β-transus temperature heat treatment conditions were used from AMS(Aerospace material specification)-H-81200 published by SAE International. Vertical specimens were heat-treated with the same conditions per 3 samples each build at the center of the tube furnace inside the tube and then furnace cooled. The arrangements of horizontal build 31 and vertical DOE samples were different from those of vertical samples, as shown in **Figure 15 (c)**, **(d),** and **(e)**. The way to perform all heat treatment was seen in **Figure 15 (b)**. When it comes to the atmosphere, all heat treatment was performed after exhausting the gas by using argon gas for 5 minutes and then filled with 15 psi argon gas as an internal pressure that maintained during the whole process by checking the flow regulator, which means argon gas was flowing while the specimens were furnace cooled in the tube furnace. The argon gas valve got closed when the temperature reached room temperature. After getting preliminary results from several specimens, only near β-transus temperature (950°C for 1 hour) heat treatment was performed with vertical/horizontal build 5, 9, 12, 16, 20, 24, and 28 to see the trend of changes in microstructure and mechanical properties. Thermo Scientific Lindberg/Blue M mini-mite tube furnace (Model TF55030A-1) was used for heat treatment, as shown in **Figure 15 (a)**. The detailed specification of the tube furnace is in **Appendix C**.

Table 5. Heat treatment conditions.

	build / direction	**temperature(°C)**	**soaking time(hr)**	**Remarks**
1	build 31 / vertical	950	1	
2	build 31 / horizontal	710	2	
3	build 31 / horizontal	950	1	

4	build 31 / horizontal	1050	1	
5	build 1 / vertical	950	1	DOE(16-18)
6	build 1 / vertical	950	1	DOE(19-21)
7	build 1 / vertical	1050	1	DOE
8	Wrought titanium	710	2	STA,Grade5
9	Wrought titanium	950	1	STA,Grade5
10	Wrought titanium	1050	1	STA,Grade5
11	build 5,9,12,16,20,24,28 / vertical	950	1	
12	build 5,9,12,16,20,24,28 / horizontal	950	1	

(a)

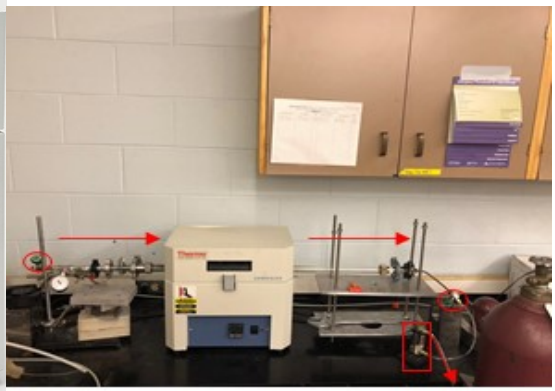

(b)

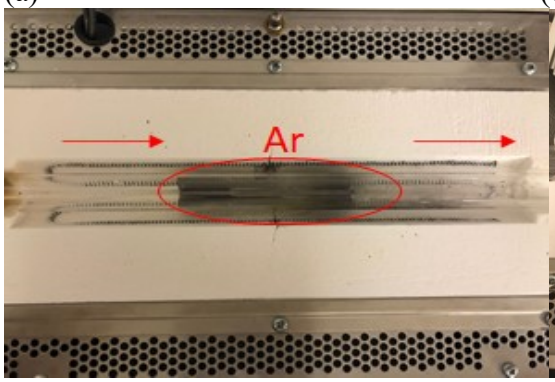

(c)

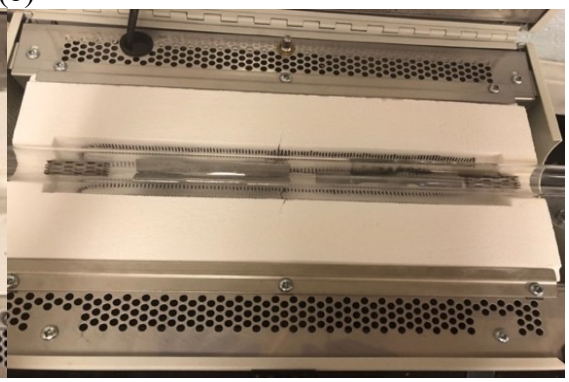

(d)

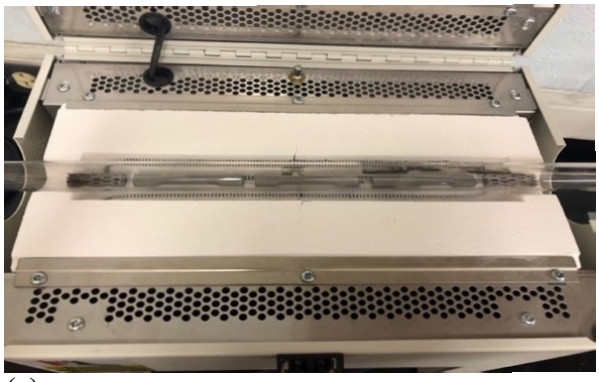

(e)

Figure 15. (a) Thermo Scientific Lindberg/Blue M Mini-Mite Tube furnace used in these experiments captured from Thermo Fisher Scientific company website, (b) the schematic of heat treatment process with red arrows indicating the direction of argon and exhausted gas and a red rectangle showing the flow regulator to check the internal pressure, (c) the arrangement of vertical samples from build 5, 9, 12, 16, 20, 24 and 28, (d) the arrangement of horizontal build 31 samples and (e) the arrangement of vertical DOE samples.

3.1.5 Tensile Testing

All tensile tests were carried out with sub-size rectangular specimens including as-built and heat-treated samples, based on ASTM E08. Three samples per each build were used for the tensile properties analysis, except vertical DOE samples which had six machined samples. In the case of the vertical DOE samples, three machined specimens labeled 16 to 18 were used to compare the results of near β-transus heat treatment. Other three machined specimens labeled 19 to 21 were used to compare the results of super β-transus heat treatment. There was no as-built data of vertical DOE samples because all vertical DOE samples were machined before the tensile testing to get rid of

surface roughness in the previous study. Before the tests began, surface preparation was performed by machining at the gauge section after the support structures were removed. A total of eight vertical and eight horizontal from the fifth (build 5: b5) to the last (build 31: b31) in increments of about every 4th build were measured to see a trend of mechanical properties and compare between as-built and heat-treated specimens. The rest of the tensile specimens not used for the test from build 1 to 30 was reserved for future use.

When it comes to equipment for the tensile tests, the Instron 5585H load frame with a 30kN grip, clip-on extensometer, and 50kN load cell (**Appendix D**) was used. The rate of displacement was 1.27mm/minute. True stress-true strain curves for each specimen measured were generated by using the load and displacement data from the testing. Several mechanical properties such as % elongation, modulus of elasticity, ultimate tensile strength, yield strength (0.2% offset) were taken out from the curves.

3.1.6 SEM Analysis and Optical Microscopy

After the tensile testing, all specimens were prepared for optical microscopy (OM) and SEM analysis to determine the trend and changes in microstructure between as-built and heat-treated Ti6Al4V from each build. The specimens were sectioned with round shape cutting saw made of diamond. Only the gauge section of all tensile specimens that were only machined was used for SEM analysis, as seen in **Figure 16**. Three parts of the samples per build were taken by SEM. Since the microstructure could vary depending on the build height [85], the same areas of the samples were taken for the microstructural analysis, indicating red rectangles in **Figure 16**. The parts sectioned

were mounted using conductive graphite-based powder with a Buehler Pneumet I hot mounting press and then polished from # 240, 400, 600, to # 800 grit SiC papers. Fine polishing was done before the final polishing step by using felt pads and 6-micron DiaLube diamond suspensions. Each polishing step was followed by cleaning the samples with deionized water to get rid of debris and dust on the surface of the samples. The final polishing step was performed to obtain a mirror finish using a solution made of 10 drops of hydrogen peroxide, 5ml ammonium hydroxide, and 100ml of 0.05µm diamond colloidal suspension. As a final step before taking SEM images, Etching was conducted with Kroll's etchant (2% HF, 6% HNO3, 92% water) for 10 seconds. After the etching, optical microscopy (OM) using an Olympus SC30 stereomicroscope and SEM analysis using JEOL-6010 SEM were performed, as seen in **Figure 17**. Three locations indicated with orange squares on the prepared surface of each sample were examined through the equipment. In **Figure 18 (b) and (c)**, OM images were taken with Olympus SC30 (100X magnification for measurement of prior β grains, 200X and 500X magnification for the overall observations of changes in the microstructure to measure prior β grain widths) by using the line intercept method for columnar and equiaxed grains, according to ASTM standard E112-13 [84]. Three optical micrographs per each sample were taken with the size of 1305µm X 975µm (100X magnification), in which each image was drawn with six parallel lines perpendicular to the columnar grains axis and the build direction. The final prior β grain width was measured with the average line length counted for each line. When it comes to the measurement of prior β grain in equiaxed structure, not only just six straight lines perpendicular to the build direction but also twelve additional lines including six diagonal lines with two lines connecting two vertices facing each other and four lines connecting the middle of length and width

of the picture and six straight lines parallel to the build direction were added to measure the grain size, based on ASTM E112-13 [84]. Following this ASTM standard, these total eighteen lines were used to yield at least fifty intercepts which refer to segments of test line overlaying one grain. Also, the measurements were done by adding these six diagonal lines and six straight lines parallel to build direction to consider the possibility of variant grain size depending on the orientations, which was why these eighteen lines in the equiaxed structure having four orientations were used unlike only six straight lines perpendicular to the build orientation were used for the columnar structure even though these 6 straight lines also included at least fifty intercepts. The average of measurements was calculated from the three images per sample by using the software named Image J.

When it comes to SEM analysis, compared to OM (50X, 200X, 500X), higher magnification (2500X) pictures were taken and analyzed to measure the α lath thickness. Also, the samples were distributed onto conductive tape before SEM analysis. The definition of the lath thickness is the shortest distance between two adjacent parallel β ribs. The way to calculate the α lath thickness is based on Searles et al. [72] by computing the distance between two parallel β ribs using Adobe Photoshop. There are five steps to measure thickness [67]. First of all, segmenting image grayscale is carried out. Next, at an angle intersecting β ribs, parallel lines are drawn. The average line length is recorded followed by measurement of the length of each line segment. This process is iterated by rotating parallel lines by 30 degrees to a total of 360 degrees, as seen in **Figure 18 (a)**. α lath thickness is calculated with an equation 1/1.5*1/λ. The value of the thickness is computed on average from three images per sample.

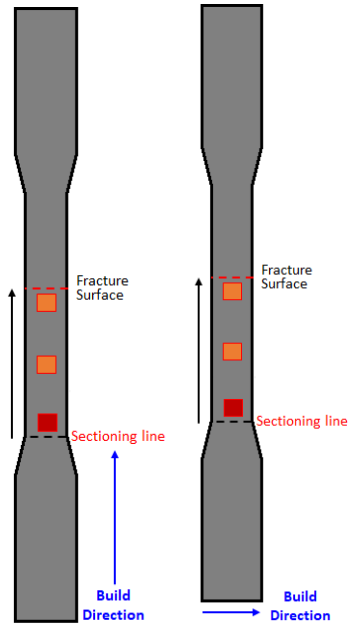

Figure 16. A schematic diagram of the tensile specimens used in the SEM and OM analyses. Gauge section from black dash line to red dash line was used for OM and SEM. Black dotted line means a spot sectioned by diamond saw and red dotted line refers to fracture surface from tensile testing. Blue arrows indicate build direction, which means (a) vertical specimens and (b) horizontal specimens. Black arrows demonstrate the order of pictures taken and orange color cubes show the area analyzed by SEM and OM. For the consistency of the analysis, the same build height was used, as shown in red rectangles.

(a) (b)

Figure 17. (a) OM and (b) SEM equipment.

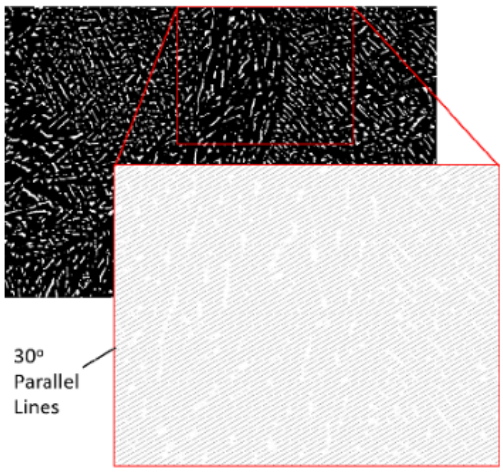

(a)

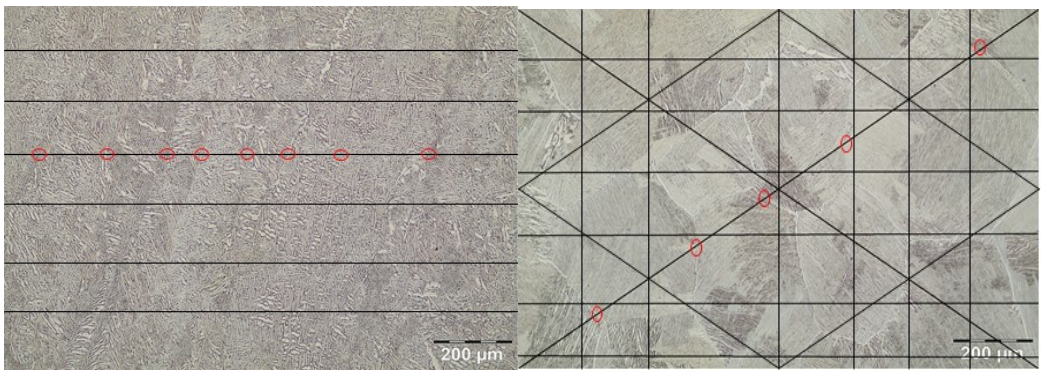

(b) (c)

Figure 18. Measurement of the microstructure in Ti6Al4V for (a) α lath thickness [85], (b) prior β width in columnar structure and (c) prior β grain size in equiaxed structure [84].

Chapter 4. Results

Optical microscopy was performed with 100X for the prior β grain measurement, 200X for 1050°C heat-treated samples to observe changed structures better, and 500X for the rest of the samples. For SEM analysis, 2500X magnification was used to measure alpha lath thickness. When it comes to heat treatment, sub β-transus temperature (710°C for 2 hours), near β-transus temperature (950°C for 1 hour), and super β-transus temperature heat treatment (1050°C for 1 hour) were carried out with vertical/horizontal build 31 (31st build, the final build of 50kg of virgin powder) and Grade 5 wrought titanium in STA (solution treated and aged) conditions samples. Vertical virgin powder (design of experiments, DOE) samples were heat-treated without sub β-transus temperature heat treatment because of the result from the horizontal build 31 samples, which will be discussed specifically in **4.2** (Tensile Testing). Due to a lack of specimens and future use, only near β-transus temperature heat treatment was performed from build 5 to build 31 in increments of about every 4th build.

4.1 SEM Analysis and Optical Microscopy

4.1.1 Horizontal build 31 (optical microscopy)

The microstructure of EBM printed as-built Ti6Al4V is a columnar α+β structure. In **Figure 19**, the results of sub β-transus heat treatment are not much different from the microstructure of as-built samples. Both images show the same

columnar β grain structure with no significant sign of coarsening of α lath structure. In contrast to the insignificant changes of the microstructure from sub β-transus heat treatment, the near β-transus heat treatment resulted in a more coarse α lath structure, as shown in **Figure 20**. Obvious changes in microstructure were observed in **Figure 21,** showing an equiaxed morphology with full recrystallization. Furthermore, transformed prior β grains from columnar to equiaxed structure show a small portion of coarse Widmanstatten structures, indicating that specimens were cooled slowly in the tube furnace. Comparisons of prior β grain width among the samples were seen in **Figure 22**, showing that only samples heat-treated above β-transus temperature indicated significant changes in the grain size. The rest of the samples showed an average of 54μm while super β-transus heat treatment resulted in an average of 292μm.

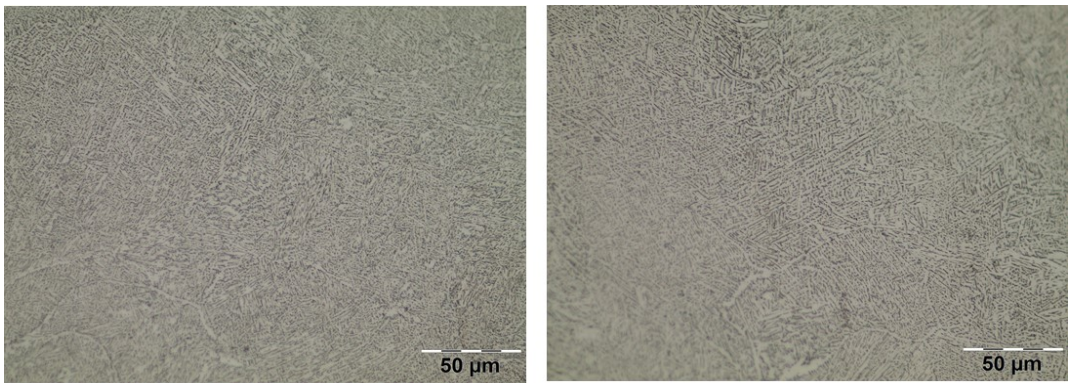

(a) (b)

Figure 19. Comparison of the microstructure of horizontal build 31 (a) as-built and (b) heat-treated (710°C, 2 hours) samples. 500X magnification images.

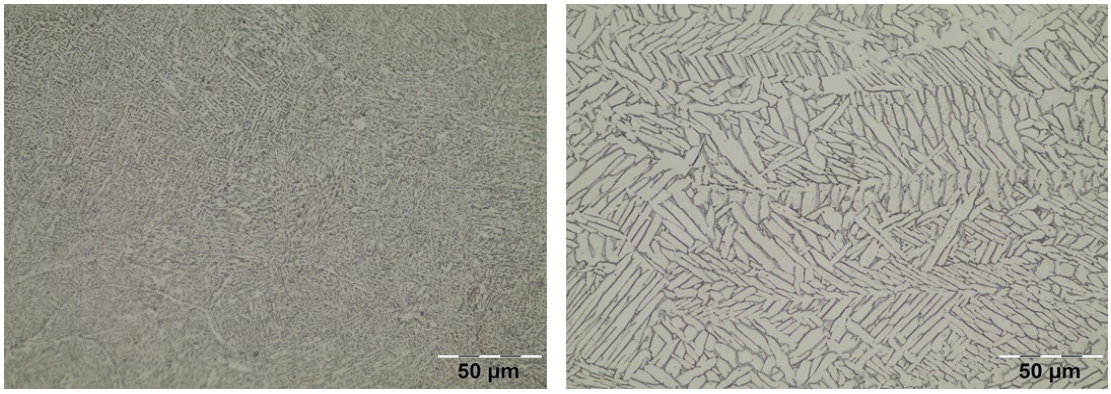

(a) (b)

Figure 20. Comparison of the microstructure of horizontal build 31 (a) as-built and (b) heat-treated (950°C, 1 hour) samples. 500X magnification images.

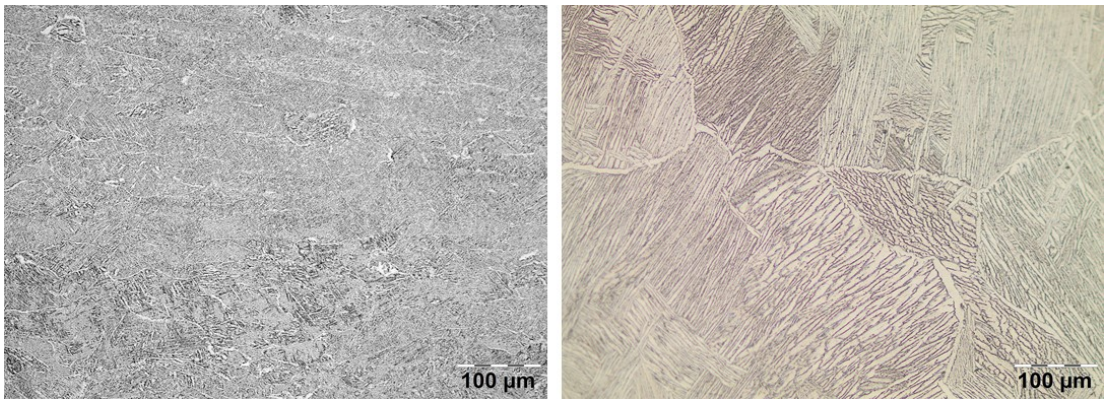

(a) (b)

Figure 21. Comparison of the microstructure of horizontal build 31 (a) as-built and (b) heat-treated (1050°C, 1 hour) samples. 200X magnification images.

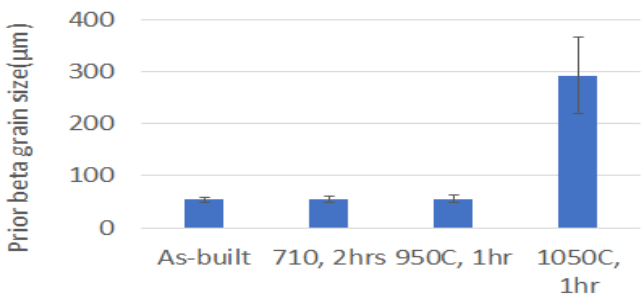

Figure 22. Plots of prior β grain size from horizontal build 31 samples with different conditions treated.

4.1.2 Horizontal build 31 (SEM analysis)

Figure 23 shows SEM images with 2500X magnification. The microstructure of Ti6Al4V with sub β-transus heat treatment is not much different from that of an as-built structure. However, samples with near β-transus heat treatment showed a more apparent coarse α lath structure and super β-transus heat treatment, which resulted in a completely transformed equiaxed prior β grains with coarse α lath thickness. Comparisons of α lath thickness among the samples were seen in **Figure 24**. Average α lath thickness values of as-built, heat-treated below, near, and above the β-transus temperature were 1.18µm, 1.3µm, 2.59µm, and 2.6µm respectively.

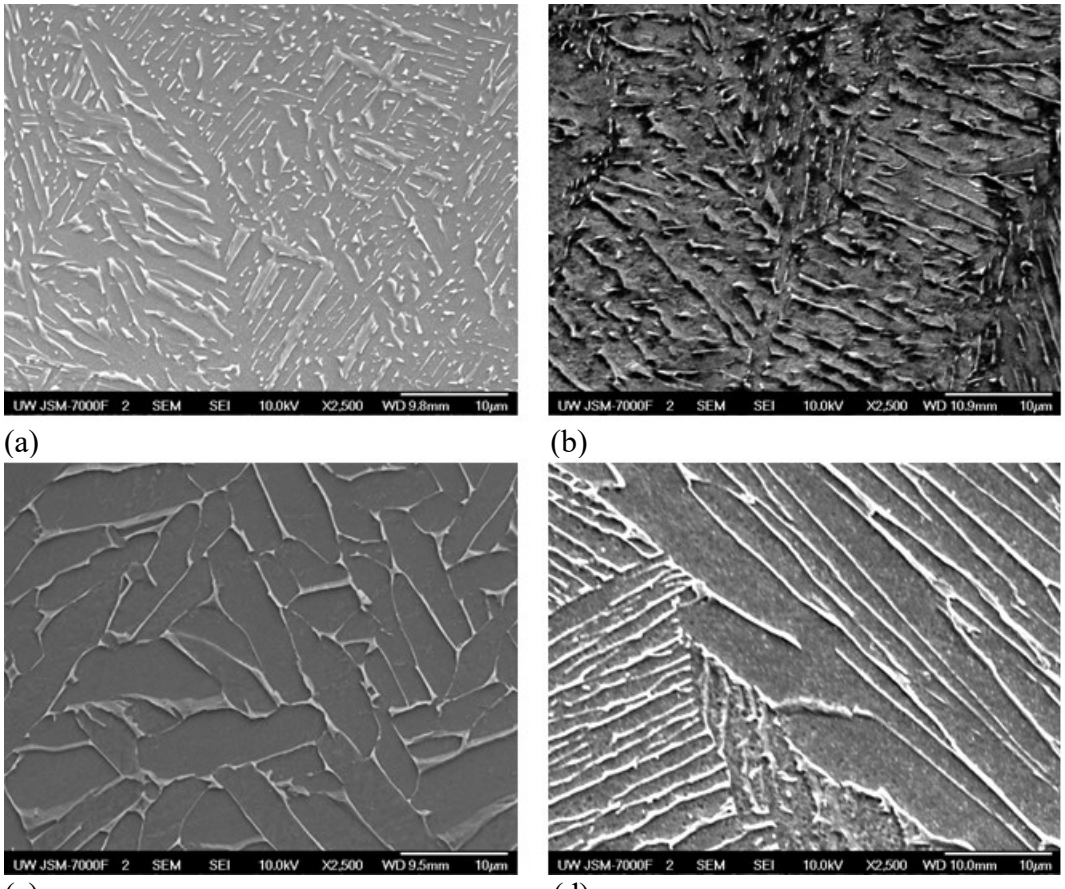

(a) (b)

(c) (d)

Figure 23. Comparison of the microstructure of horizontal build 31 (a) as-built and (b) heat-treated (710°C, 2 hours), (c) heat-treated (950°C, 1 hour), and (d) heat-treated (1050°C, 1 hour) samples. 2500X magnification images.

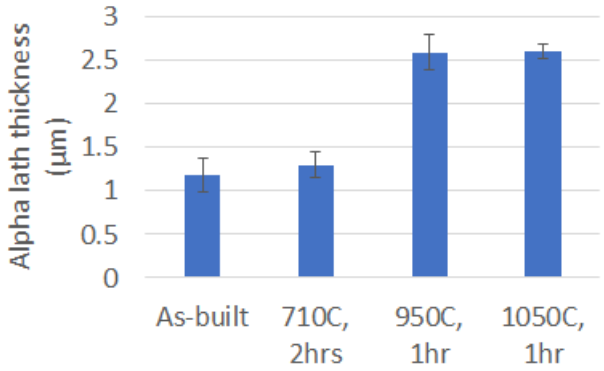

Figure 24. Plots of α lath thickness from horizontal build 31 samples with different conditions treated.

4.1.3 Vertical DOE (nearly virgin powder, optical microscopy)

In **Figure 25,** similar to the result of horizontal build 31, a more coarse α lath structure was observed. Also, a uniform equiaxed prior β grain and a portion of Widmanstatten structure were seen in **Figure 25 (d)**. The average β grain size of machined, heat-treated samples near β-transus temperature and above β-transus temperature was 85µm,86µm, and 280µm respectively, as shown in **Figure 26**.

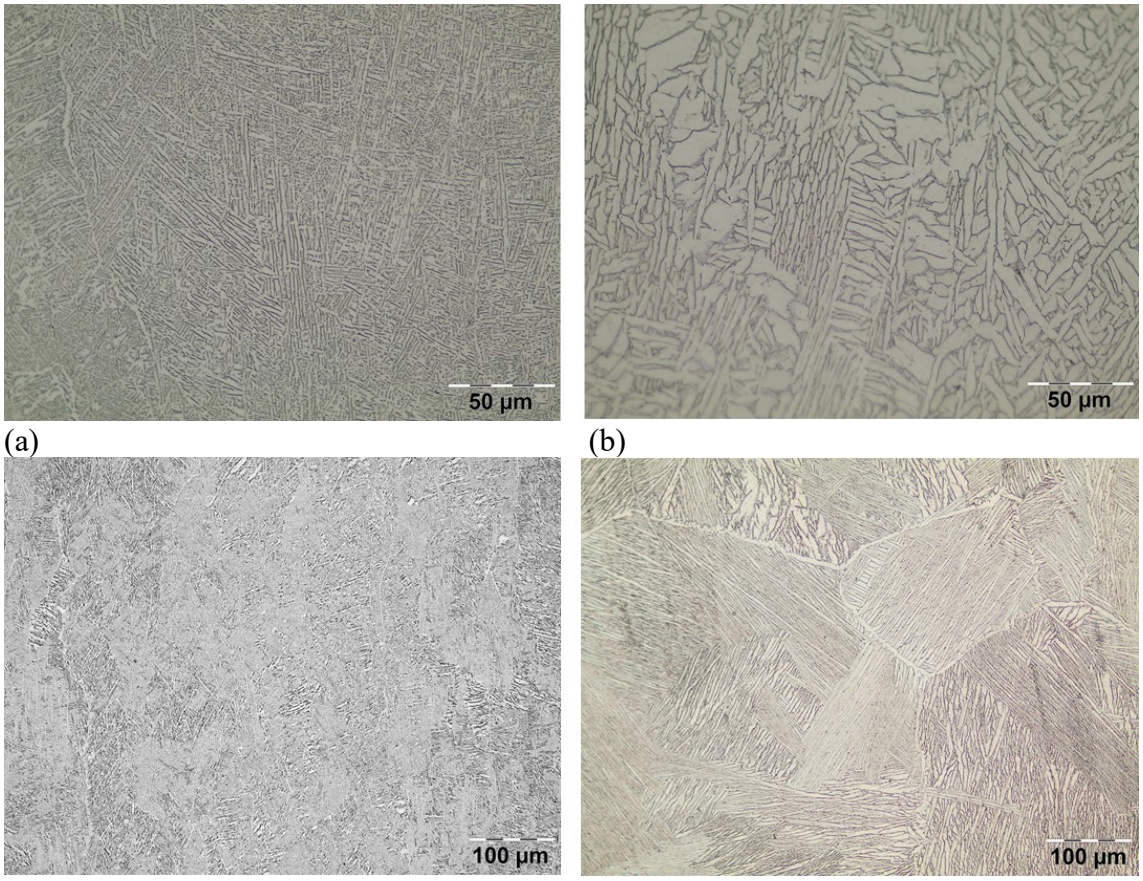

(a) (b)

(c) (d)

Figure 25. Comparison of the microstructure of vertical DOE (a) machined and (b) heat-treated (950°C, 1 hour), (c) machined and (d) heat-treated (1050°C, 1 hour) samples. 500X magnification was used for (a) and (b). 200X magnification was used for (c) and (d) to show equiaxed structure more clearly.

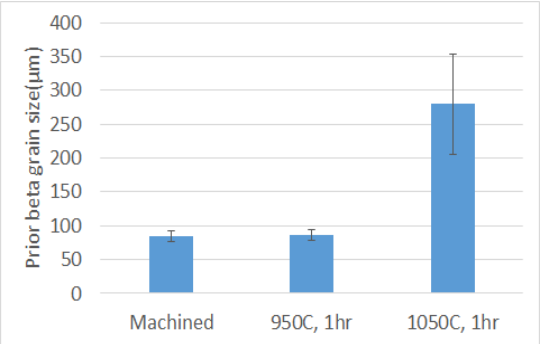

Figure 26. Plots of prior β grain size from vertical DOE samples with different conditions treated.

4.1.4 Vertical DOE (nearly virgin powder, SEM analysis)

SEM images in **Figure 27** were nearly the same as the result of horizontal build 31 in terms of the changes in the microstructure depending on the heat treatments. However, when it comes to α lath thickness, the result of near β-transus heat treatment looks similar to that of the super β-transus heat treatment. **In Figure 28**, a comparison of α lath thickness was shown. The average thickness of machined, heat-treated samples near β-transus temperature and above β-transus temperature was 0.97μm, 1.86μm, and 1.97μm, respectively.

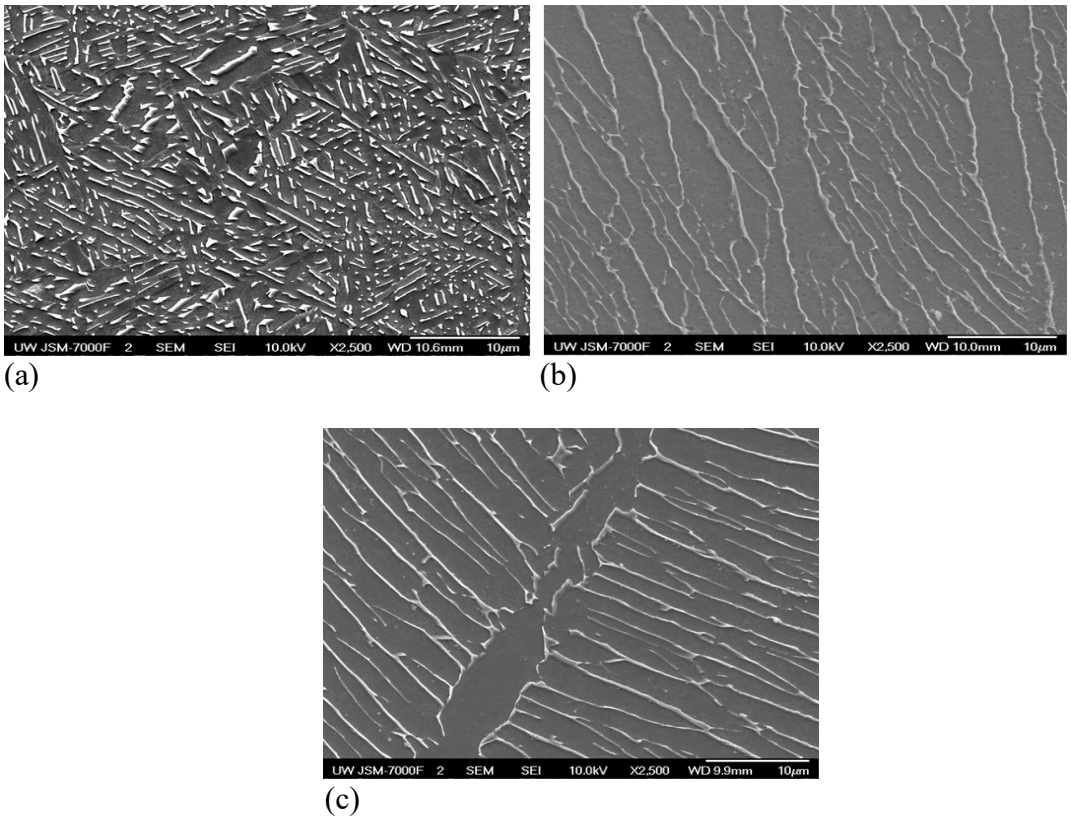

(a) (b)

(c)

Figure 27. Comparison of the microstructure of vertical DOE (a) machined and (b) heat-treated (950°C, 1 hour) and (c) heat-treated (1050°C, 1 hour) samples. 2500X magnification used.

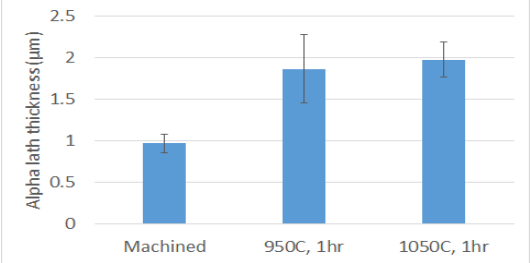

Figure 28. Plots of α lath thickness from vertical DOE samples with the different heat treatment conditions.

4.1.5 Wrought titanium (optical microscopy)

In these experiments, wrought titanium (solution treated and aged, Grade 5) was used as reference material to validate heat treatment with the tube furnace, as shown in **Figure 29** and **Figure 30**. Compared to non-heat-treated samples that have equiaxed α (light) and intergranular β (dark) grains, more coarse α structure was found resulting from near β-transus heat treatment. However, there were no apparent changes in the microstructure between non-heat treated and heat-treated samples with 710°C for 2 hours. When it comes to super β-transus heat treatment, the microstructure changed into plate-like α (light) and intergranular β (dark) structures. These structures from these experiments are all the same as microstructures in Metal Handbook published by American Society for Metals [74], as shown in **Figure 31** from the reference.

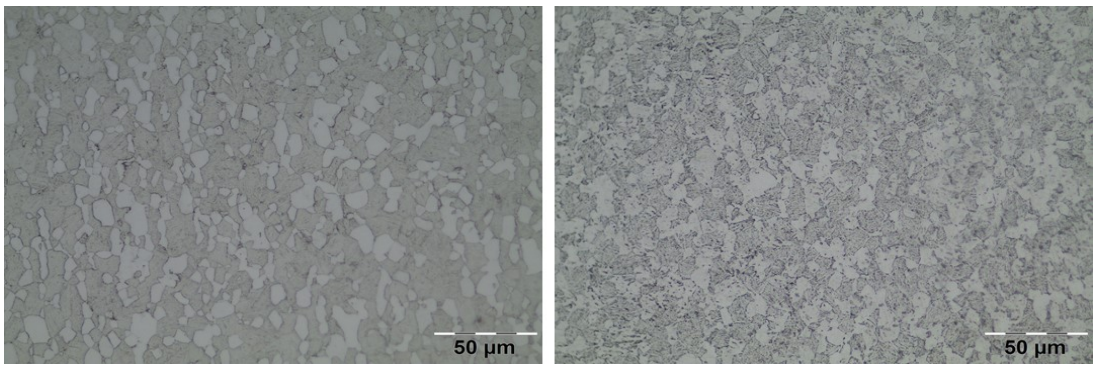

(a) (b)

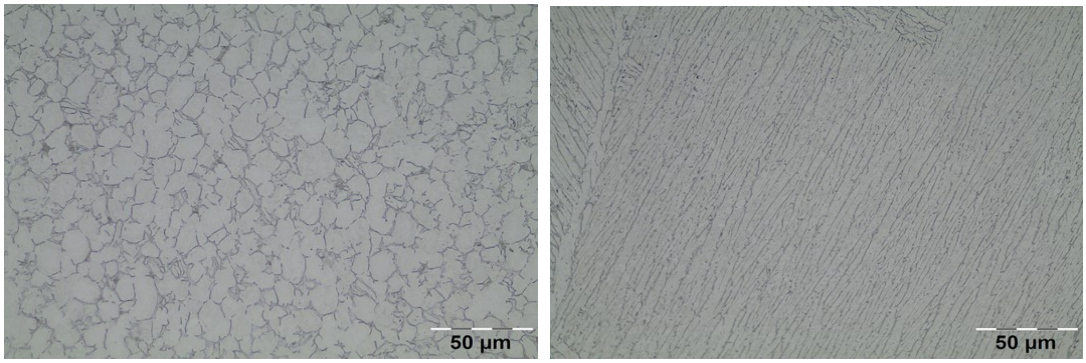

(c) (d)

Figure 29. Comparison of the microstructure of wrought titanium (a) non-heat treated and (b) heat-treated (710°C, 2 hours), (c) heat-treated (950°C, 1 hour) and (d) heat-treated (1050°C, 1 hour) samples. 500X magnification was used.

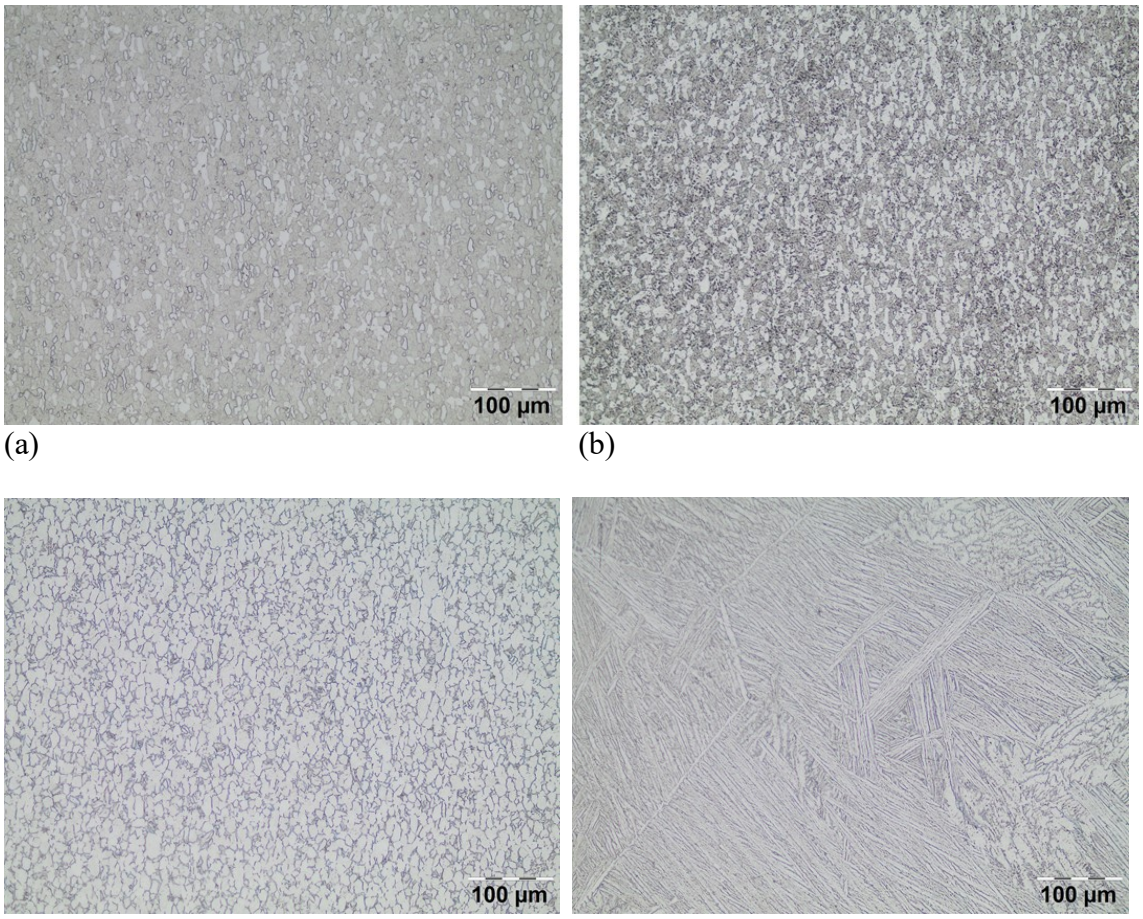

(a) (b)

(c) (d)

Figure 30. Comparison of the microstructure of wrought titanium (a) non-heat treated and (b) heat-treated (710°C, 2 hours), (c) heat-treated (950°C, 1 hour) and (d) heat-treated (1050°C, 1 hour) samples. 200X magnification was used for showing equiaxed structure more clearly.

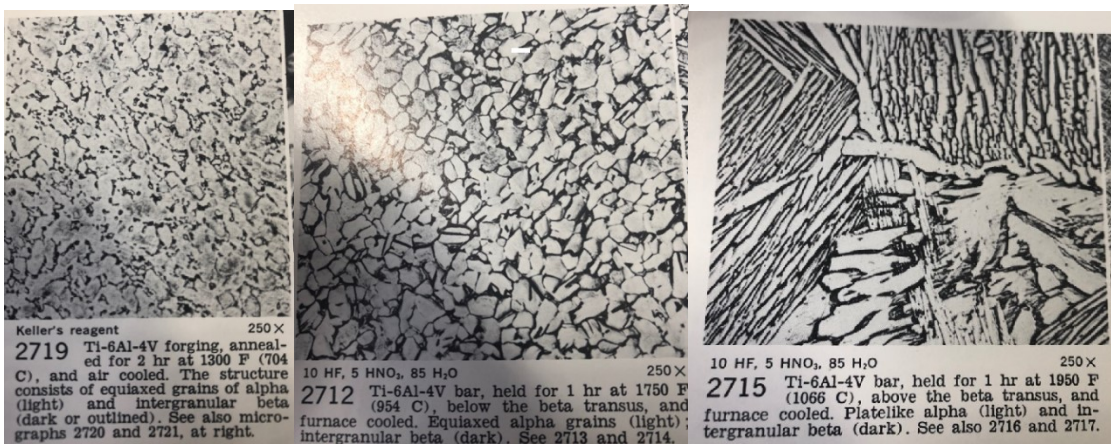

(a) (b) (c)

Figure 31. Microstructure of wrought titanium captured from Metals Handbook by American Society for Metals [74]. (a) microstructure the same as non-heat treated wrought titanium (b) the structure same as wrought titanium with near β-transus heat treatment (c) the structure same as super β-transus heat treatment.

4.1.6 Vertical build results

Near β-transus heat treatment was performed with vertical samples from build 5 to 28 in increments of about every 4th build. The machining process was done before tensile testing was carried out. The microstructure of all samples showed coarse α lath

thickness, as seen in **Figure 18 (b)**. When it comes to prior β grain size, as shown in **Figure 32 (a)**, there were no significant changes among the samples, whose range of average grain size was from 78µm to 101µm. In **Figure 32 (b)** [85], powder reuse could increase α lath thickness. However, the thickness varies depending on other variables such as build height and defects. In brief, powder reuse does not affect both α lath thickness and prior β grain width. But super β-transus heat treatment increased the β grain size by three times. Also, near and super β-transus heat treatments increased the α lath thickness by two times, as shown in **Figure 26** and **28.** Based on the result of vertical DOE samples, the effect of heat treatment on the microstructure of vertical heat-treated samples might be 1) significant increase of prior β grain when super β-transus heat treatment was applied and 2) magnificent increase of α lath thickness when near β-transus heat treatment and super β-transus heat treatment were applied.

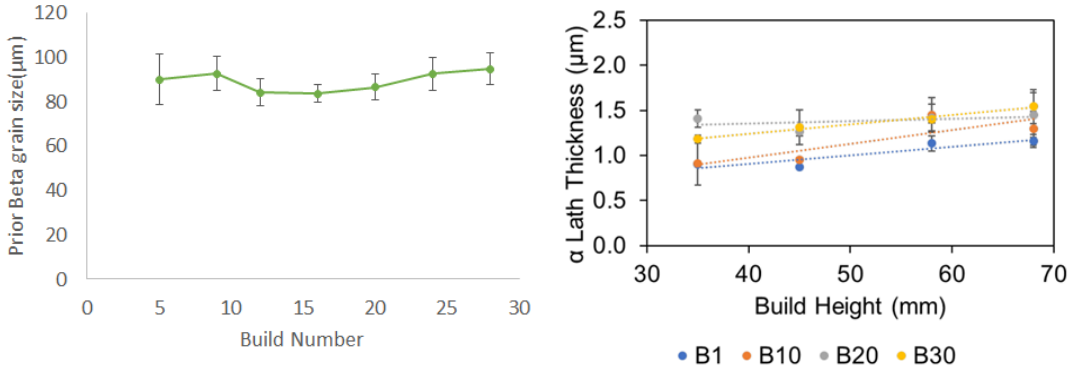

(a) (b)

Figure 32. (a) Average prior β grain size for columnar structure with powder reuse and (b) Alpha lath thickness for the tensile gauge section with powder reuse and build height [85].

4.1.7 Horizontal build results

There were limitations of using the lab and SEM machine due to COVID 19. Near β-transus heat treatment was done with heat-treated horizontal samples. However, the machining process was limited. Also, using the SEM machine was not available. Based on the results of vertical heat-treated samples, α lath thickness and prior β grain width of horizontal heat-treated samples with powder reuse might not change and show any trends clearly. Heat treatment could affect both characteristics in the same manner as vertical samples. Super β-transus heat treatment might increase prior β grain size and α lath thickness while near β-transus heat treatment only increases α lath thickness.

4.2 Tensile Testing

For each tensile specimen, including as-built and heat-treated samples, true stress-true strain curves were made. Three specimens are analyzed each build to measure the average mechanical properties such as % elongation, tensile strength, and modulus of elasticity. For example, representative samples from vertical build 5 are seen with a stress-strain curve plotted with the raw data from the tensile testing in **Figure 33**. The curve shows a typical elastic relationship between stress and strain with a linear line until the deformation starts at yield strength. When strength reaches up to the yield strength, a small portion of necking takes place and then failure happens. A comparison between as-built and heat-treated samples was analyzed starting horizontal build 31, vertical DOE, and wrought titanium. Furthermore, representative true stress-true strain curves are seen in Section **4.2.4** and **4.2.5** for build 5, 9, 12, 16, 20, 24, 28, and 31 for both build directions. Several trends were discussed from these curves. All tensile properties and stress-strain curves were plotted and are presented in **Appendix G** and

Appendix H, respectively. The data of 12-1 sample, one of build 12 specimens in **Appendix G** was not used for the analysis due to system errors during the testing.

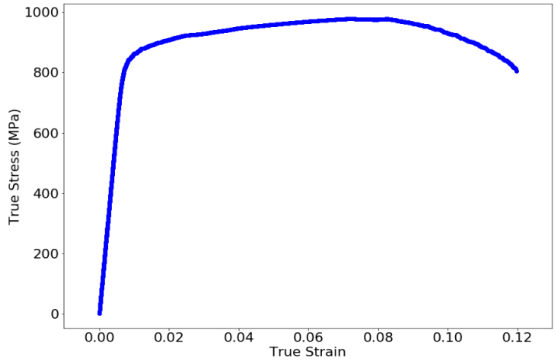

Figure 33. True stress-true strain curve from a build 5 vertical specimen.

4.2.1 Horizontal build 31 Tensile Testing Results

The primary purpose of these experiments is to observe the changes in mechanical properties in terms of strength and % elongation in particular because the heat treatment is well known as post-processing to relieve stress and improve ductility. In **Figure 34**, yield strength decreased with increasing temperature. However, % elongation showed a different trend from the result of yield strength. Sub and near β-transus heat treatment resulted in the increase in ductility, but the ductility of the samples with super β-transus heat treatment decreased. When it comes to sub β-transus heat treatment, ductility increased slightly at the expense of a small decrease in yield strength.

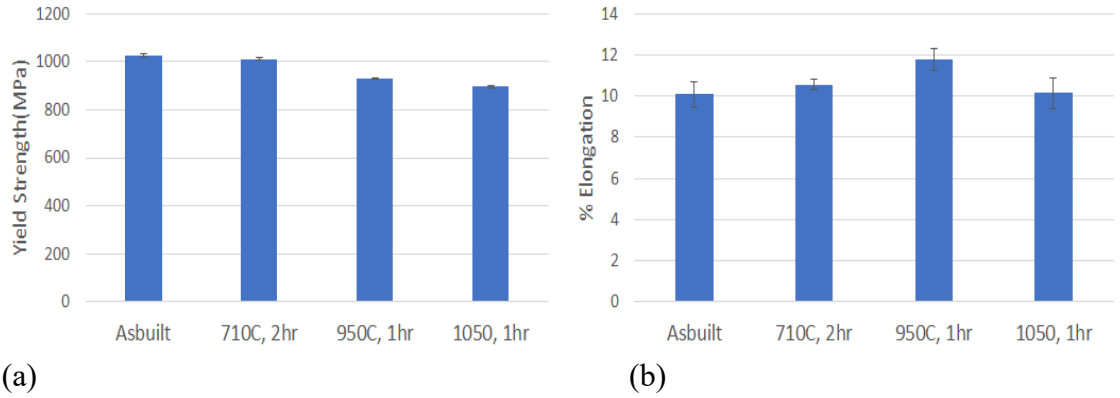

(a) (b)

Figure 34. Plots of (a) yield strength and (b) % elongation. from horizontal build 31.

4.2.2 Vertical DOE Tensile Testing Results

The trends of yield strength and % elongation curves with vertical DOE made of nearly virgin powder were different from those of the curves with horizontal build 31 that was made from heavily used powder samples, as shown in **Figure 35**. In the case of near β-transus heat treatment, both yield strength and % elongation decreased while super β-transus heat treatment resulted in an increase of % elongation with a decrease of the yield strength compared to each machined sample. However, on average, the value of % elongation heat-treated near β-transus (13.3%) was higher than that of % elongation heat-treated above β-transus (10.8%).

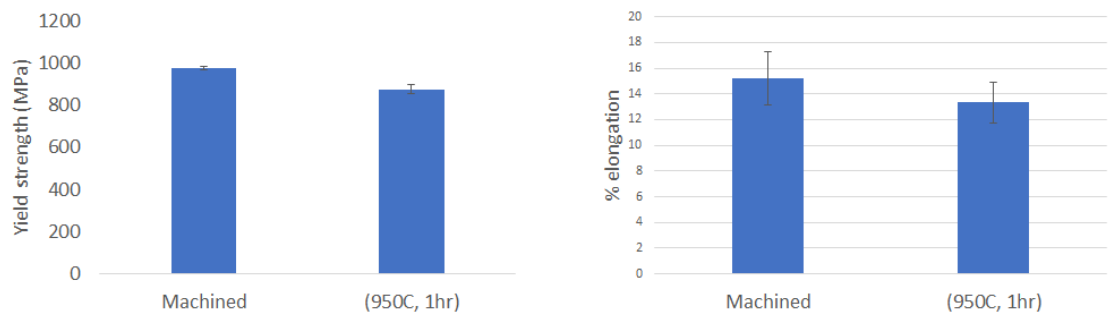

(a) (b)

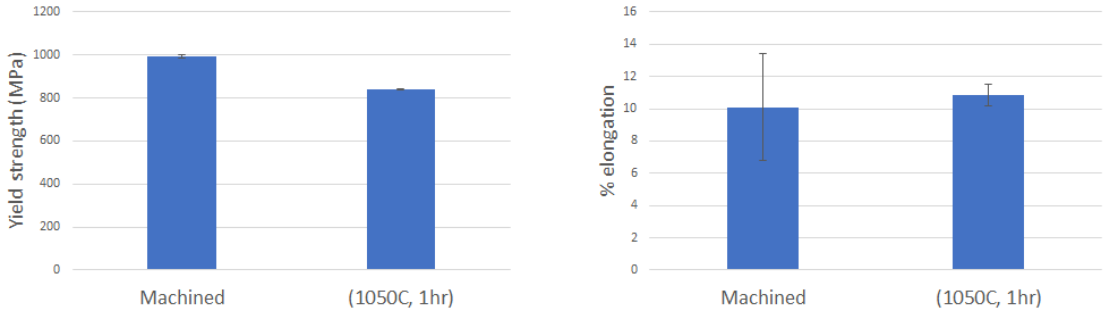

(c) (d)

Figure 35. Plots of (a) yield strength, (b) % elongation of machined but not heat-treated and heat-treated vertical DOE samples at 950°C for an hour, (c) yield strength and (d) % elongation of machined but not heat-treated and heat-treated vertical DOE samples at 1050°C for an hour.

4.2.3 Wrought Titanium Tensile Testing Results

In **Figure 36**, yield strength decreased with an increase in temperature, while % elongation showed different trends from the results of other samples. The result of sub β-transus heat treatment and near β-transus heat treatment showed similar % elongation values on average. In contrast, % elongation of the samples with super β-transus heat treatment decreased rather than that of as-received wrought titanium samples.

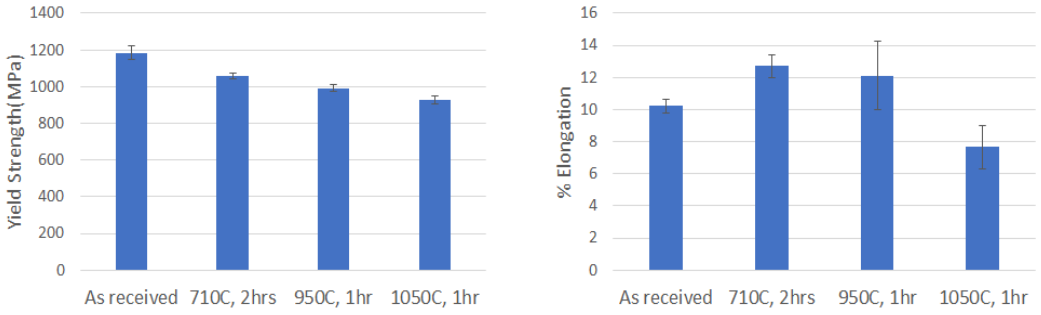

(a) (b)

Figure 36. Plots of (a) yield strength and (b) % elongation of wrought titanium samples.

4.2.4 Trends of Vertical specimens

Representative ultimate tensile strength, % elongation, yield strength, and elastic modulus with powder reuse curves are shown in **Figure 37** for build 5 from 28 for vertical build directions. All samples were heat-treated with 950°C for an hour and then furnace cooled. To analyze trends more quantitatively, yield strength, the modulus of elasticity, % elongation, and ultimate tensile strength were measured for each tensile specimen. Tensile properties were calculated on average. The mechanical properties were plotted following the build number in order. These trends were described for each mechanical properties below. Specific quantitative values of the properties were shown in **Table 6**.

The elastic modulus of as-built specimens and heat-treated samples, shown in **Figure 37 (a)**, did not indicate a clear trend with powder reuse (maximum 136GPa and minimum 118GPa). The reason why the elastic modulus of build 12 exhibited lower than expected modulus compared with the general trend was possibly due to a preheat problem during the build process, according to BARC paper reported by Prof. Ramulu and Arola. Overall, machining and heat treatment increased the elastics modulus of all samples. The magnitude increased by an average of 16 GPa.

Figure 37 (b) shows the yield strength of heat-treated vertical samples with powder reuse. Unlike the result of elastic modulus, yield strength significantly increased with powder reuse by 22% for as-built and 15% for heat-treated samples, compared to build 5 and build 28. The machining process increased the yield strength, which magnitude was average 7.45MPa. However, build 20, 24, and 28 showed a slight decrease in yield strength due to heat treatment that resulted in a decrease of the strength.

Figure 37 (c) plots the UTS. The trend seen is similar to that of the yield strength, which shows a significant increase of UTS with powder reuse by 19% for as-built and 18% for heat-treated samples, compared to build 5 and build 28. Machining and heat treatment resulted in an increase of magnitude by average 45.2MPa.

In Figure 37 (d), % elongation (ductility) of heat-treated samples with an average % elongation of 12.2% increased by approximately 3% on average on each build, compared to that of as-built ones with an average % elongation of 9.17%. With powder reuse, the ductility appears to increase by about 1%. Ductility of build 12 in **Figure 37 (d)** was lower than expected ductility compared with the general trend because of possible preheat issue. As an exceptional case, in **Figure 37 (e)** and **(f)**, the ductility of as-built build 31 samples drastically decreased compared to other builds while tensile strength relatively less decreased. The average % elongation values of as-built build 31 samples were 1.5%. The ductility of heat-treated build 31 increased insignificantly about 0.6%.

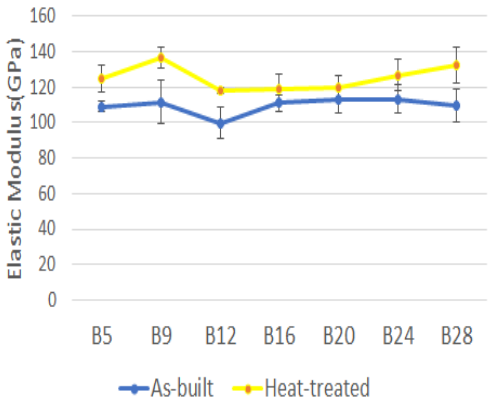

(a)

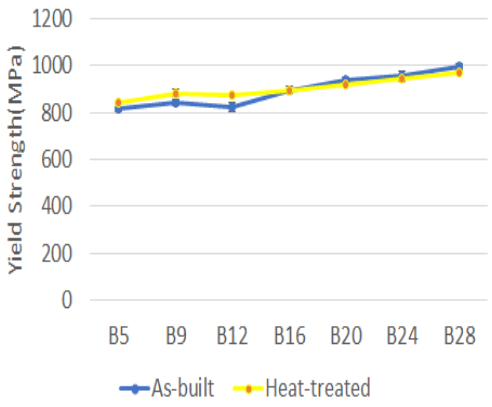

(b)

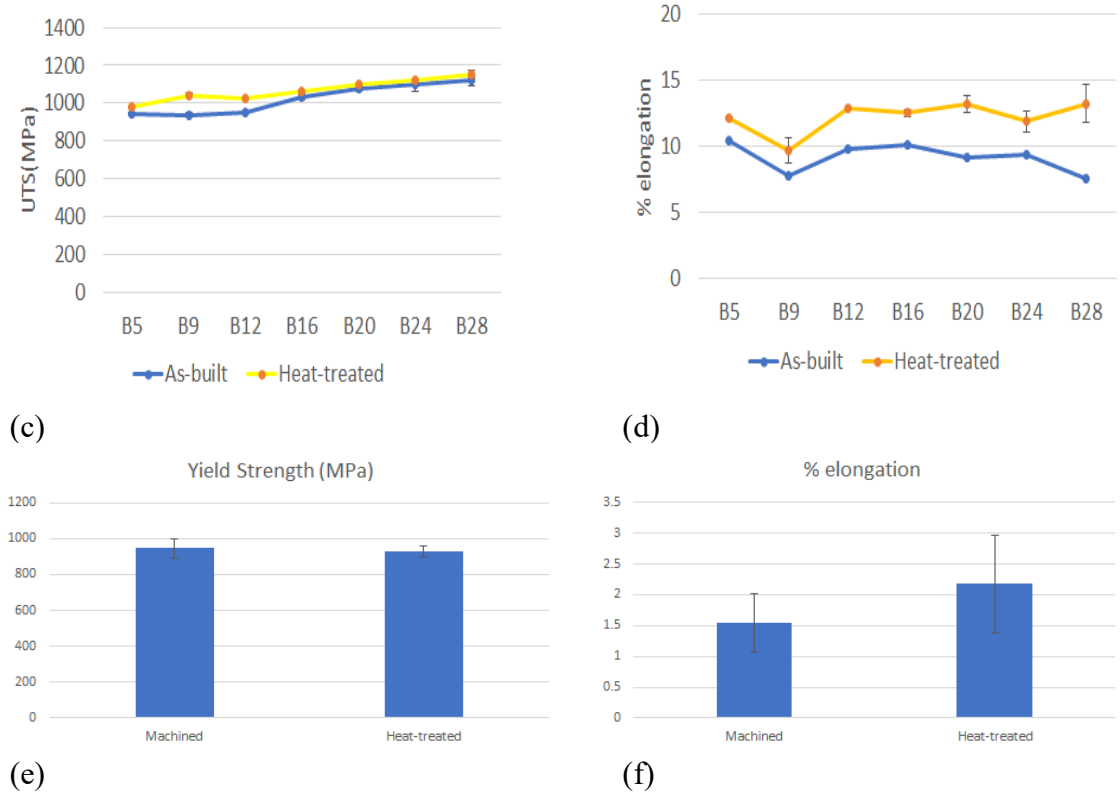

Figure 37. Comparisons between as-built (not-machined) and heat-treated vertical samples with powder reuse in terms of (a) elastic modulus , (b) yield strength, (c) ultimate tensile strength and (d) % elongation. (e) yield strength of as-built and heat-treated(950°C, 1hr)vertical build 31 and (f) % elongation of machined and heat-treated(950°C, 1hr) vertical build 31.

Table 6. Comparison of vertical as-built and heat-treated samples from build 5 to 28, except build 31 machined.

AB : as-built, HT : heat-treated with 950°C for an hour, MA : machined

Sample	**% Elongation**	**Yield Strength (MPa)**	**Ultimate Tensile Strength (MPa)**	**Elastic Modulus(GPa)**
Build 5, AB	10.4±0.6	813±7.4	942±9.5	108±3.1

Build 5, HT	12.1±0.1	839±1.8	977±1.2	124±7.9
% increase	16.3±4.4	3.10±0.7	3.7±0.9	14.6±4.5
Build 9, AB	7.8±0.4	843±13.9	938±14.6	111±11.9
Build 9, HT	9.7±1	882±13.9	1041±9.3	136±5.9
% increase	24.6±7.8	4.6	10.9±0.6	22.1±5.4
Build 12, AB	9.8±1.1	821±18.8	948±6.4	99±8.6
Build 12, HT	12.9	871±2.5	1027±5.1	118±1.5
% increase	31.4±10.7	6.1±2	8.3±0.1	18.4±7.1
Build 16, AB	10.1±0.5	895±16.6	1032±12.1	111±4.6
Build 16, HT	12.5±0.3	895±4.7	1059±12	118±8.1
% increase	23.8±1.4	-0.1±1.3	2.50	7.2±3.2
Build 20, AB	9.2±1.2	938±9.2	1074±13.8	112±7.2
Build 20, HT	13.2±0.7	916±5.5	1096±12	120±6
% increase	43.8±6.1	-2.4±0.4	2±0.2	6.7±1
Build 24, AB	9.4±0.5	955±22.3	1095±34.8	113±8.1
Build 24, HT	11.9±0.8	945±13.4	1119±11.8	126±8.8
% increase	26.7±2.8	-1.1±0.9	2.1±2.1	11.8±0.6
Build 28, AB	7.6±1.2	995±9.9	1122±27.5	109±9.5
Build 28, HT	13.2±1.4	966±5.7	1151±18.1	132±10
% increase	73.9±2.8	-2.8±0.4	2.6±0.8	20.8±0.5
Build 31, MA	1.5±0.5	945±55	964±72	108±7.3
Build 31, HT	2.2±0.8	926±29	987±51	129±6.5
% increase	41±20.3	-2±2.8	2.3±2.2	19.3±0.7

4.2.5 Trends of Horizontal specimens

Due to COVID 19, machining heat-treated horizontal samples was limited, which will be left as one of future works. The trends of horizontal samples could be expected and might be different from those of vertical samples because of build orientation that could affect the tensile properties, based on the result of the BARC paper. The elastic modulus might increase because of machining and heat treatment. With powder reuse, the modulus will not show any clear trends. Yield strength possibly will increase with powder reuse. The machining process also could increase yield strength. However, heat treatment will be able to decrease the strength, in which means the total yield strength might be able to decrease. The magnitude of the yield strength will be also different between horizontal and vertical samples. When it comes to UTS, this property will increase not only with powder reuse but with heat treatment and machining process, although the magnitude might be different. % elongation might decrease significantly with powder reuse, which the magnitude of decrease of % elongation will be higher compared to vertical samples. According to the BARC paper, % elongation decreased even though the machining process was done. Instead, the ductility of horizontal samples decreased with a slower rate compared to as-built samples. Future work will be done to observe the effect of heat treatment because heat treatment could result in higher % elongation.

Chapter 5. Discussion

The results of SEM analysis and tensile testing are discussed in the following section. Furthermore, the effect of heat treatment in terms of the mechanical properties and the microstructure is demonstrated.

5.1 SEM Analysis and Optical Microscopy

The microstructure of as-built EBM printed Ti6Al4V samples is columnar prior β grains with fine α lamellae, as seen in **Figure 7 (a)** and **8 (a)**. The fact that an α+β dual-phase exists at room temperature means the samples went through a slow solidification process since the α' (martensitic) phase resulting from fast cooling such as the SLM process from above β transus temperature was not observed.

Sub β-transus heat treatment resulted in a negligible difference of microstructures compared to as-built build 31 samples, as seen in **Figure 19**. That is because the heat treatment conditions were not much different from preheating conditions. Furthermore, these conditions cannot change as much as not only α lath coarsened enough but also prior β grain grew since the α phase limited the growth of the β grain below the β transus temperature, as shown in **Figure 22** and **24**. The result from wrought titanium also showed trivial changes in microstructure formed with equiaxed α and intergranular β phase in **Figure 29**.

For near β-transus heat treatment in **Figure 26**, based on the columnar morphology, the growth of β grain seems to be still hindered by the α phase. However, α lath thickness coarsened much more than that of sub β-transus heat treatment (about two times), as shown in **Figure 28**. The magnitude of the coarsening of α lath thickness depends on the overall cooling rate. For instance, processes with slow cooling rates such

as furnace cooling show more coarse α lamellae while other processes with relatively fast cooling rates such as air cooling or water quenching show a rather acicular α' phase. Also, the coarsening of α lath increases with increasing annealing temperature and time according to several works of literature [17,9].

In contrast to sub and near β-transus heat treatment, super β-transus heat treatment showed changed prior β grains from columnar to equiaxed structure with Widmänstatten and colony structures in **Figure 21** and **25**. Above the β transus temperature, prior β grain growth could happen massively and the α phase was able to be dissolved completely. That is the reason why the prior β grain size of the samples heat-treated above the super β-transus temperature was four times larger than that of as-built ones, as shown in **Figure 22** and **26**. However, based on the images taken, the microstructures from super β -transus heat treatment with nearly virgin (vertical DOE, build 5) and heavily used (build 28, 30, and 31) looked more alike equiaxed prior β grain containing parallel α plate formed along α_{GB} layer located at the β grain boundaries rather than a fully equiaxed β structure. The existence and size of α colonies that consist of new α lamellae in the equiaxed β grain could explain the reason why the yield strength of the samples heat-treated above the β transus temperature was the lowest among heat-treated samples [15].

The result of wrought titanium was the same as expectations according to the Metals Handbook [74], as shown in **Figure 30** and **31**. As-received wrought titanium samples were in STA condition. From an equiaxed prime α and secondary α+β lamellae to platelike α and intergranular β, the results of heat treatments showed a good validation of experiments in this study as reference.

When it comes to the correlation between the microstructure and heat treatment, according to Galarraga et al. [12] in **Figure 38**, α lath thickness could increase with annealing time and temperature, based on the equation below.

$$\delta_{\alpha_{lath}} = \delta_{\alpha_{lath}(t=0)} \cdot t^{\left(\frac{T-850}{1000}\right)}$$

δ αlath is α lath thickness in μm and δαlath(t=0) is α lath thickness of the starting material (ELI Ti6Al4V) in μm. Value t is annealing time and T is the temperature in K. All values were measured and plotted with the equation above. This plot indicates that annealing time used in this study (1 hour and 2 hours) could not affect the microstructure much compared to annealing temperature. α lath thickness affected by near-β transus heat treatment was similar to the results of super-β transus heat treatment in this study. Based on this result, the plot of super-β transus heat treatment would be similar to that of 900°C in **Figure 38**, which will be done in the future to compare the results.

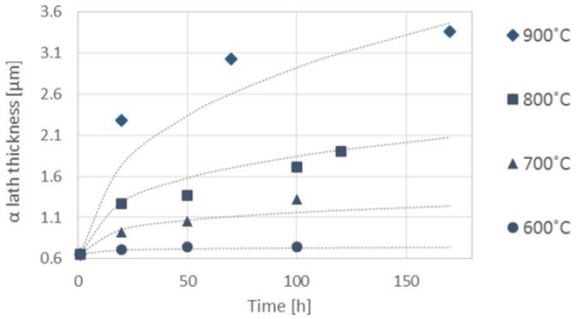

Figure 38. Plot of α lath thickness as a funcion of annealing time and temperature [17].

When it comes to the effect of powder reuse on the microstructure, oxygen content could increase with powder reuse and then affect α lath thickness since

oxygen is an α phase stabilizer. α lath thickness is affected by the overall cooling rate from β-transus temperature to the preheat temperature. When the cooling rate is lower, the thickness is getting larger. On the other hand, β grain size is affected by the cooling time from the solidus (about 1600°C) to the β-transus temperature (about 980°C, depending on the amount of oxygen content). The increase of oxygen content leads to the increase of β-transus temperature, which has more influence on α lath thickness than β grain size due to the temperature range [85]. In these experiments, prior β grain size seemed not to be affected by powder reuse while α lath thickness might increase with powder reuse if other variables such as build height and defects could be controlled, as shown in **Figure 32(a)** and **(b).** Comparisons of α lath thickness and prior β width with horizontal build 31 and vertical DOE samples were shown in **Table 7**.

Table 7. Comparison of α lath thickness and morphology on average.

HB : horizontal build 31, VT : vertical DOE samples

Sample	**α lath thickness**	**prior β grain size**	**Microstructure**
HB / as-built	1.2μm	53.5μm	columnar β / α lamellae
HB / 710°C, 2hrs	1.3μm	54.6μm	columnar β / α lamellae
HB / 950°C, 1hr	2.6μm	55.5μm	columnar β / α lamallae
HB / 1050°C, 1hr	2.6μm	292.4μm	equiaxed β / α platelet
VT / machined	1μm	84.5μm	columnar β / α lamallae
VT / 950°C, 1hr	1.9μm	85.9μm	columnar β / α lamallae
VT / 1050°C, 1hr	2μm	279.8μm	equiaxed β / α platelet

5.2 Tensile Testing

The mechanical properties that include % elongation, ultimate tensile strength, yield strength, and elastic modulus are seen in **Table 8**. The minimum values to meet the ASTM requirements [56] and the properties that Arcam company claims [66] are shown as well. As an exceptional case, vertical build 31 showed very low % elongation while other tensile properties showed similar trends compared to other samples. This result could be explained by high porosity. Although porosity also exists in other samples, the number of porosity in build 31 increased a lot and decreased % elongation.

Table 8. Comparison of mechanical properties with ASTM standards [56], heat-treated samples and values in Arcam's quote [66] The values represent an average.
H : horizontal, V : vertical, AB : as-built, HT : heat-treated, MA 1: machined(to compare the result of near β-transus heat treatment, MA 2 : machined(to compare the reulst of super β-transus heat treatment), MA : machined

	% Elongation	**Yield strength(MPa)**	**Ultimate tensile strength(MPa)**	**Elastic modulus(GPa)**
ASTM F2924	10	825	895	120
Arcam	14	950	1020	120
V DOE / **MA1**	15.2±2.1	973±8.6	1140±6.3	117±2.1
VDOE **HT,950°C,1hr**	13.3±1.6	874±21.9	1042±32.6	120±7.3
V DOE / **MA2**	10.1±3.3	995±7.8	1141±19.6	116±5.1
VDOE **HT,1050°C,1hr**	10.8±0.7	840±2	988±5.9	114±3.6
H build 31 / **AB**	10.1±0.6	1025±9	1167±2.6	100±2.3
H build 31 /	10.6±0.3	1012±5.2	1166±2	118±7

HT,710°C, 2 hrs				
H build 31 / **HT, 950°C, 1hr**	11.8±0.5	929±3.2	1110±6.6	116±8.6
H build 31 / **HT,1050°C, 1hr**	10.2±0.7	898±4.8	1060±9.5	105±4.1
V build 31 / **MA**	1.5±0.5	945±55	964±72	108±7.3
V build 31 / **HT, 950°C, 1 hr**	2.2±0.8	926±29	987±51	129±6.5

Sub β-transus heat treatment resulted in a slight increase of % elongation (about 0.5-1%) and elastic modulus and a decrease of yield and ultimate tensile strength. **In Table 8**, the tensile properties of horizontal build 31 samples with sub β-transus heat treatment met the ASTM requirement even though % elongation was below Arcam's quote. The reason why this sub β-transus heat treatment brought out insignificant mechanical improvement could be related to moderate microstructural changes. The microstructure of the samples with sub β-transus heat treatment was nearly the same as that of as-built samples, which meant columnar prior β grains still maintained as a lamellar structure even though there was a slight increase of α lath thickness. Since the build plate was preheated to about 700°C during the EBM process, similar conditions of sub β-transus heat treatment (710°C for 2 hours, furnace cooling) might not be able to cause significant impact to the microstructure and properties.

Compared to the result of sub β-transus heat treatment, near β-transus heat treatment showed higher elongation approximately 1-2%. The extent of the decrease of tensile strength was higher than the result of sub β-transus heat treatment while elastic

modulus rather increased or did not change much. This could be attributed to the changes in the microstructure that affected the properties. Near β-transus heat treatment coarsened the α lath with columnar prior β grains remained. The increase of α lath thickness could increase the ductility and decrease the tensile strength. However, vertical DOE samples showed an exception. The average % elongation of heat-treated samples near β transus decreased compared to that of machined samples even though yield strength and ultimate tensile strength decreased. This result might be attributed to 1) temperature profile inside the tube furnace due to locations that the samples were put in **Figure 15 (d) and (e)**, 2) possible oxygen embrittlement through the thickness of the material and 3) a lack of the number of specimens to get clear trends. In **Figure 15 (d) and (3)**, horizontal build 31 and vertical DOE sample underwent temperature profile inside the tube furnace because the locations of the samples were different while vertical heat-treated samples from build 5, 9, 12, 16, 20, 24, and 28 were put on the same location in the tube. Oxygen embrittlement might not happen because of heat treatment and machining process. However, further measurement of oxygen amount through the thickness of the samples could be done just in case in the future. % elongation of six machined samples used in this study was high (15.2% and 10.1%) in general compared to horizontal and other vertical heat-treated samples whereas % elongation of machined samples chosen for heat treatments could be relatively low among machined vertical DOE samples.

When it comes to the relationship between the microstructure and mechanical properties of AM Ti6Al4V, Lütjering et al. [75] reported that α lamellae size affects the effective slip length that has a huge influence on the yield strength. Syed et al. [51] also demonstrated that the properties were primarily influenced by α lath thickness

determining the effective slip length.

Several works of literature covered the relationship called the Hall-Petch relation between α lath thickness and strength following the equation below [18, 48].

$$\sigma_y = \sigma_0 + \frac{k_y}{\sqrt{d}}$$

σy is the yield stress and σ0 is the starting stress for dislocation movement depending on the material. The value 'ky' is the strengthening coefficient that is a constant specific to each material. 'd' value is the average thickness that could be a grain diameter or lamellae thickness, meaning that 'd' value in this study is α lath thickness. The result of this study followed the relationship. In **Table 7 (Section 5.1)**, near β-transus heat treatment led to the coarsening of α lath thickness twice as much compared to sub β-transus heat treatment that only showed a slight increase of the thickness while yield strength and ultimate tensile strength decreased both.

Several works of literature found that the decrease of cooling rates results in the increase of the α lath thickness and decrease of yield strength, ultimate tensile strength, and microhardness [75,76,77], which makes sense because furnace cooling used in this study has the slowest cooling rates among other methods including air cooling or quenching.

Also, build orientation could be one of the factors which affect the properties. Hayes et al. [79] showed that not only tensile strength but also ductility could depend on the build direction. In this study, the result of near β-transus heat treatment with vertical and horizontal build 31 samples showed a significant difference in terms of % elongation in particular in **Table 8**. Vertical build 31 specimens showed relatively much low ductility values compared to horizontal samples. A possible explanation could be

too much porosity which is one of the crucial factors to affect the properties and lack of fusion voids from vertical specimens compared to horizontal samples. Also, the amount of oxygen content in the powder might explain the too low ductility since the powder was used over 31 times.

Contrary to the result of near β-transus heat treatment, super β-transus heat treatment showed different phenomena. All tensile properties were lower than the result of near β-transus heat treatment. In particular, % elongation of both nearly virgin and heavily used powder samples was nearly the same as that of as-built samples. Furthermore, the result of wrought titanium showed the same trend as that of nearly virgin powder and heavily used powder samples; tensile strength decreased with increasing temperature and ductility of super β-transus heat treatment was the lowest value even though tensile strength was also the lowest among the samples.

As the columnar structure was changed to a uniform equiaxed structure with α-β morphology showing Widmänstatten and colony structures, mechanical properties could have been changed differently, compared to sub and near β-transus heat treatment. Ductility of metals normally increases with decreasing the strength. In this study, however, super β-transus heat treatment led to decrease of both properties. The purposes of the heat treatments in this study were improving the ductility, relieving internal residual stresses and getting particular microstructures. The effect of heat treatments in this study might not be as much effective as the HIP process because heat treatments could not close internal pores which affect the properties significantly. Formanior et al. stated that [15] super β-transus heat treatment with furnace cooling resulted in the formation of new α lamellae clustered in large colonies within equiaxed prior β grains transformed from columnar structure, instead of coarsening of α lath thickness.

However, this result did not cause significant improvement of tensile properties, which was similar to the result in this study.

Galarraga et al. [17] studied the influence of α lath thickness on the tensile strength and the effect of the α lath thickness on the ductility in terms of cooling rates and fracture mode. Compared to the linear correlation showing the decrease of strength with the increase of α lath thickness, the refinement of the columnar structure increased the ductility until a certain maximum peak and then decreased drastically depending on cooling rates in **Figure 39 (a)** and **(b)** [86], which means the lowest cooling rate does not result in the highest % elongation. The average cooling rate was measured experimentally in this study and was about 3-5°C/min. Based on **Figure 39 (b)**, increasing cooling rates could result in higher % elongation until a certain peak, which will be studied more in detail in future work. Also, plotting the cooling rate curve during the whole process should be necessary for the future, as shown in **Appendix C**. By comparing tensile elongation between 100μm and 600μm in the lameallar structure of Ti6Al4V, it can be concluded that reducing prior β grain could improve the ductility. Also, this result could be due to the fracture mode changing from transcrystalline to intercrystalline [75], as shown in **Figure 40**. Galarraga et al. [17] only covered transcrystalline fracture mode occurring at the α_{GB} layer in the paper, showing an empirical relation that ductility decreases with increasing α lath thickness. According to the book Titanium [86], intercrystalline dimple type of fracture takes place along the continuous α_{GB} layer in the β grains. The influence of the α_{GB} layer on % elongation has to do with the preferential deformation and following crack initiation among these layers. Furthermore, how much the ductility decreases predominantly depends on not only the strength difference between α_{GB} layers and equiaxed β grains but also the β

grain size. According to the result of the book, reducing β grain size led to an improvement of tensile properties including ductility, based on the low tensile ductility from a fine lamellar structure with intercrystalline fracture mode and relatively high tensile ductility from a coarse lamellar structure with transcrystalline fracture mode.

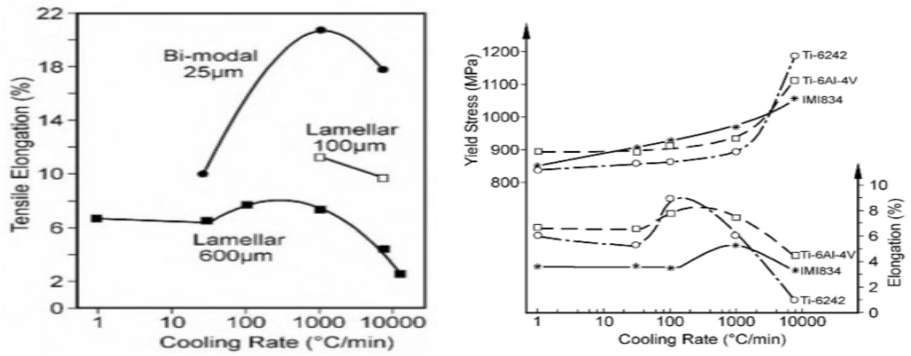

(a) (b)

Figure 39. (a) Tensile elongation of Ti6Al4V with β grain size as a function of cooling rate [86] and (b) yield stress and % elongation as a function of cooling rate [86].

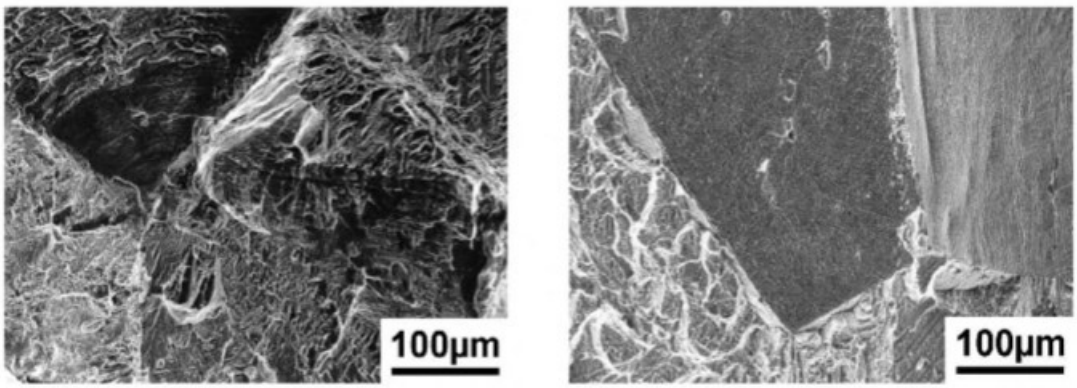

(a) (b)

Figure 40. Fracture modes of lamellar Ti6Al4V (a) a ductile transcrystalline and (b) intercrystalline mode [86].

This fact could explain why the ductility of the samples above the super β-

transus heat treatment in this study decreased even though tensile strength also decreased. Since the size of equiaxed prior β grains got bigger than that of columnar β grains, intercrystalline fracture might happen at α_{GB} layers leading to crack initiation and then a decrease of ductility even though heat treatment was done with a low cooling rate (furnace cooled).

5.3 Powder reuse and heat treatment

The main effect of the powder reuse on the microstructure and tensile properties would be an increase of oxygen amount, which leads to an increase of β-transus temperature. When it comes to the microstructure, increasing β-transus does not affect α lath or β grain size clearly because there are other variables such as build height and internal defects, as seen in **Figure 32(a)** and **(b)**. However, tensile properties could be affected significantly. According to the BARC paper in **Figure 41**, the elastic modulus, yield strength, and ultimate tensile strength increased with powder reuse while % elongation decreased with the powder reuse. The machining process restored % elongation values based on the result of the paper. Compared to the results of the BARC paper, the result of samples machined and heat-treated near β-transus showed different phenomena, as shown in **Figure 37**. Elastic modulus did not indicate any clear trends, but heat treatment with the machining process increased the elastic modulus of all samples. Ultimate tensile strength increased with heat treatment and machining while some results of yield strength rather decreased. This is because near β-transus heat treatment improved % elongation to some extent at the expense of yield strength. Powder reuse resulted in a decrease in the ductility of as-built specimens. The machining process was proved to restore decreased the ductility of the specimens in

BARC paper. Compared to % elongation of machined but non-heat-treated samples, machined and heat-treated samples showed an average 1.2% higher ductility. Based on this result, the machining and heat treatment as post processing are essential for Ti6Al4V components to obtain enough good properties for the applications.

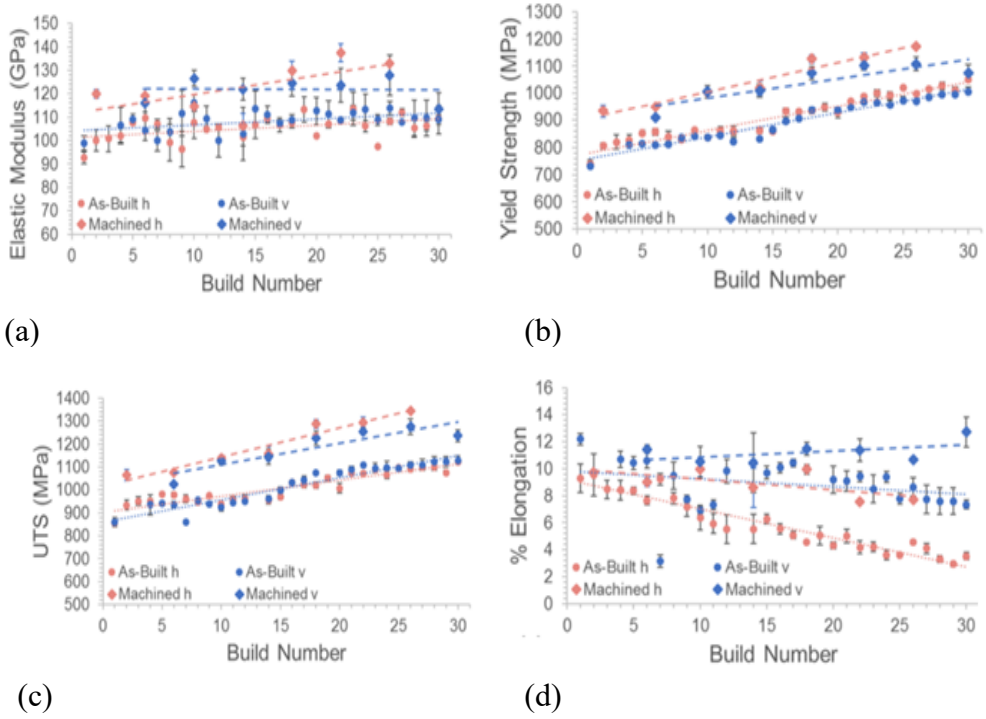

Figure 41. Plots of tensile properties over 30 builds with powder reuse. (a) The elastic modulus, (b) Yield strength, (c) ultimate tensile strength and (d) % elongation. Source from BARC paper that Prof. Ramulu and Arola reported in 2019.

5.4 Applications and reliability of the results

To consider the reliability of the results in these experiments, the coefficient of variation (COV) of all data was measured on average in **Appendix H**, **I**, **J**, and **K**. COV values are used to compare the variation of distributions. It can be measured by dividing the standard deviation by the mean. Large values mean low reliability since the

distribution is wide. **Figure 42** and **43** presents the plot of the COV of the microstructure. Horizontal build 31 samples heat-treated above β-transus showed the largest value in terms of prior β grain width while vertical DOE samples heat-treated near β-transus resulted in the largest COV of α lath thickness. Based on this result, further study is needed to standardize the way to measure the average prior β grain size for consistency. Furthermore, vertical DOE samples showed large COV values of α lath thickness, which might be attributed to various factors such as dimension differences.

In the case of tensile properties, the COV values of all properties generally decreased, as shown in **Figure 44 and 46**. % elongation showed large COV values in general compared to other tensile properties. This result indicates that mechanisms of ductility are complicated because the ductility is relatively affected more than other properties by various factors such as α lath thickness, prior β grain size, cooling rates, dimensions of specimens, internal defects with powder reuse, and post-processing. The COV plots of vertical DOE samples in **Figure 45** showed different trends from horizontal build 31 and vertical samples. Super β-transus heat treatment showed lower COV values compared to near β-transus heat treatment. Also, near β-transus heat treatment increased the COV values of the tensile properties except those of % elongation. That also could explain three factors: 1) temperature profile, 2) possible oxygen embrittlement, and 3) a lack of the number of specimens to get clear trends. However, further analysis should be done to find the exact factors that affect COV values.

Other than that, heat treatment resulted in a decrease of COV values compared to as-built COV values in terms of the ductility, which further study should be necessary because this could mean heat treatment can improve the reliability of the material.

Developing additive manufacturing techniques and optimization of post processings results in better mechanical performances of additively manufactured metals for the replacement of spare parts such as equipment, which eventually leads to an improvement of the reliability of the equipment. However, more in-depth and further studies must be done for practical industrialization. Not only the EBM process but also other PBF processes such as SLM or DED process could be studied to get better mechanical performances and improved reliability of materials. In the case of the DED process, for instance, Ti6Al4V showed similar or better mechanical performances with the machining process and heat treatment [8]. If heat treatment conditions and machining process used in this study could be optimized through further studies, applying these post processings to DED or SLM process might be possible.

The COV plots of all properties except some exceptions generally seem to increase with powder use in **Figure 47.** However, further analysis is needed to clarify the trends and find variables that affect the COV with powder reuse. The COV values of the properties with powder reuse were shown in **Appendix K**.

(a) (b)

Figure 42. Plots of Coefficient of variation (COV) of the microstructure of horizontal build 31. COV of (a) α lath thickness, and (b) prior β grain size.

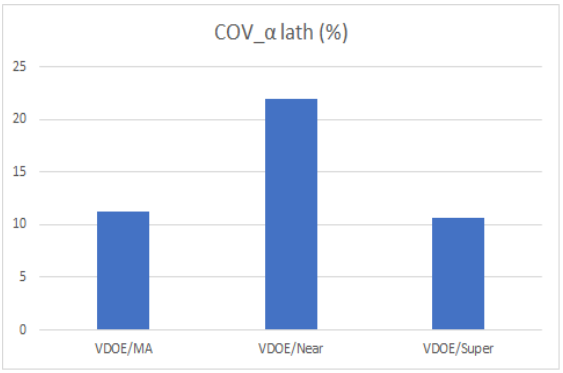

(a)

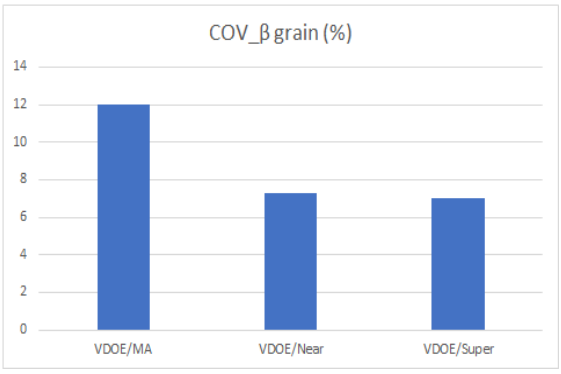

(b)

Figure 43. Plots of Coefficient of variation (COV) of the microstructure of vertical DOE samples. (a) COV of α lath thickness, and (b) COV of prior β grain size.

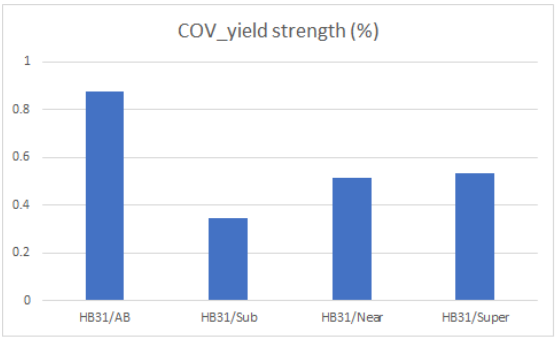

(a)

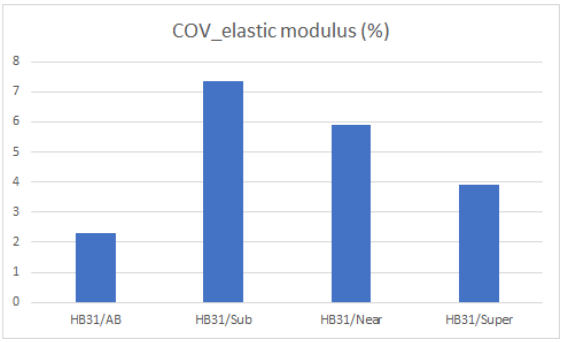

(b)

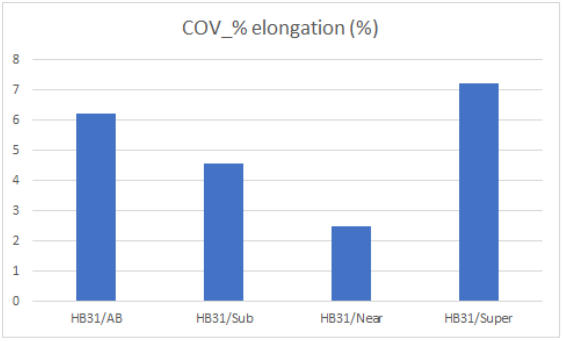

(c)

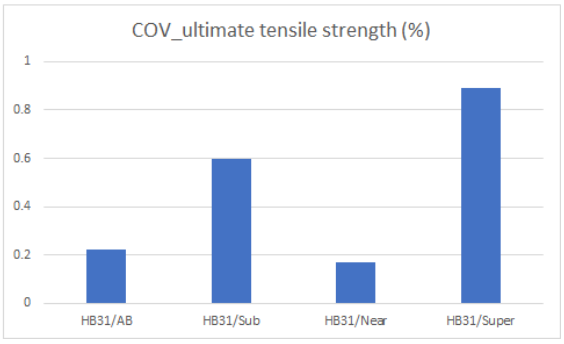

(d)

Figure 44. Plots of Coefficient of variation (COV) of the tensile properties of horizontal build 31. COV of (a) yield strength, (b) elastic modulus, (c) % elongation, and (d) ultimate tensile strength.

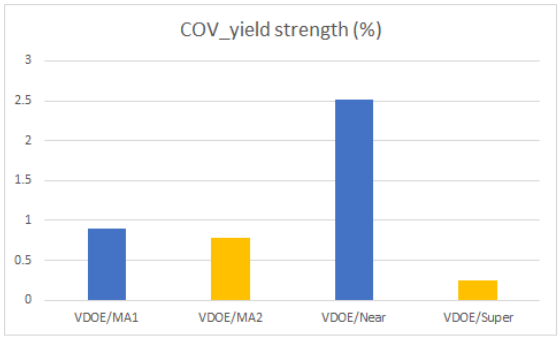

(a)

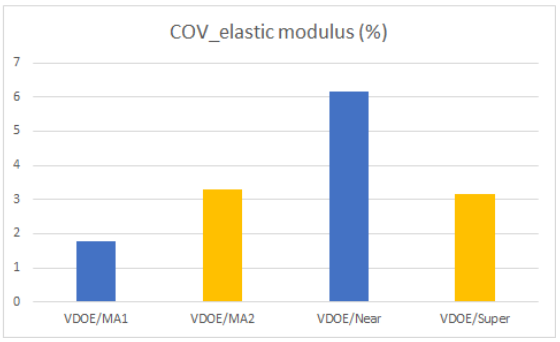

(b)

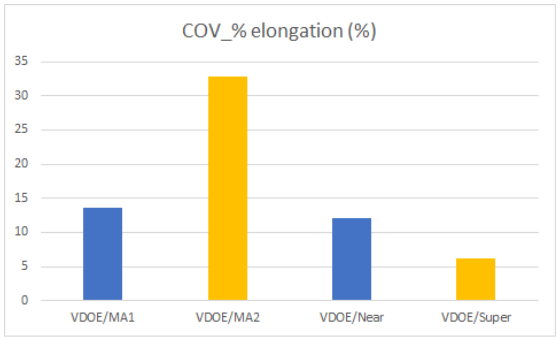

(c)

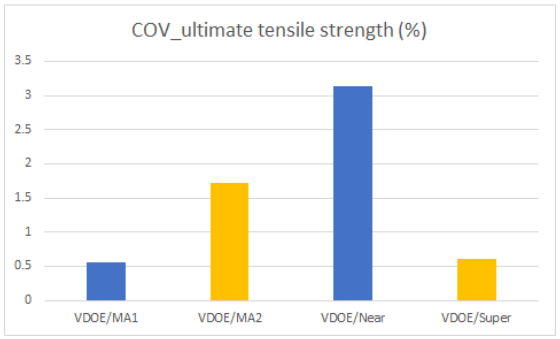

(d)

Figure 45. Plots of Coefficient of variation (COV) of the tensile properties of vertical DOE samples. COV of (a) yield strength, (b) elastic modulus, (c) % elongation, and (d) ultimate tensile strength.

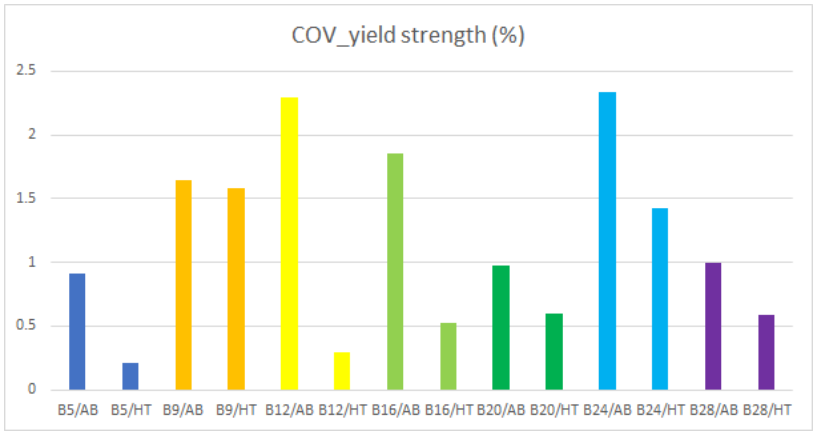

(a)

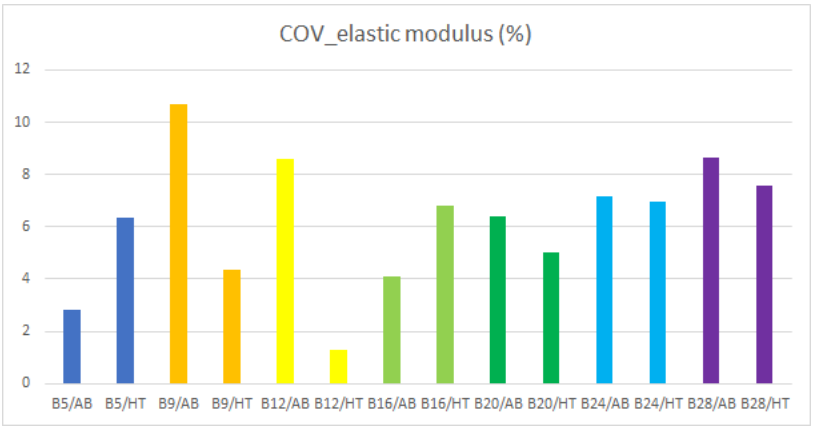

(b)

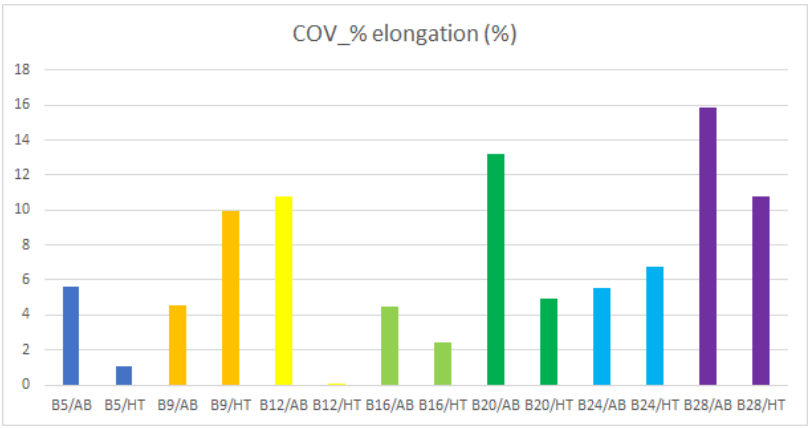

(c)

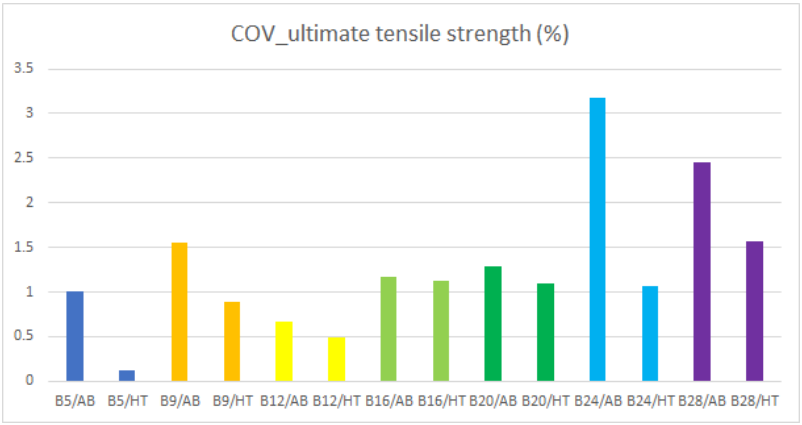

(d)

Figure 46. Plots of Coefficient of variation (COV) of the tensile properties of vertical samples. COV of (a) yield strength, (b) elastic modulus, (c) % elongation, and (d) ultimate tensile strength.

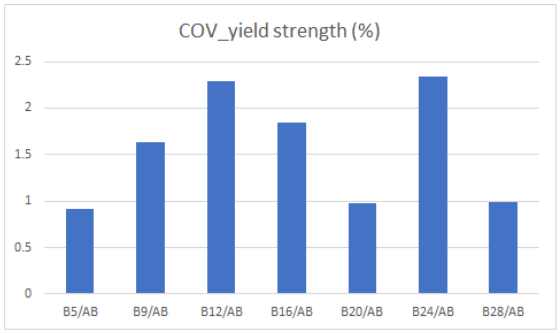

(a)

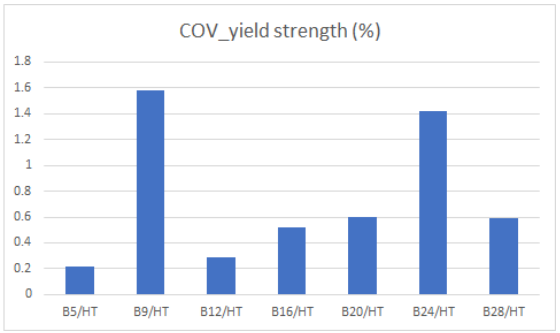

(b)

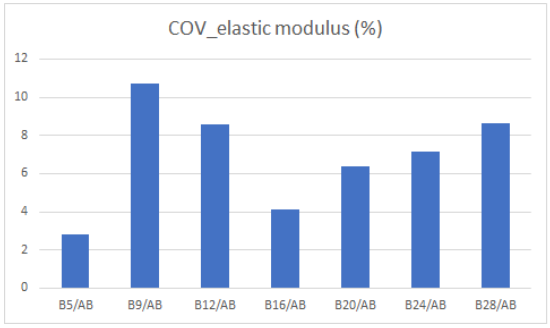

(c)

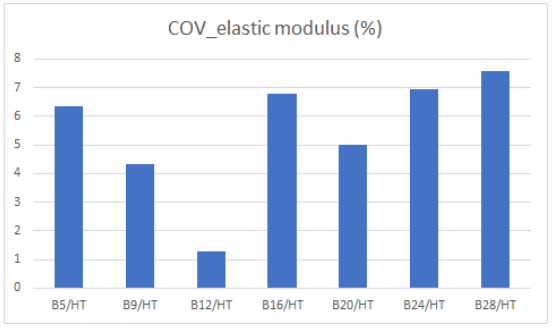

(d)

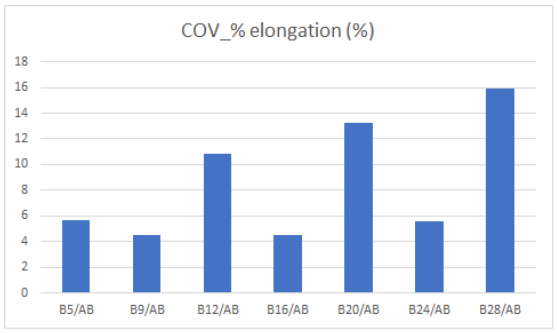

(e)

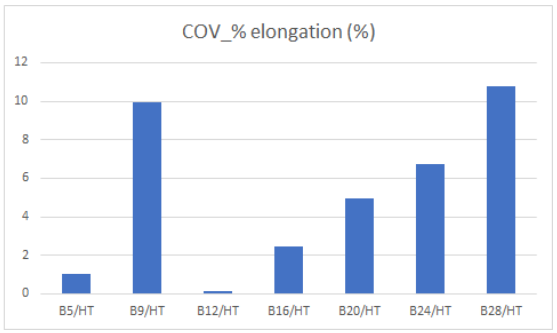

(f)

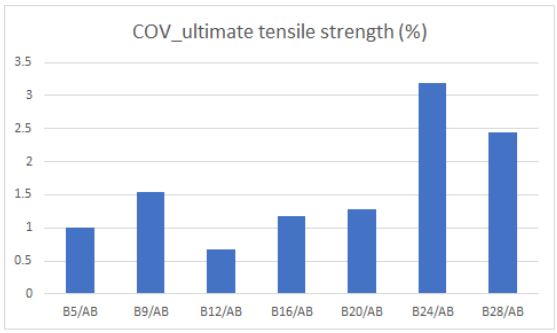

(g)

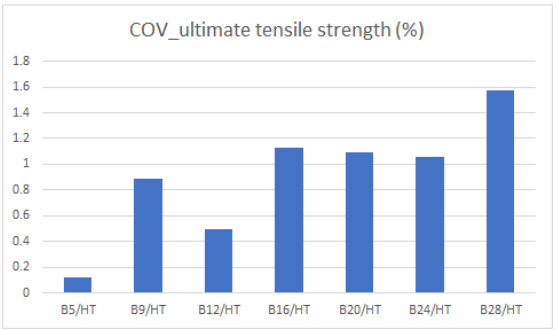

(h)

Figure 47. Plots of Coefficient of variation (COV) of the tensile properties of vertical samples with powder reuse. COV of (a) the yield strength of as-built vertical samples,

(b) the yield strength of heat-treated vertical samples, (c) the elastic modulus of as-built vertical samples, (d) the elastic modulus of heat-treated vertical samples, (e) % elongation of as-built vertical samples, (f) % elongation of heat-treated vertical samples, (g) the ultimate tensile strength of as-built vertical samples, and (h) the ultimate tensile strength of heat-treated vertical samples.

Chapter 6. Conclusions and Future Work

6.1 Conclusions

In this study, the microstructure and tensile properties of EBM printed as-built and heat-treated Ti6Al4V components based on the β-transus temperature (~1000°C) were characterized over 31 consecutive builds with conclusions below:

● post-process heat treatments under sub β-transus temperature (710°C, 2 hours) barely increased % elongation and decreased tensile strength enough. This could be attributed to existent α lamellae including the α_{GB} layer that inhibited the growth of the columnar β phase. Also, since heat treatment conditions were not much different from the preheating process, the effect of this sub β-transus heat treatment to improve the mechanical properties was negligible. α lath thickness slightly increased, compared to as-built samples.

● Near β-transus heat treatment (950°C, 1 hour) showed an increase of ductility 3% on average while the other two heat treatments did not even result in significant improvement, which could be the best option for refinement in tensile properties at the expense of the strength. α lath thickness of the samples heat-treated near β transus temperature increased as twice as much as that of as-built samples. Columnar prior β grains remained even though there were quite a few coarsening of α lath structure with large α precipitate.

● Super β-transus heat treatment changed the microstructure from columnar prior β grains with α lamellae to equiaxed prior β grains with α platelets. % elongation decreased even though tensile strength decreased as well, which were different from the results of the other two heat treatments. This might be related to an intercrystalline fracture occurring along the continuous α_{GB} layer in the equiaxed prior β grains because

the effect of the layers on the ductility caused preferential deformation and crack initiation from the strength difference between the layers and the grains. Furthermore, the large size of equiaxed β grains could be the reason why ductility decreased.

● For the microstructural analysis related to tensile properties, the increase of α lath thickness caused an increase of ductility at the expense of the strength under the beta transus temperature. However, this Hall-Petch relationship could not be applied above the β-transus temperature, based on the fact that % elongation and tensile strength decreased at the same time.

● Powder reuse decreased % elongation due to an increase in oxygen amount. The machining process and heat treatment could improve the ductility by an average of 3% at the expense of yield strength. However, heat treatment as post-processing worked slightly to heavily used powder samples because of internal defects, which meant just normal annealing process with machining was not likely to counteract some effects of oxidation and affect significantly improved ductility. Therefore, the ductility of heavily used powder appears not to be improved enough to meet the ASTM requirement.

● Heat treatment and machining process could improve the reliability of Ti6Al4V components. Additional experiments should be needed to verify.

6.2 Future Work

1) Further analysis such as a fractography test is needed to determine the effect of two kinds of fracture modes on the ductility more in detail.

2) Other heat treatments with powder reuse will be performed to improve tensile properties enough.

3) A more in-depth investigation of the microstructure and mechanical properties below should be done.

- plotting α lath thickness as a function of annealing time and temperature (super β transus temperature in particular) with the equation
- plotting cooling rate curves during the whole process
- finding an optimized cooling rate to get the highest % elongation
- defining the correlation between heat treatment and reliability more in detail
- Heat treatment of metals printed by different techniques such as DED or SLM and finding the effect of the heat treatment on the microstructure and properties

Appendices

A. Arcam A2X Printer and Powder Recovery System


* processing parameters used in this study

Parameters	Values
Beam Speed	4530 nm/s
Speed Function	45
Beam Current	15 mA
Max Current	20 mA
Speed Factor	1.5 mm
Thickness Factor	0 mm
Line Offset	0.2 mm
Line Order	1
Snake	True
Randomized Hatch	False
Hatch Depth	0.05 mm
Focus Offset	25 mA

B. Powder Certification

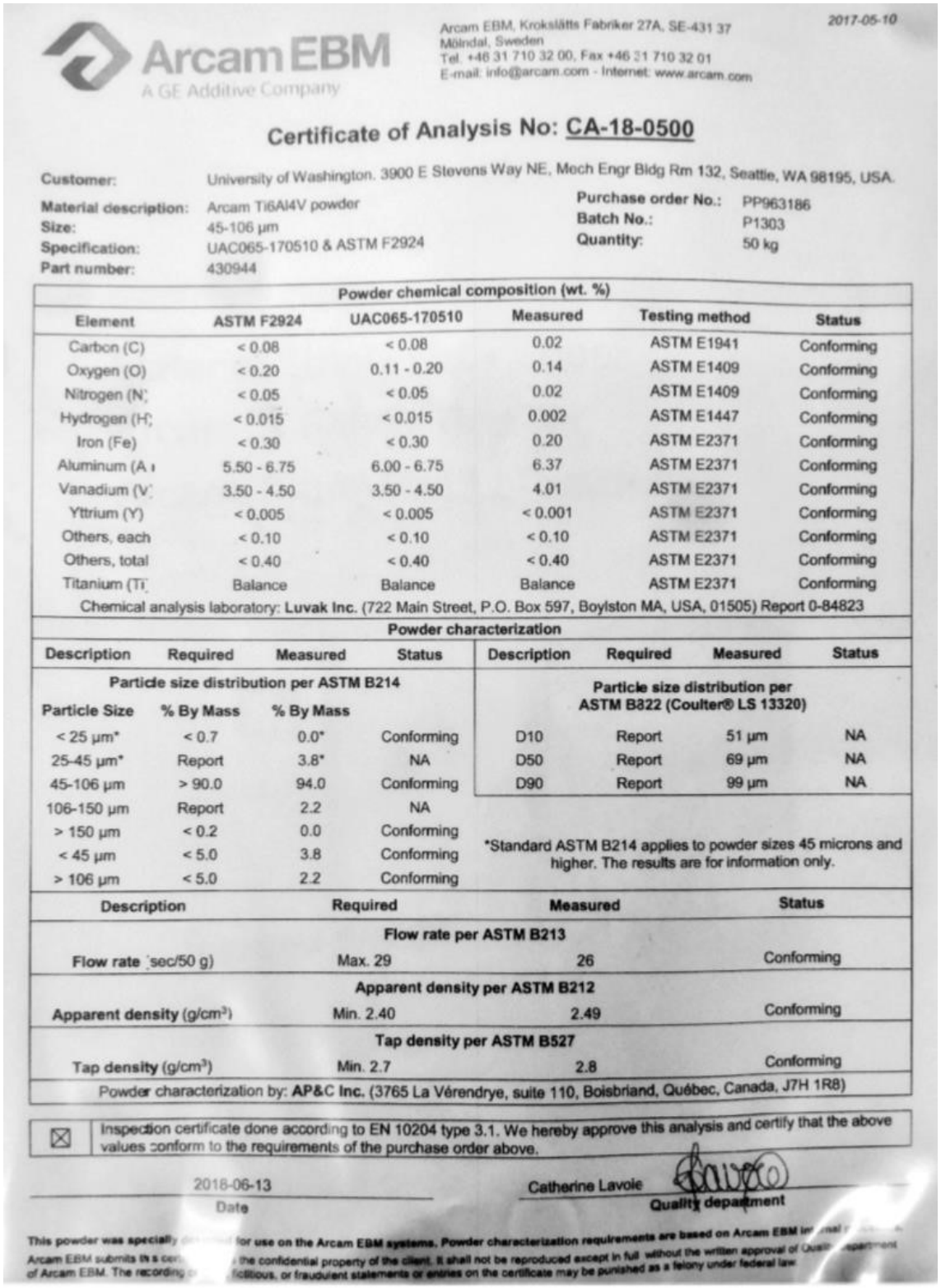

Arcam EBM
A GE Additive Company

Arcam EBM, Krokslätts Fabriker 27A, SE-431 37
Mölndal, Sweden
Tel. +46 31 710 32 00, Fax +46 31 710 32 01
E-mail: info@arcam.com - Internet: www.arcam.com

2017-05-10

Certificate of Analysis No: CA-18-0500

Customer: University of Washington. 3900 E Stevens Way NE, Mech Engr Bldg Rm 132, Seattle, WA 98195, USA.

Material description: Arcam Ti6Al4V powder
Size: 45-106 µm
Specification: UAC065-170510 & ASTM F2924
Part number: 430944

Purchase order No.: PP963186
Batch No.: P1303
Quantity: 50 kg

Powder chemical composition (wt. %)

Element	ASTM F2924	UAC065-170510	Measured	Testing method	Status
Carbon (C)	< 0.08	< 0.08	0.02	ASTM E1941	Conforming
Oxygen (O)	< 0.20	0.11 - 0.20	0.14	ASTM E1409	Conforming
Nitrogen (N)	< 0.05	< 0.05	0.02	ASTM E1409	Conforming
Hydrogen (H)	< 0.015	< 0.015	0.002	ASTM E1447	Conforming
Iron (Fe)	< 0.30	< 0.30	0.20	ASTM E2371	Conforming
Aluminum (Al)	5.50 - 6.75	6.00 - 6.75	6.37	ASTM E2371	Conforming
Vanadium (V)	3.50 - 4.50	3.50 - 4.50	4.01	ASTM E2371	Conforming
Yttrium (Y)	< 0.005	< 0.005	< 0.001	ASTM E2371	Conforming
Others, each	< 0.10	< 0.10	< 0.10	ASTM E2371	Conforming
Others, total	< 0.40	< 0.40	< 0.40	ASTM E2371	Conforming
Titanium (Ti)	Balance	Balance	Balance	ASTM E2371	Conforming

Chemical analysis laboratory: **Luvak Inc.** (722 Main Street, P.O. Box 597, Boylston MA, USA, 01505) Report 0-84823

Powder characterization

Particle size distribution per ASTM B214

Particle Size	% By Mass	% By Mass	Status
< 25 µm*	< 0.7	0.0*	Conforming
25-45 µm*	Report	3.8*	NA
45-106 µm	> 90.0	94.0	Conforming
106-150 µm	Report	2.2	NA
> 150 µm	< 0.2	0.0	Conforming
< 45 µm	< 5.0	3.8	Conforming
> 106 µm	< 5.0	2.2	Conforming

Particle size distribution per ASTM B822 (Coulter® LS 13320)

Description	Required	Measured	Status
D10	Report	51 µm	NA
D50	Report	69 µm	NA
D90	Report	99 µm	NA

*Standard ASTM B214 applies to powder sizes 45 microns and higher. The results are for information only.

Description	Required	Measured	Status
Flow rate per ASTM B213			
Flow rate (sec/50 g)	Max. 29	26	Conforming
Apparent density per ASTM B212			
Apparent density (g/cm³)	Min. 2.40	2.49	Conforming
Tap density per ASTM B527			
Tap density (g/cm³)	Min. 2.7	2.8	Conforming

Powder characterization by: **AP&C Inc.** (3765 La Vérendrye, suite 110, Boisbriand, Québec, Canada, J7H 1R8)

☒ Inspection certificate done according to EN 10204 type 3.1. We hereby approve this analysis and certify that the above values conform to the requirements of the purchase order above.

2018-06-13
Date

Catherine Lavoie
Quality department

This powder was specially [illegible] for use on the Arcam EBM systems. Powder characterization requirements are based on Arcam EBM [illegible]
Arcam EBM submits this [illegible] the confidential property of the client. It shall not be reproduced except in full without the written approval of [illegible]
of Arcam EBM. The recording [illegible] fictitious, or fraudulent statements or entries on the certificate may be punished as a felony under federal law.

C. Furnace specification

1100°C Mini-Mite™ Split-Hinge, Single Zone, Integrated Controller, Temperature Range 100 to 1100°C

Furnace Model No.	Electrical Volts, Hz, 1Ø	Watts	Integral Controller	Exterior Dimensions H x F-B x W in" (mm)	*Process Tube Diameter, in" (mm)	Heated Length in" (mm)	Ship Weight lbs (kg)
Digital, Single Segment Control, 1100°C							
TF55030A	120V, 50/60 Hz	800	1 Segment	15" (381) x 11" (279.4) x 16" (406.4)	1" (25.4)	12" (304.8)	35 (16)
Digital, Multi Segment Programmable, 1100°C							
TF55035A	120V, 50/60 Hz	800	16 Segment	15" (381) x 11" (279.4) x 16" (406.4)	1" (25.4)	12" (304.8)	35 (16)

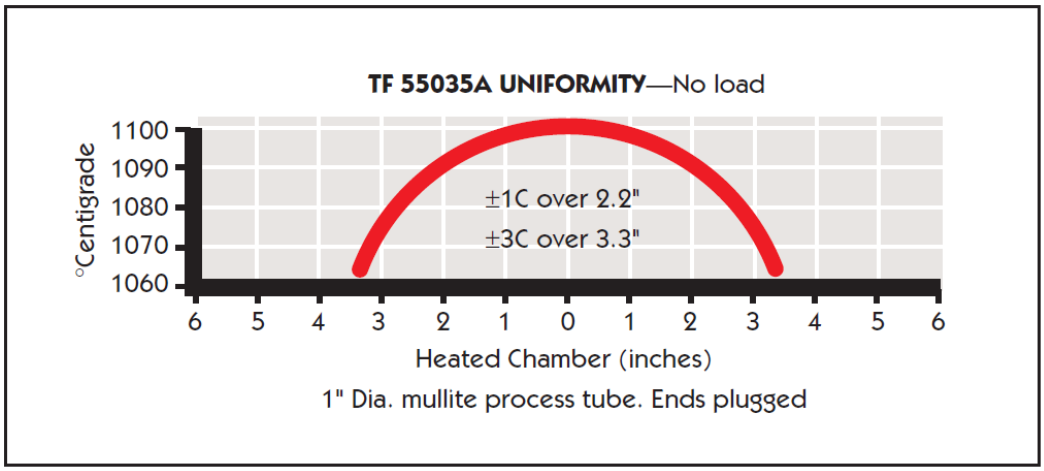

Model TF55035A Uniformity Profile, No Load

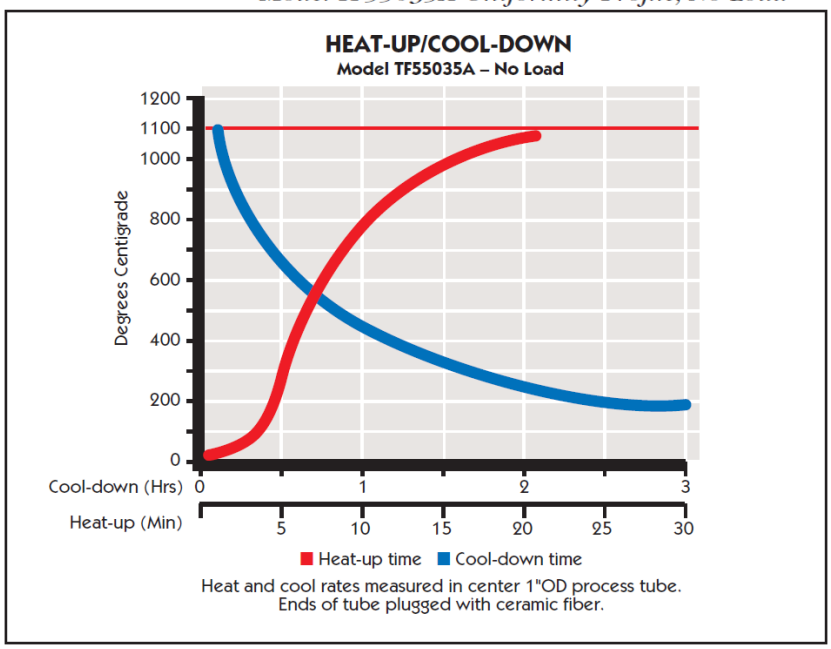

Model TF55035A Heat-Up/Cool-Down

D. Tensile Testing Equipment

Instron 5585H load frame with 50kN load cell, 30kN wedge grips and clip on extensometer.

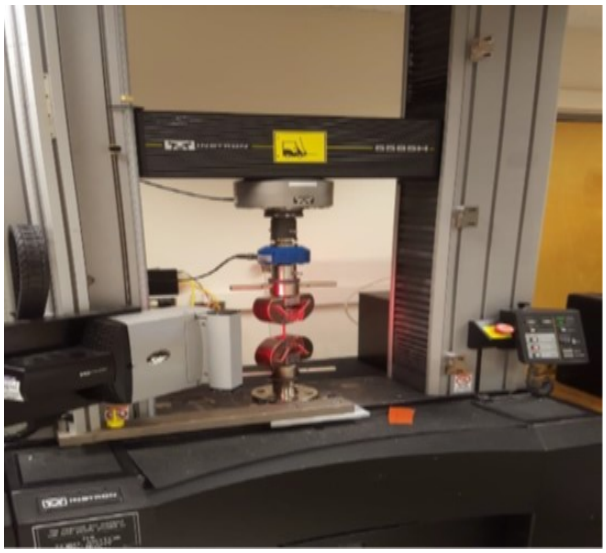

E. Powder Chemistry

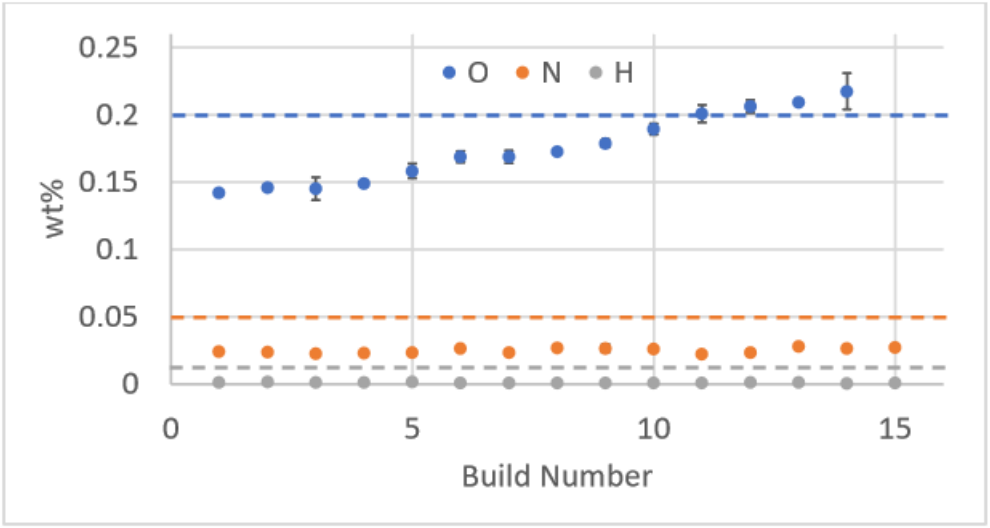

O, N and H content obtained by Sean Ghods using inert gas fusion courtesy of Boeing Everett

F. Tensile properties of horizontal build 31, vertical DOE and vertical heat-treated (at 950°C for an hour) samples from build 5 to 28. 3 specimens per build were used.

* The data of 12-1 sample were skipped due to system errors during the testing.

HB : Horizontal Build 31 samples // AB : As-Built // VDOE : Vertical Design Of Experiments samples

SB : Sub beta transus temperature heat treatment // NB : Near beta transus temperature heat treatment

SSB : Super beta transus temperature heat treatment // MA : Machined vertical DOE samples for comparisons of the results from near beta transus heat treatment // MA2 : Machined vertical DOE samples for comparisons of the results from super beta transus heat treatment.

Specimens	Elastic Modulus(GPa)	Yield Strength(MPa)	Ultimate Tensile Strength(MPa)	% elongation
HB-AB_1	98	1012	1165	11
HB-AB_2	103	1031	1166	9.5
HB-AB_3	99	1032	1171	9.9
HB-SB_1	124	1007	1164	10.5
HB-SB_2	109	1019	1169	10.9
HB-SB_3	122	1009	1166	10.3
HB-NB_1	105	929	1107	11.4
HB-NB_2	126	932	1119	12.5
HB-NB_3	119	925	1103	11.4
HB-SSB_1	100	898	1052	9.1
HB-SSB_2	108	892	1054	10.7
HB-SSB_3	109	904	1073	10.6
VDOE-MA_1	119	967	1137	15.7
VDOE-MA_2	115	969	1135	17
VDOE-MA_3	116	983	1147	13
VDOE-NB_1	122	890	1066	15.1
VDOE-NB_2	109	843	996	11.3
VDOE-NB_3	127	890	1065	13.6
VDOE-MA2_1	113	991	1161	13.9
VDOE-MA2_2	115	989	1122	7.8
VDOE-MA2_3	121	1004	1140	8.6
VDOE_SSB_1	113	838	980	11.5
VDOE_SSB_2	110	842	991	11
VDOE_SSB_3	119	838	993	9.9
5-1	119	840	978	12
5-2	121	837	976	12.2
5-3	134	840	977	12
9-1	131	898	1036	6.8
9-2	136	873	1036	9.5
9-3	142	876	1052	12.7
12-2	117	870	1024	13
12-3	119	873	1031	12.9
16-1	117	900	1073	12.7
16-2	111	893	1052	12.2
16-3	127	892	1052	12.8
20-1	127	919	1110	13.9
20-2	116	910	1091	12.8
20-3	118	919	1089	12.8
24-1	131	948	1115	11

24-2	133	931	1110	12.6
24-3	116	957	1133	12
28-1	129	972	1147	12.9
28-2	144	961	1137	12
28-3	125	968	1172	14.8

G. Stress-strain curves of horizontal build 31, vertical DOE and vertical heat-treated samples

※ Horizontal build 31

* As-built_1

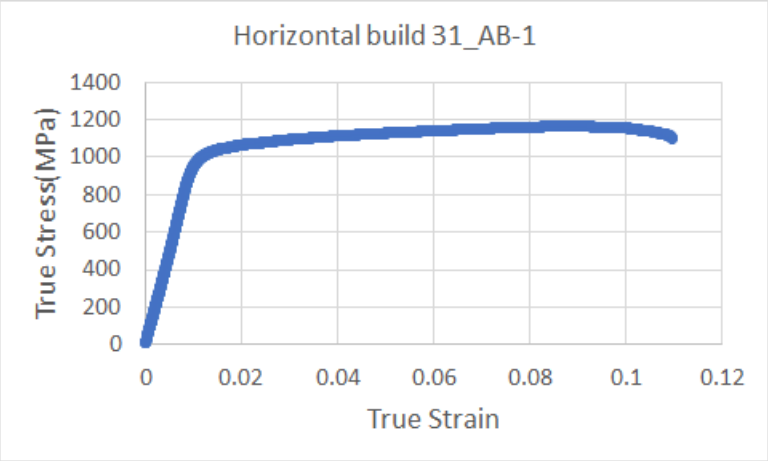

* As-built_2

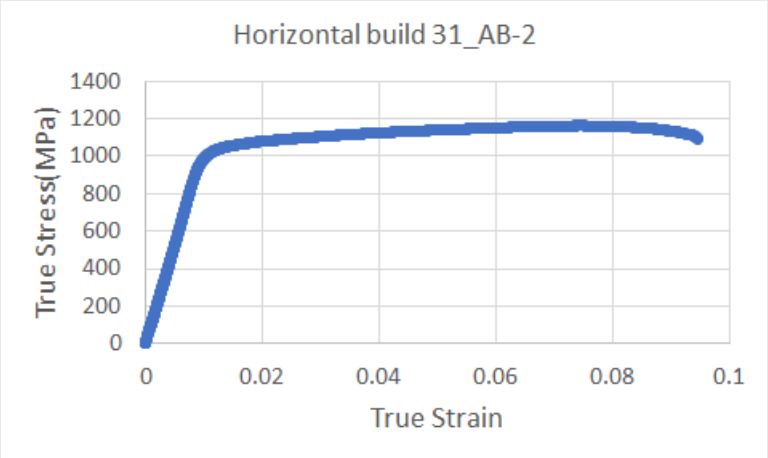

* As-built_3

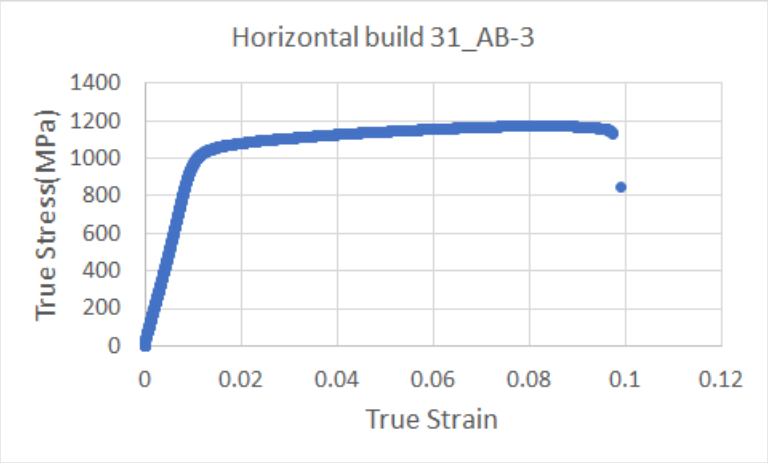

* Sub β-transus heat treatment (710°C, 2 hours)_Sample 1

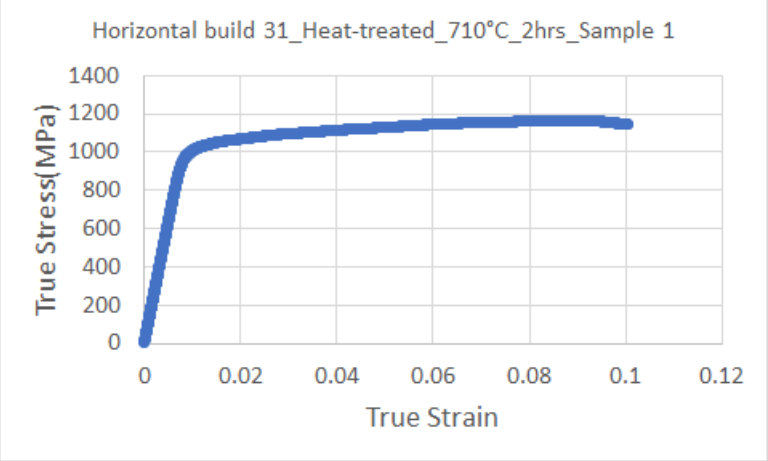

* Sub β-transus heat treatment (710°C, 2 hours)_Sample 2

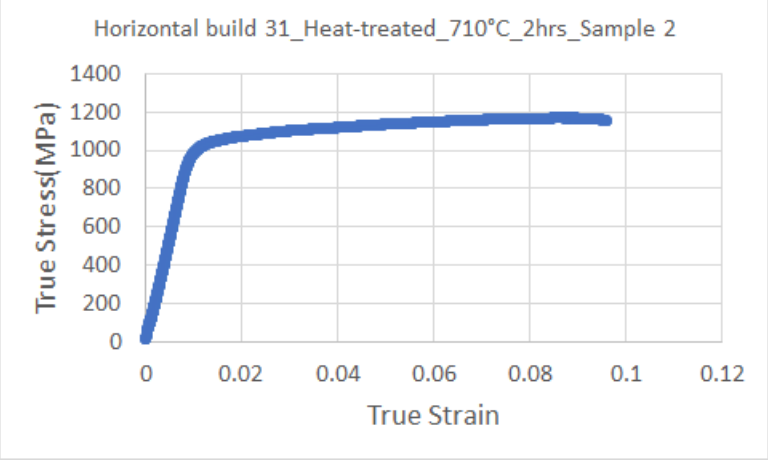

* Sub β-transus heat treatment (710°C, 2 hours)_Sample 3

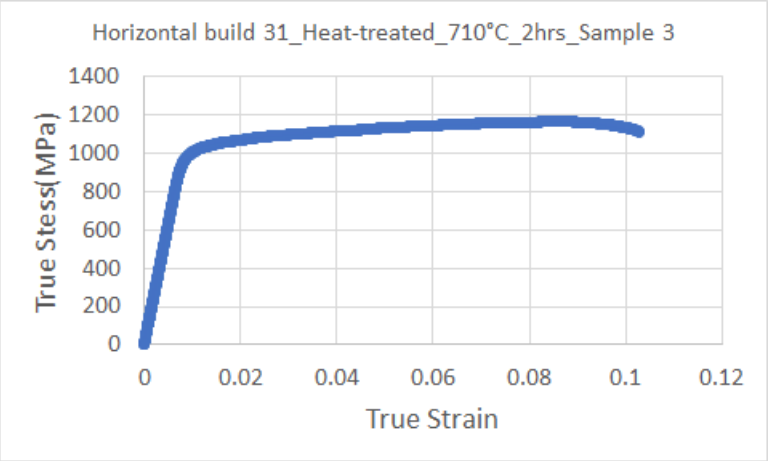

* Near β-transus heat treatment (950°C, 1 hour)_Sample 1

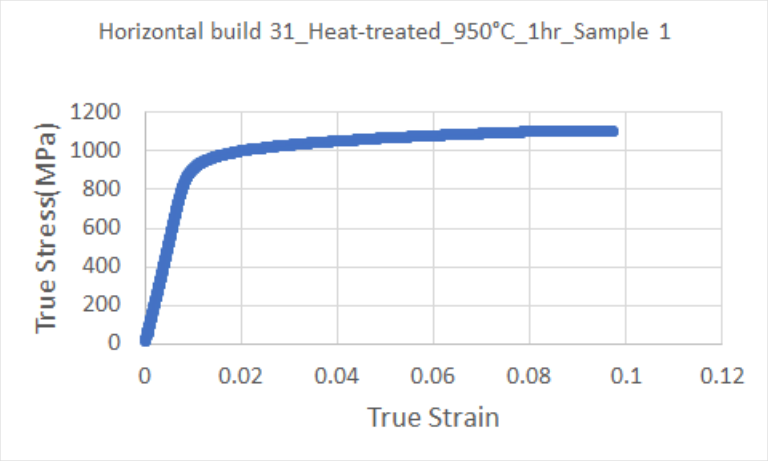

* Near β-transus heat treatment (950°C, 1 hour)_Sample 2

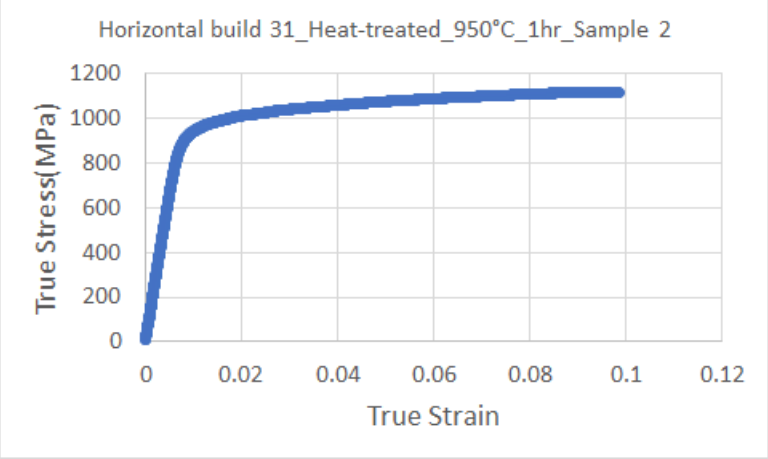

* Near β-transus heat treatment (950°C, 1 hour)_Sample 3

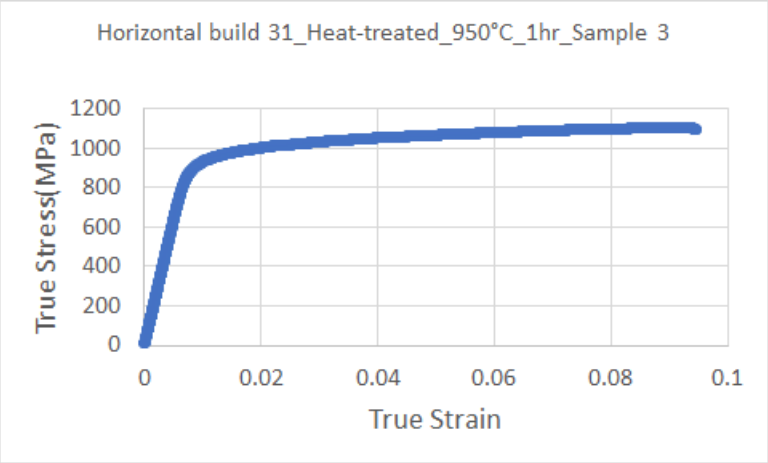

* Super β-transus heat treatment (1050°C, 1 hour)_Sample 1

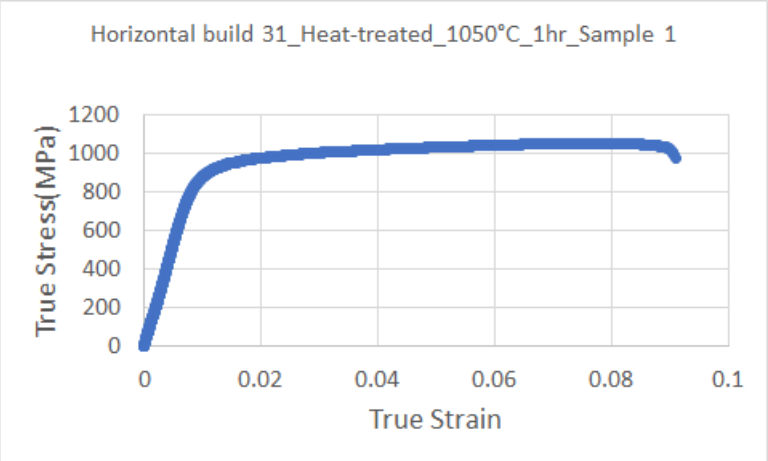

* Super β-transus heat treatment (1050°C, 1 hour)_Sample 2

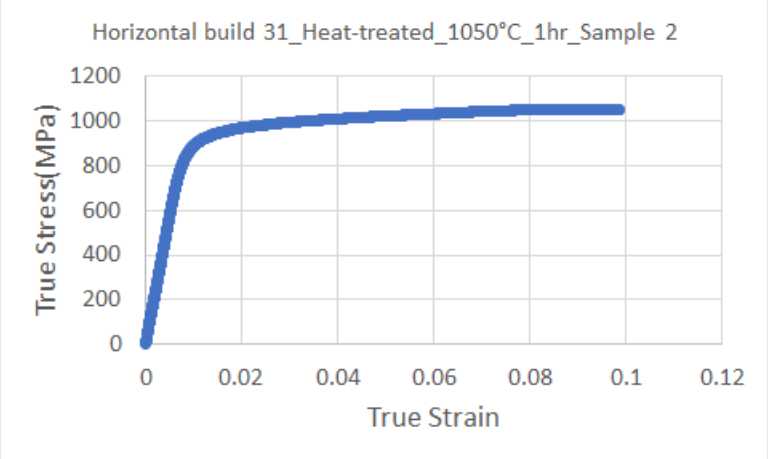

* Super β-transus heat treatment (1050°C, 1 hour)_Sample 3

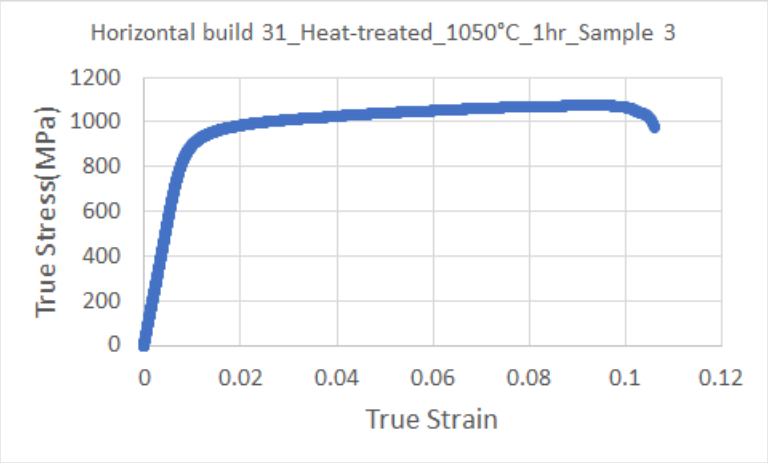

※ Vertical DOE

* Machined_1 (to compare the results of **near** β-transus heat treatment)

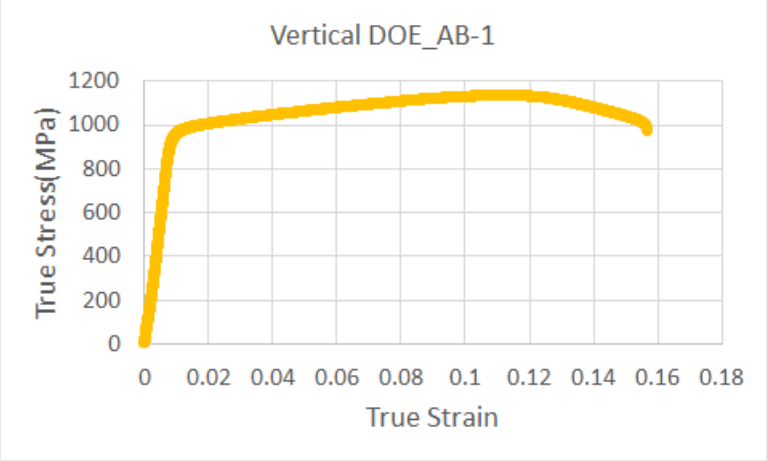

* Machined_2 (to compare the results of **near** β-transus heat treatment)

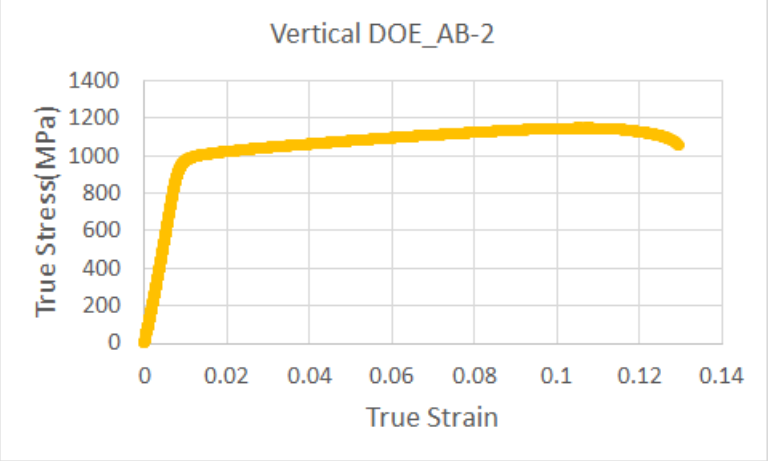

* Machined_3 (to compare the results of **near** β-transus heat treatment)

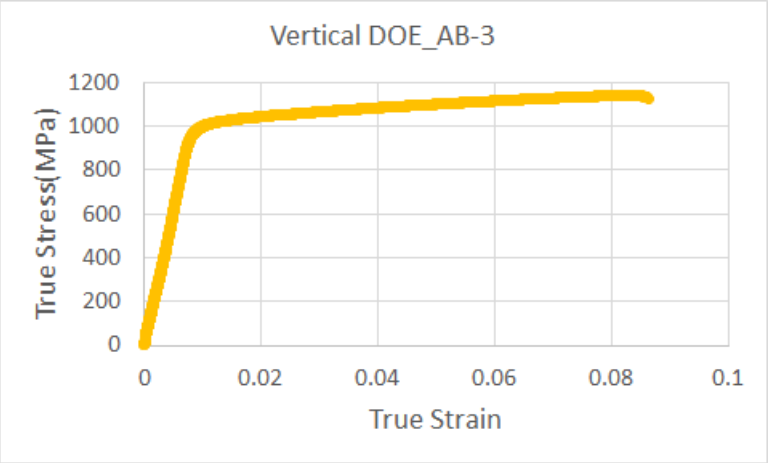

* Machined_4 (to compare the results of **super** β-transus heat treatment)

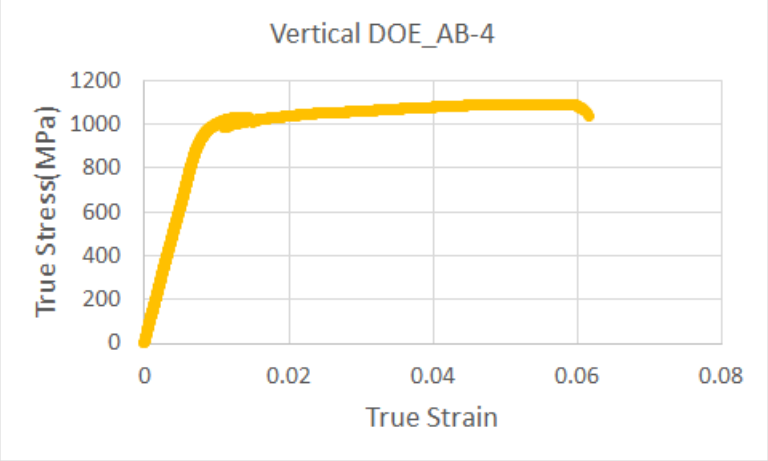

* Machined_5 (to compare the results of **super** β-transus heat treatment)

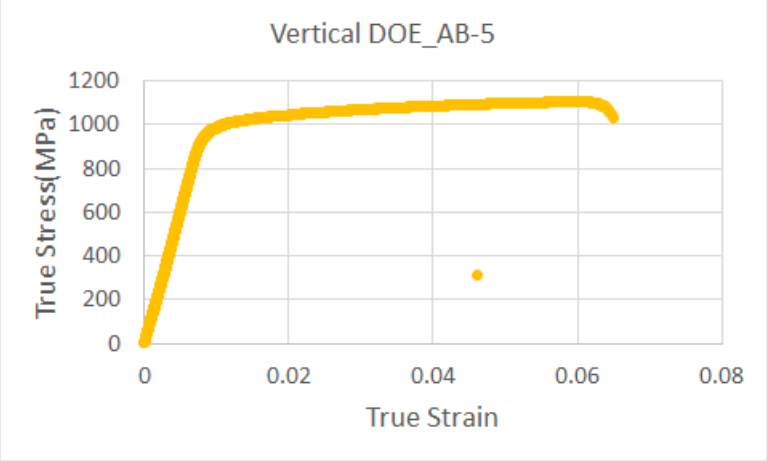

* Machined_6 (to compare the results of **super** β-transus heat treatment)

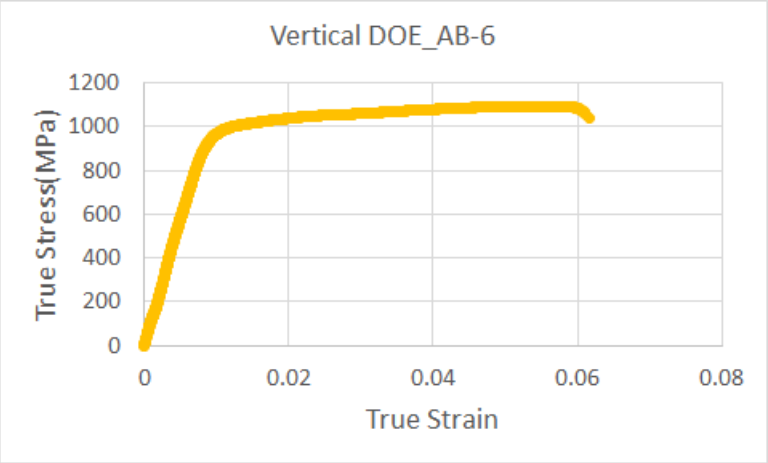

* Near β-transus heat treatment (950°C, 1 hour)_Sample 1

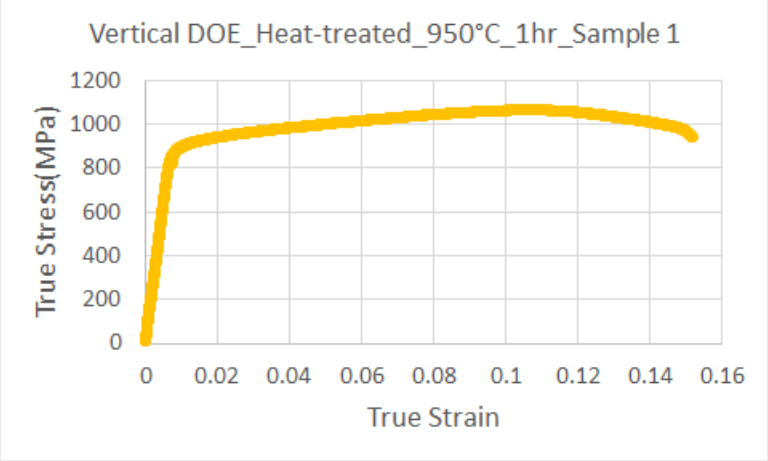

* Near β-transus heat treatment (950°C, 1 hour)_Sample 2

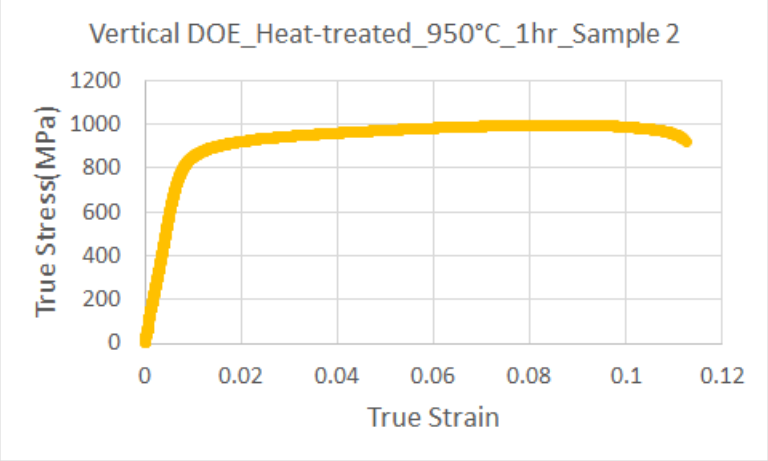

* Near β-transus heat treatment (950°C, 1 hour)_Sample 3

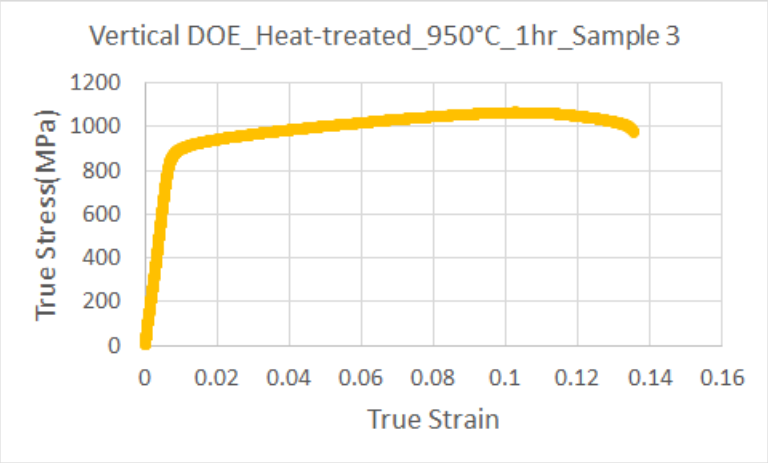

* Super β-transus heat treatment (1050°C, 1 hour)_Sample 1

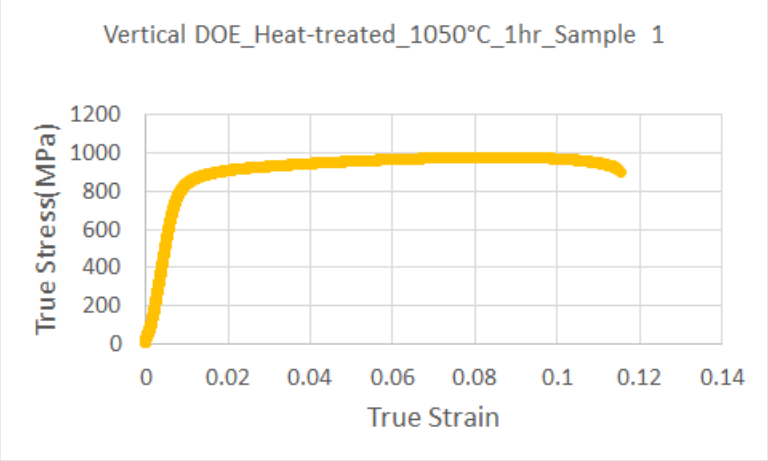

* Super β-transus heat treatment (1050°C, 1 hour)_Sample 2

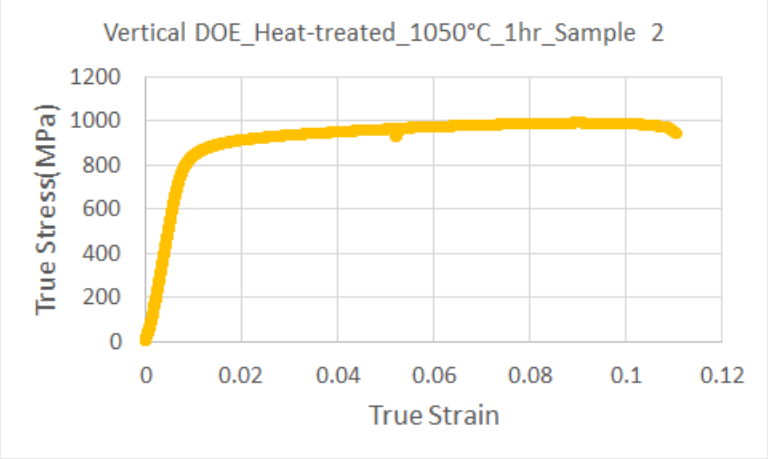

* Super β-transus heat treatment (1050°C, 1 hour)_Sample 3

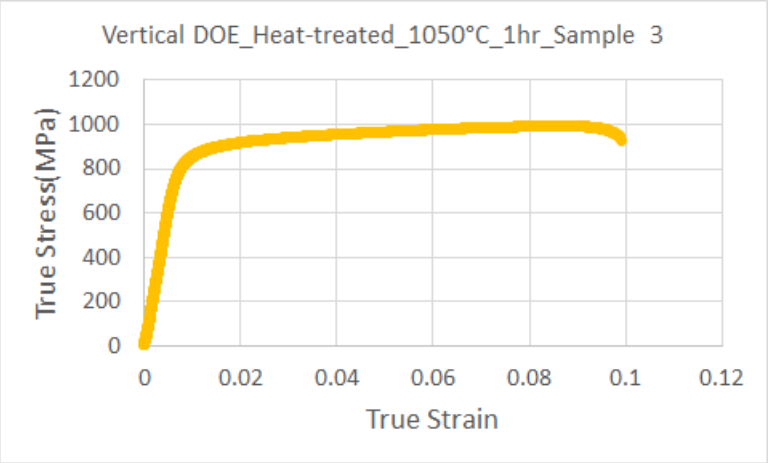

※ Vertical heat-treated samples of build 5, 9, 12, 16, 20, 24 and 28

* 5-1

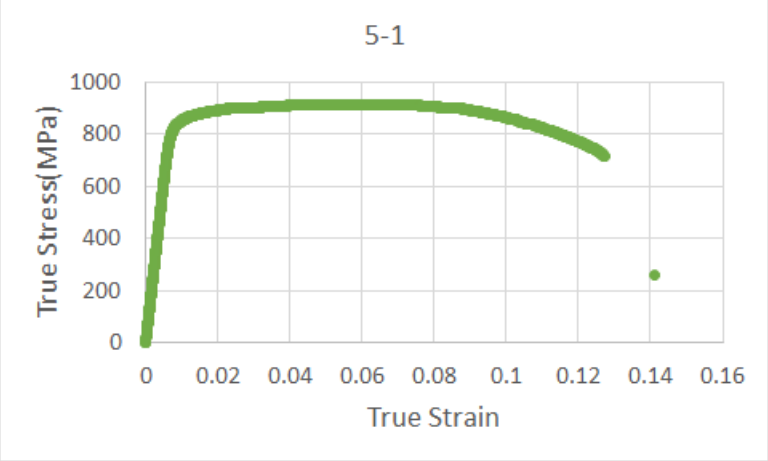

* 5-2

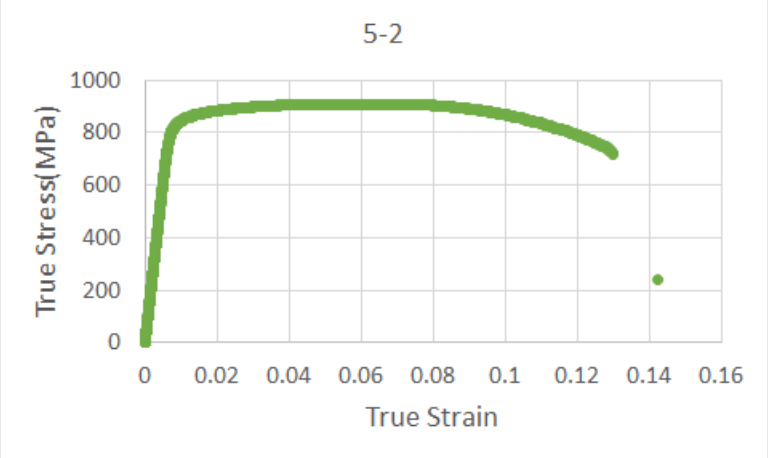

* 5-3

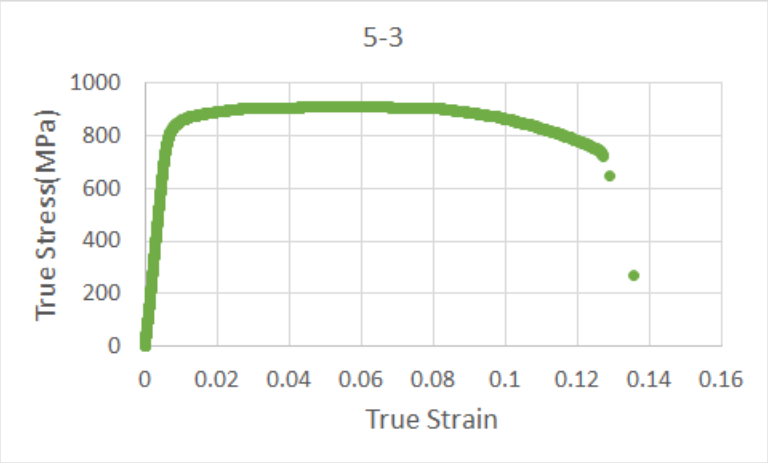
5-3
True Stress(MPa)
1000
800
600
400
200
0
0
0.02
0.04
0.06
0.08
0.1
0.12
0.14
0.16
True Strain

* 9-1

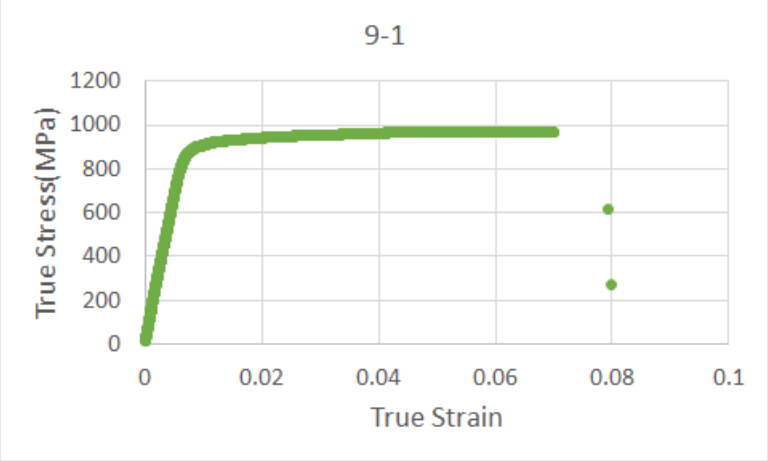
9-1
True Stress(MPa)
1200
1000
800
600
400
200
0
0
0.02
0.04
0.06
0.08
0.1
True Strain

* 9-2

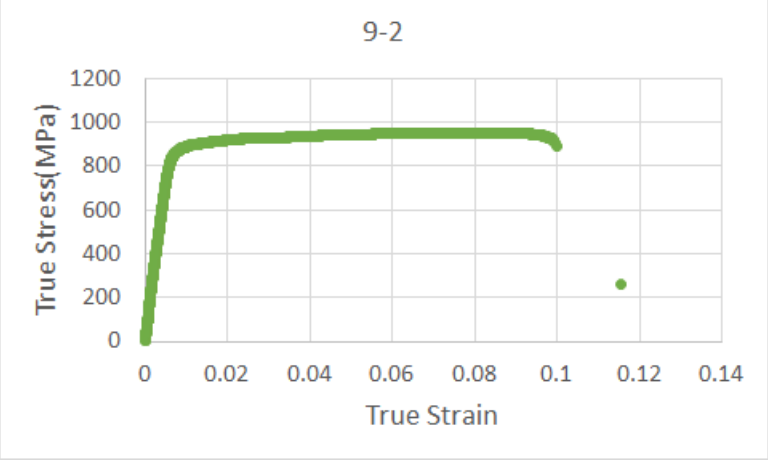
9-2
True Stress(MPa)
1200
1000
800
600
400
200
0
0
0.02
0.04
0.06
0.08
0.1
0.12
0.14
True Strain

* 9-3

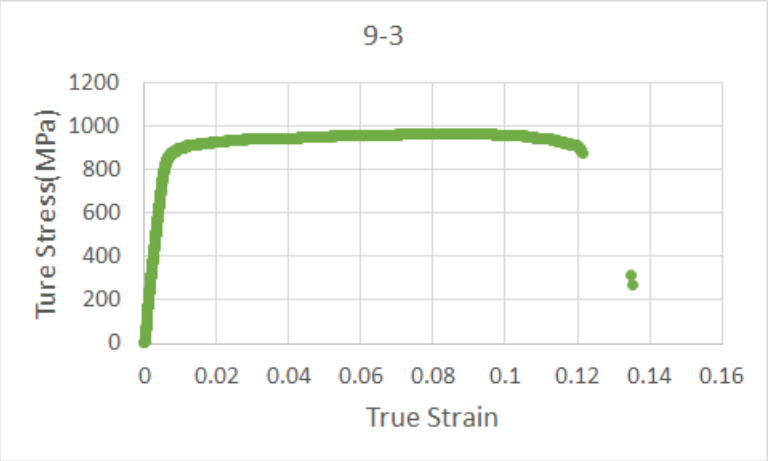
9-3
Ture Stress(MPa)
1200
1000
800
600
400
200
0
0
0.02
0.04
0.06
0.08
0.1
0.12
0.14
0.16
True Strain

* 12-1

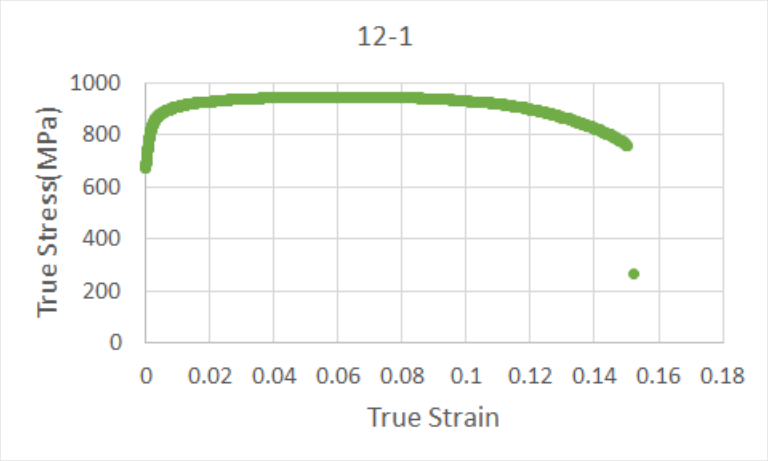
12-1
True Stress(MPa)
1000
800
600
400
200
0
0
0.02
0.04
0.06
0.08
0.1
0.12
0.14
0.16
0.18
True Strain

* 12-2

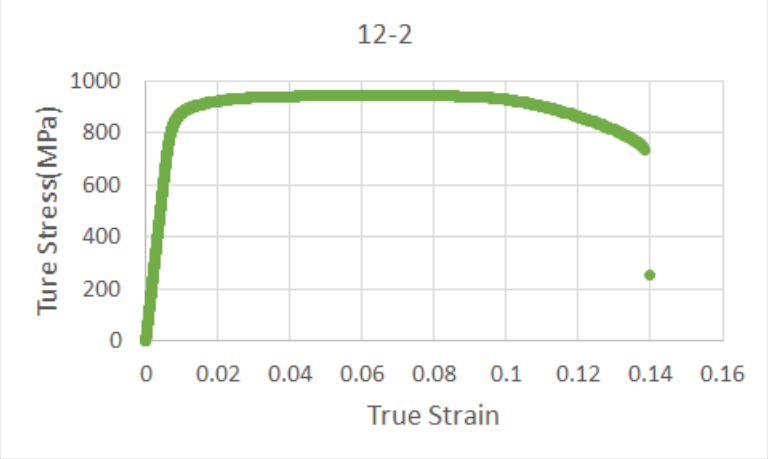
12-2
Ture Stress(MPa)
1000
800
600
400
200
0
0
0.02
0.04
0.06
0.08
0.1
0.12
0.14
0.16
True Strain

* 12-3

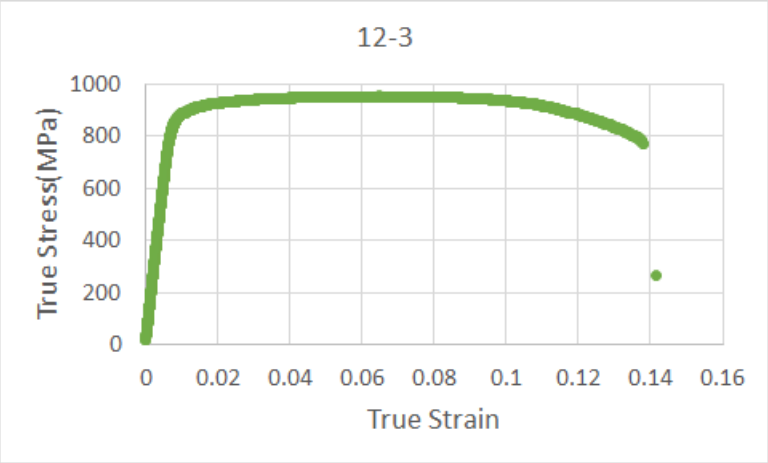
12-3
True Stress(MPa)
1000
800
600
400
200
0
0
0.02
0.04
0.06
0.08
0.1
0.12
0.14
0.16
True Strain

* 16-1

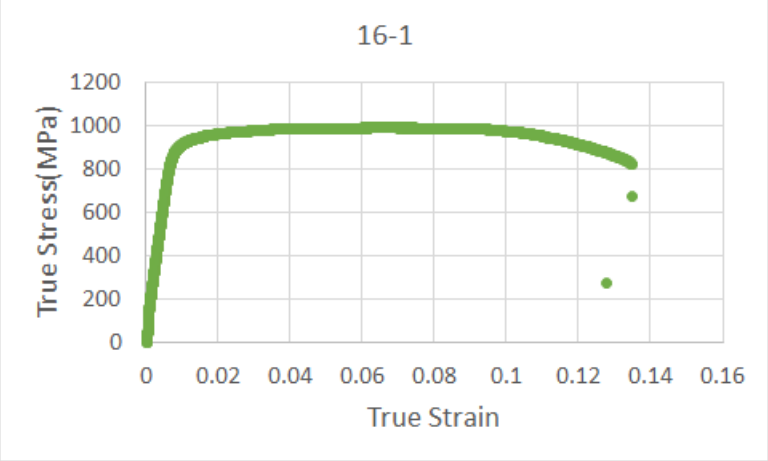
16-1
True Stress(MPa)
1200
1000
800
600
400
200
0
0
0.02
0.04
0.06
0.08
0.1
0.12
0.14
0.16
True Strain

* 16-2

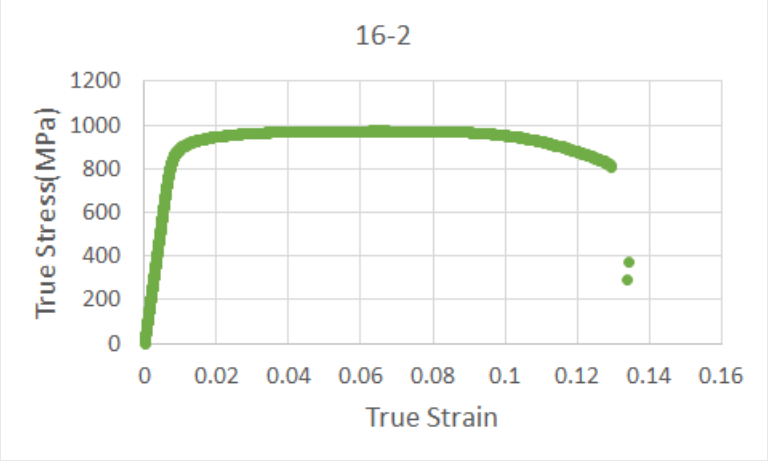
16-2
True Stress(MPa)
1200
1000
800
600
400
200
0
0
0.02
0.04
0.06
0.08
0.1
0.12
0.14
0.16
True Strain

* 16-3

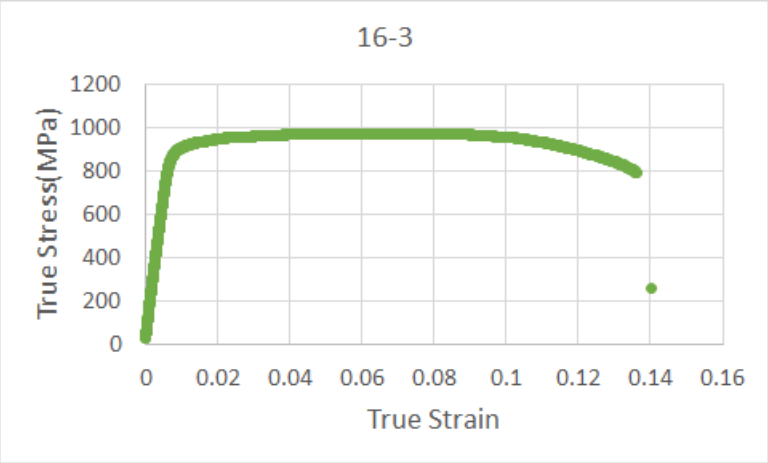
16-3
True Stress(MPa)
1200
1000
800
600
400
200
0
0
0.02
0.04
0.06
0.08
0.1
0.12
0.14
0.16
True Strain

* 20-1

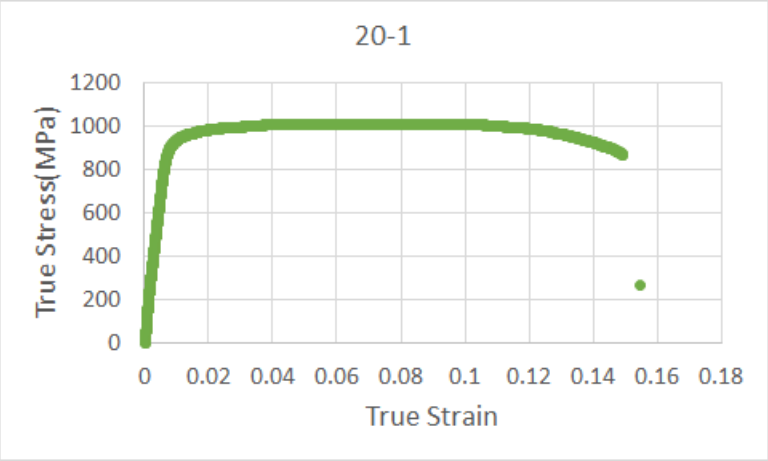
20-1
True Stress(MPa)
1200
1000
800
600
400
200
0
0
0.02
0.04
0.06
0.08
0.1
0.12
0.14
0.16
0.18
True Strain

* 20-2

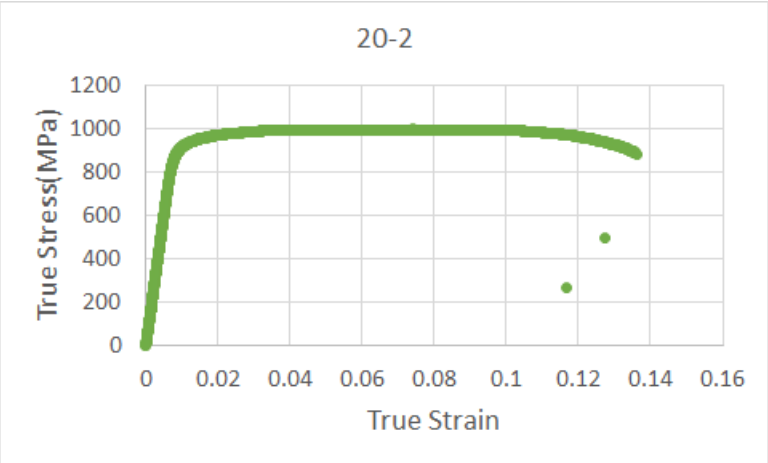
20-2
True Stress(MPa)
1200
1000
800
600
400
200
0
0
0.02
0.04
0.06
0.08
0.1
0.12
0.14
0.16
True Strain

* 20-3

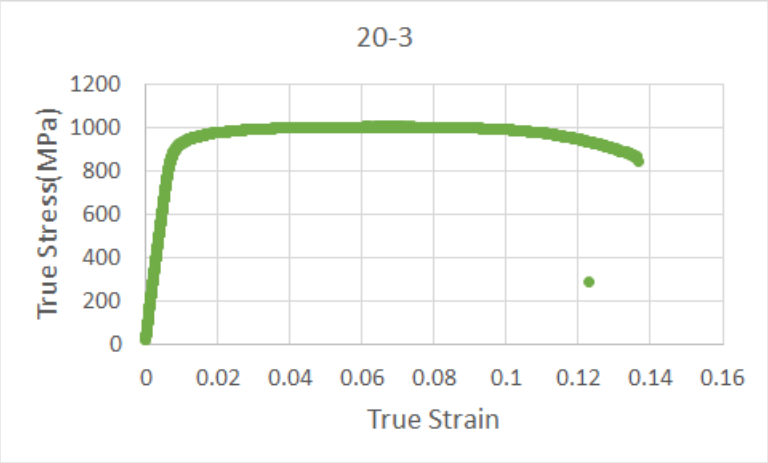
20-3
True Stress(MPa)
1200
1000
800
600
400
200
0
0
0.02
0.04
0.06
0.08
0.1
0.12
0.14
0.16
True Strain

* 24-1

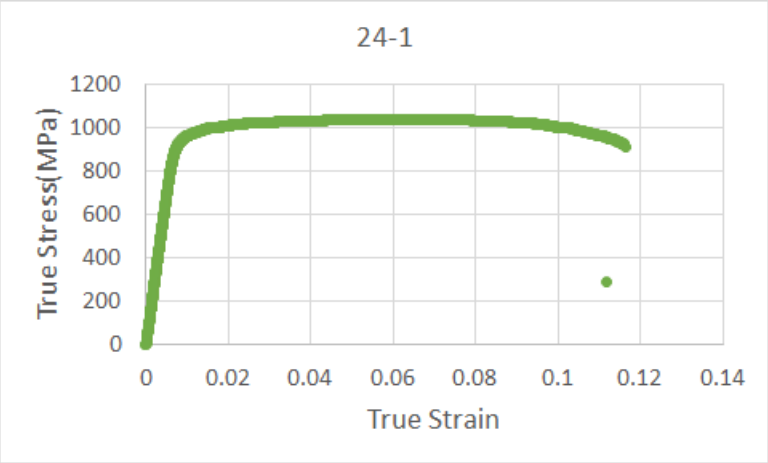
24-1
True Stress(MPa)
1200
1000
800
600
400
200
0
0
0.02
0.04
0.06
0.08
0.1
0.12
0.14
True Strain

* 24-2

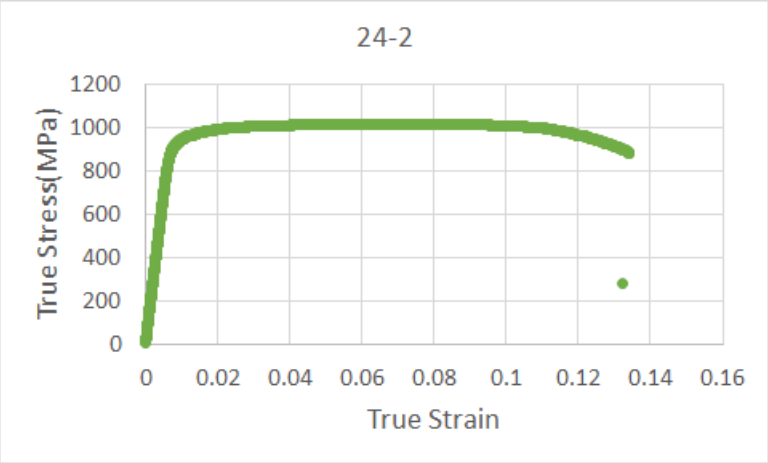
24-2
True Stress(MPa)
1200
1000
800
600
400
200
0
0
0.02
0.04
0.06
0.08
0.1
0.12
0.14
0.16
True Strain

* 24-3

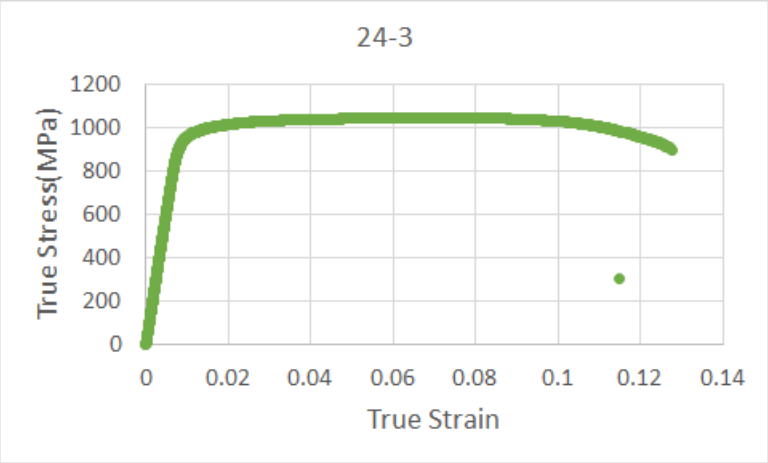
24-3
True Stress(MPa)
1200
1000
800
600
400
200
0
0
0.02
0.04
0.06
0.08
0.1
0.12
0.14
True Strain

* 28-1

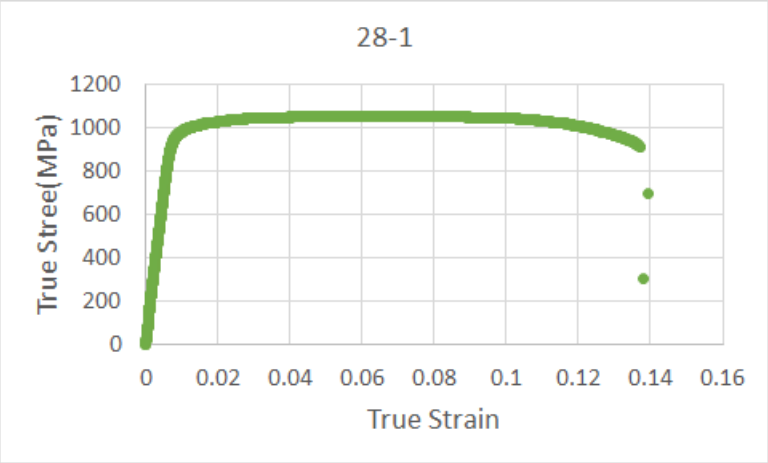
28-1
True Stree(MPa)
1200
1000
800
600
400
200
0
0
0.02
0.04
0.06
0.08
0.1
0.12
0.14
0.16
True Strain

* 28-2

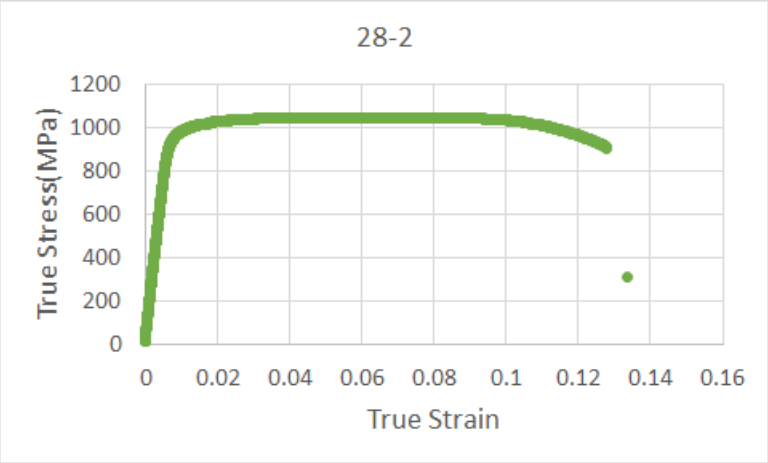
28-2
True Stress(MPa)
1200
1000
800
600
400
200
0
0
0.02
0.04
0.06
0.08
0.1
0.12
0.14
0.16
True Strain

* 28-3

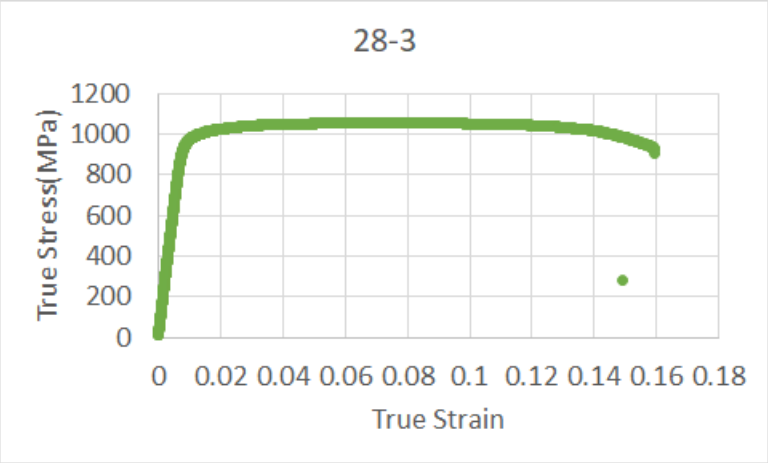
28-3
True Stress(MPa)
1200
1000
800
600
400
200
0
0 0.02 0.04 0.06 0.08 0.1 0.12 0.14 0.16 0.18
True Strain

H. Coefficient of variation (COV) in terms of the microstructure of horizontal build 31 and vertical DOE samples

HB : horizontal build, Sub : sub β-transus heat treatment, Near : near β-transus heat treatment, Super : super β-transus heat treatment, VDOE : vertical DOE sample, MA : machined vertical DOE samples.

Specimens	COV_α lath (%)	COV_β grain (%)
HB31/AB	16.1	6.3
HB31/Sub	11.5	8.6
HB31/Near	7.7	14.9
HB31/Super	3.1	25.2
VDOE/MA	11.3	12
VDOE/Near	22	7.3
VDOE/Super	10.7	7

I. Coefficient of variation of the tensile properties of horizontal build 31 and vertical DOE samples

COV : coefficient of variation, HB : horizontal build, Sub : sub β-transus heat treatment, Near : near β-transus heat treatment, Super : super β-transus heat treatment, VDOE : vertical DOE sample, MA1 : machined for comparisons with near β-transus heat treatment, MA2 : machined for comparisons with super β-transus heat treatment, AB : as-built, HT : heat-treated, V : vertical oriented.

Specimens	COV_elastic modulus (%)	COV_yield strength (%)	COV_ultimate tensile strength (%)	COV_% elongation (%)
HB31/AB	2.3	0.9	0.2	6.2
HB31/Sub	7.4	0.3	0.6	4.6
HB31/Near	5.9	0.5	0.2	2.5
HB31/Super	3.9	0.5	0.9	7.2
VDOE/MA1	1.8	0.9	0.6	13.6
VDOE/MA2	3.3	0.8	1.7	32.8
VDOE/Near	6.2	2.5	3.1	12.1
VDOE/Super	3.2	0.2	0.6	6.2

J. Coefficient of variation (COV) of the tensile properties of vertical samples

AB : as-built, HT : heat-treated

Specimens	COV_elastic modulus (%)	COV_yield strength (%)	COV_ultimate tensile strength (%)	COV_% elongation (%)
Build 5/AB	2.8	0.9	1	5.6
Build 5/HT	6.4	0.2	0.1	1
Build 9/AB	10.7	1.6	1.6	4.5
Build 9/HT	4.4	1.6	0.9	9.9
Build 12/AB	8.6	2.3	0.7	10.8
Build 12/HT	1.3	0.3	0.5	0.1
Build 16/AB	4.1	1.9	1.2	4.5
Build 16/HT	6.8	0.5	1.1	2.5
Build 20/AB	6.4	1	1.3	13.2
Build 20/HT	5	0.6	1.1	5
Build 24/AB	7.2	2.3	3.2	5.6
Build 24/HT	7	1.4	1.1	6.7
Build 28/AB	8.6	1	2.5	15.9
Build 28/HT	7.6	0.6	1.6	10.8

K. Coefficient of variation (COV) of tensile properties of the vertical samples with powder reuse

※ As-built samples

Specimens	COV_elastic modulus (%)	COV_yield strength (%)	COV_ultimate tensile strength (%)	COV_% elongation (%)
Build 5	2.8	0.9	1	5.6
Build 9	10.7	1.6	1.6	4.5
Build 12	8.6	2.3	0.7	10.8
Build 16	4.1	1.9	1.2	4.5
Build 20	6.4	1	1.3	13.2
Build 24	7.2	2.3	3.2	5.6
Build 28	8.6	1	2.5	15.9

※ Heat-treated samples

Specimens	COV_elastic modulus (%)	COV_yield strength (%)	COV_ultimate tensile strength (%)	COV_% elongation (%)
Build 5	6.4	0.2	0.1	1
Build 9	4.4	1.6	0.9	9.9
Build 12	1.3	0.3	0.5	0.1
Build 16	6.8	0.5	1.1	2.5
Build 20	5	0.6	1.1	5
Build 24	7	1.4	1.1	6.7
Build 28	7.6	0.6	1.6	10.8

References

[1] ASTM Int'l, “F2792–12a: Standard Terminology for Additive Manufacturing Technologies”, pp.1~3, 2012.

[2] I. Gibson, D. Rosen, B. Stucker, “Additive Manufacturing Technologies: 3D Printing, Rapid Prototyping, and Direct Digital Manufacturing”, Springer, pp.19~42, 2015.

[3] J. Allen, “An investigation into the comparative costs of additive manufacture vs. machine from solid for aero engine parts”, Cost Effective Manufacture Via Net Shape Processing, pp.17-1~17-10, 2006.

[4] R. Huang, M. Riddle, D. Graziano, J. Warren, S. Das, S. Nimbalkar, J. Cresko, E. Masanet, “Energy and emissions saving potential of additive manufacturing: the case of lightweight aircraft components”, Journal of Cleaner Production, pp. 1559–1570, 2016.

[5] M. Seifi, A. Salem, . Beuth, O. Harrysson, J.J. Lewandowski, “Overview of materials qualification needs for metal additive manufacturing”, JOM, Vol. 68, pp. 747~764, 2016.

[6] G.B. Kannan, D.K. Rajendran, “A review on status of research in metal additive manufacturing, Advances in 3D Printing & Additive Manufacturing Technologies”, Advanced in 3D printing & additive manufacturing techonologies, pp. 95~100, 2017.

[7] D. Herzog, V. Seyda, E.Wycisk, C. Emmelmann, “Additive manufacturing of metals”, Acta Materialia, Vol. 117, pp. 371~392, 2016.

[8] S. Liu, Yung C. Shin, “Additive manufacturing of Ti6Al4V alloy: A review”, Materials and Design, Vol. 164, pp.107~552, 2019.

[9] A. Strondl, O. Lyckfeldt, H. Brodin, U. Ackelid, “Characterization and Control of Powder Properties for Additive Manufacturing”, JOM, Vol.67, 549~554, 2015.

[10] H. P. Tang, M. Qian, N. Liu, X. Z. Zhang, G. Y. Yang, J. Wang, “Effect of Powder Reuse Times on Additive Manufacturing of Ti-6Al-4V by Selective Electron Beam Melting”, JOM, Vol. 67, No.3, pp. 555~563, 2015.

[11] Y. Sun, M. Aindow, R. J. Hebert, “The effect of recycling on the oxygen distribution in Ti-6Al-4V powder for additive manufacturing”, Materals at high temperatures, Vol. 35, pp. 217~224, 2018.

[12] H. Galarraga, Diana A. Lados, Ryan R. Dehoff, Michael M. Kirka, Peeyush Nandwana, “Effects of the microstructure and porosity on properties of Ti-6Al-4V ELI alloy fabricated by electron beam melting (EBM)”, Additive Manufacturing, Vol. 10, pp. 47~57, 2016.

[13] S. Raghavan, Mui Ling Sharon Nai, Pan Wang, Wai Jack Sin, Tao Li, Jun Wei, “Heat treatment of electron beam melted (EBM) Ti-6Al-4V: microstructure to mechanical property correlations”, Rapid Prototyping Journal, Vol. 24, pp.774~783, 2018.

[14] C. de Formanoir, Alice Brulard, Solange Vivès, Guilhem Martin, Frédéric Prima, Sébastien Michotte, Edouard Rivière, Adrien Dolimont & Stéphane Godet, “A strategy to improve the work-hardening behavior of Ti–6Al–4V parts produced by additive manufacturing”, Materials Research Letters, Vol. 5, pp. 201~208, 2017.

[15] C. de Formanoir, Sébastien Michotte, Olivier Rigo, Lionel Germain, Stéphane Godet, “Electron beam melted Ti-6Al-4V: Microstructure, texture and mechanical behavior of the as-built and heat-treated material”, Materials Science & Engineering A, Vol. 652, pp. 105~119, 2016.

[16] X. Tao , Z. Yao, S. Zhang, Z. Li, Yi Xu, “Correlation Between Heat-Treated Microstructure and Mechanical and Fretting Wear Behavior of Electron Beam Freeform-Fabricated Ti6Al4V Alloy”, JOM, Vol. 71, pp. 2313~2320, 2019.

[17] H. Galarraga, R. J. Warren, Diana A. Lados, Ryan R. Dehoff, Michael M. Kirka, Peeyush Nandwana, “Effects of heat treatments on microstructure and properties of Ti-6Al-4VELI alloy fabricated by electron beam melting (EBM)”, Materials Science & Engineering A, Vol. 685, pp. 417~428, 2017.

[18] Xiaoli Zhao, Shujun Li, Man Zhang, Yandong Liu, Timothy B. Sercombe, Shaogang Wang, Yulin Hao, Rui Yang, Lawrence E. Murr, “Comparison of the microstructures and mechanical properties of Ti–6Al–4V fabricated by selective laser melting and electron beam melting”, Materials and Design, Vol. 95, pp. 21~31, 2016.

[19] Daniel Greitemeier, Frank Palm, Freerk Syassen, Tobias Melz, “Fatigue performance of additive manufactured TiAl6V4 using electron and laser beam melting”, International Journal of Fatigue, Vol. 94, pp. 211~217, 2017.

[20] Hong, H, Riga, A.T Gahoon, J.M Scott, C.G, “Machinability of steels and titanium alloys under lubrication”, Wear, Vol.162, pp. 34~39, 1993.

[21] R. Huang, M. Riddle, D. Graziano, J. Warren, S. Das, S. Nimbalkar, J. Cresko, E. Masanet, “Energy and emissions saving potential of additive manufacturing: the case of lightweight aircraft components”, Journal of Cleaner Production, Vol. 135, pp. 1559~1570, 2016.

[22] P. Li, D.H. Warner, A. Fatemi, N. Phan, “Critical assessment of the fatigue performance of additively manufactured Ti–6Al–4V and perspective for future research”, International Journal of Fatigue, Vol. 85, pp. 130~143, 2016.

[23] Hiemenz, J, “Electron beam melting”. Advanced Materials & Process, Vol. 165, pp. 45~46, 2007.

[24] B. Wysocki, P. Maj, R. Sitek, J. Buhagiar, K. Kurzydłowski, W. Święszkowski, “Laser and electron beam additive manufacturing methods of fabricating titanium bone implants”, Applied Science, Vol. 657, pp. 1~20, 2017.

[25] Y. Zhai, H. Galarraga, D.A. Lados, “Microstructure, static properties, and fatigue crack growth mechanisms in Ti-6Al-4V fabricated by additive manufacturing: LENS and EBM”, Engineering Failure Analysis, Vol. 69, pp. 3~14, 2016.

[26] A. Safdar, L.Y. Wei, A. Snis, Z. Lai, “Evaluation of microstructural development in electron beam melted Ti-6Al-4V”, Materials Characterization., Vol 65, pp. 8~15, 2012.

[27] M. Koike, P. Greer, K. Owen, G. Lilly, L.E. Murr, S.M. Gaytan, E. Martinez, T. Okabe, “Evaluation of titanium alloys fabricated using rapid prototyping technologies electron beam melting and laser beam melting”, Materials, Vol. 4-10, pp. 1776~1792, 2011.

[28] M. Strantza, R. Vafadari, D. de Baere, B. Vrancken,W. van Paepegem, I. Vandendael, H. Terryn, P. Guillaume, D. van Hemelrijck, “Fatigue of Ti6Al4V structural health monitoring systems produced by selective laser melting”, Materials, Vol. 9, pp. 1~15, 2016.

[29] N. Biswas, J.L. Ding, V.K. Balla, D.P. Field, A. Bandyopadhyay, “Deformation and fracture behavior of laser processed dense and porous Ti6Al4V alloy under static and dynamic loading”, Materials Science and Engineering A, Vol. 549, pp. 213~221, 2012.

[30] S. Beretta, S. Romano, “A comparison of fatigue strength sensitivity to defects for

materials manufactured by AM or traditional processes", Intenational Journal of Fatigue, Vol. 94, pp. 178~191, 2017.

[31] E.Wycisk, A. Solbach, S. Siddique, D. Herzog, F.Walther, C. Emmelmann, "Effects of defects in laser additive manufactured Ti-6Al-4V on fatigue properties", Physics Procedia, Vol. 56, pp. 371~378, 2014.

[32] L. Parry, I.A. Ashcroft, R.D.Wildman, "Understanding the effect of laser scan strategy on residual stress in selective laser melting through thermo-mechanical simulation", Additive Manufacturing, Vol. 12, pp. 1~15, 2016.

[33] G. Vastola, G. Zhang, Q.X. Pei, Y.W. Zhang, "Controlling of residual stress in additive manufacturing of Ti6Al4V by finite element modeling", Additive Manufacturing, Vol. 12, pp. 231~239, 2016.

[34] N.S. Bailey, W. Tan, Y.C. Shin, "Predictive modeling and experimental results for residual stresses in laser hardening of AISI 4140 steel by a high power diode laser", Surface & Coatings Technology, Vol. 203, pp. 2003~2012, 2009.

[35] N.S. Bailey, C. Katinas, Y.C. Shin, "Laser direct deposition of AISI H13 tool steel powder with numerical modeling of solid phase transformation, hardness, and residual stresses", Journal of Material Processing Technology, Vol. 247, pp. 223~233, 2017.

[36] P. Mercelis, J.P. Kruth, "Residual stresses in selective laser sintering and selective laser melting", Rapid Prototyping Jounral, Vol. 12, pp. 254~265, 2006.

[37] Y. Liu, Y. Yang, D.Wang, "A study on the residual stress during selective laser melting (SLM) of metallic powder", International Journal of Additive

Manufacturing Technology, Vol. 87, pp. 647~656, 2016.

[38] L.D. Bobbio, S. Qin, A. Dunbar, P. Michaleris, A.M. Beese, “Characterization of the strength of support structures used in powder bed fusion additive manufacturing of Ti-6Al-4V”, Additive Manufacturing, Vol. 14, pp. 60~68, 2017.

[39] J.-P. Järvinen, V.Matilainen, X. Li, H. Piili, A. Salminen, I.Mäkelä, O. Nyrhilä, “Characterization of effect of support structures in laser additivemanufacturing of stainless steel”, Physics. Procedia, Vol. 56, pp. 72~81, 2014.

[40] H. Weiwei, J. Wenpeng, L. Haiyan, T. Huiping, K. Xinting, H. Yu, “Research on preheating of titanium alloy powder in electron beam melting technology”, Rare Metal Materials and Engineering, Vol. 40, pp. 2072~2075, 2011.

[41] V. Chastand, P. Quaegebeur, W. Maia, E. Charkaluk, “Comparative study of fatigue properties of Ti-6Al-4V specimens built by electron beam melting (EBM) and selective laser melting (SLM)”, Materials Characterization, Vol. 143, pp. 76~81, 2018.

[42] T. Vilaro, C. Colin, J.D. Bartout, “As-fabricated and heat-treated microstructures of the Ti-6Al-4V alloy processed by selective laser melting”, JOM, Vol. 42, pp. 3190~3199, 2011.

[43] S. Leuders, M. Thöne, A. Riemer, T. Niendorf, T. Tröster, H.A. Richard, H.J. Maier, “On the mechanical behaviour of titanium alloy TiAl6V4 manufactured by selective laser melting: fatigue resistance and crack growth performance”, International Journal of Fatigue, Vol. 48, pp. 300~307, 2013.

[44] U. Ackelid, M. Svensson, “Additive manufacturing of dense metal parts by

electron beam melting", Materials Science and Technology Conferenceand Exhibition, pp. 2711~2719, 2009.

[45] P.-H. Li, W.-G. Guo, W.-D. Huang, Y. Su, X. Lin, K.-B. Yuan, "Thermomechanical response of 3D laser-deposited Ti–6Al–4V alloy over a wide range of strain rates and temperatures", Materials Science and Engineering A, Vol. 647, pp. 34~42, 2015.

[46] S. Tammas-Williams, H. Zhao, F. Léonard, F. Derguti, I. Todd, P.B. Prangnell, "XCT analysis of the influence of melt strategies on defect population in Ti–6Al–4V component manufactured by selective electron beam melting", Materials Characterization, Vol. 102, pp. 47~61, 2015.

[47] S.M. Gaytan, L.E. Murr, F. Medina, E. Martinez, M.I. Lopez, R.B. Wicker, "Advan ced metal powder based manufacturing of complex components by electron beam melting", Materials Technology, Vol. 24, pp. 180~190, 2009.

[48] Murr L. E et al, "Microstructures and mechanical properties of electron beam-rapid manufactured Ti-6Al-4V biomedical prototypes compared to wrought Ti-6Al-4V", Materials Characterization, pp. 96~105, 2009.

[49] Tan X, Kok Y, Tan Y.J, "Graded microstructure and mechanical properties of additive manufactured Ti-6Al-4V via electron beam melting". Acta Materialia, Vol. 97, pp. 1~16, 2015.

[50] ASTM Int'l, "F136 - 13 Standard Specification for Wrought Titanium-6Aluminum-4Vanadium ELI (Extra Low Interstitial) Alloy for Surgical Implant Applications (UNS R56401)", 2002.

[51] Abdul Khadar Syed, Mustafa Awd, Frank Walther, Xiang Zhang, “Microstructure and mechanical properties of as-built and heat-treated electron beam melted Ti–6Al–4V”, Materials Science and Technology, Vol. 35, pp. 653~660, 2019.

[52] J. Alcisto, A. Enriquez, H. Garcia, S. Hinkson, T. Steelman, E. Silverman, P. Valdovino, H. Gigerenzer, J. Foyos, J. Ogren, J. Dorey, K. Karg, T. McDonald, O.S. Es-Said, “Tensile properties and microstructures of laser-formed Ti–6Al–4V”, Journal of Materials Engineering Performance, Vol. 20, pp. 203~212, 2011.

[53] M.J. Bermingham, L. Nicastro, D. Kent, Y. Chen, M.S. Dargusch, “Optimising the mechanical properties of Ti-6Al-4V components produced by wire + arc additive manufacturing with post-process heat treatments”, Journal of Alloys Compounds, Vol. 753, pp. 247~255, 2018.

[54] H. Gong, K. Rafi, H. Gu, T. Starr, and B. Stucker, “Analysis of defect generation in Ti-6Al-4V parts made using powder bed fusion additive manufacturing processes”, Additive. Manufacturing, Vol. 1, pp. 87~98, 2014.

[55] Y.-L. Hao, S. J. Li, R. Yang, “Biomedical titanium alloys and their additive manufacturing”, Rare Metals, Vol. 35, pp. 661~671, 2016.

[56] ASTM Int'l, “F2924 -14: Standard Specification for Additive Manufacturing Titanium-6 Aluminum-4 Vanadium with Powder Bed Fusion”, 2014.

[57] N. Hrabe, T. Quinn, “Effects of processing onmicrostructure andmechanical properties of a titaniumalloy (Ti–6Al–4V) fabricated using electron beam melting (EBM), part 2: energy input, orientation, and location”, Materials Science and Engineering A, Vol. 573, pp. 271~277, 2013.

[58] H. Conrad, “Effect of interstitial solutes on the strength and ductility of titanium”, Progress in Materials Science, Vol. 26, pp. 123~403, 1981.

[59] Michaela Fousová, Dalibor Vojtˇech, Karel Doubrava, Matˇej Daniel, Chiu-Feng Lin, “Influence of Inherent Surface and Internal Defects on Mechanical Properties of Additively Manufactured Ti6Al4V Alloy: Comparison between Selective Laser Melting and Electron Beam Melting”, Materials, Vol. 11, pp.1~18, 2018.

[60] N. S. Pushilina, E. N. Stepanova, V. N. Kudiiarov, R. S. Laptev, and M. S. Syrtanov, “Heat treatment of the Ti-6Al-4V alloy manufactured by electron beam melting”, AIP Conference Proceedings 2167, pp. 1~4, 2019.

[61] Y.Y. Sun, S. Gulizia,C.H. Oh, D. Fraser,M. Leary,Y.F. Yang, M. Qian, “The Influence of As-Built Surface Conditions on Mechanical Properties of Ti-6Al-4V Additively Manufactured by Selective Electron Beam Melting”, JOM, Vol. 68, pp. 791-798, 2016.

[62] V. Cain, L. Thijs, J. Van Humbeeck, B. Van Hooreweder, R. Knutsen, “Crack propagation and fracture toughness of Ti6Al4V alloy produced by selective laser melting”, Additive Manufacturing, Vol. 5, pp. 68~76, 2015.

[63] S. Hashmi, “Comprehensive Materials Processing”, 2014.

[64] H. P. Tang, M. Qian, N. Liu, X. Z. Zhang, G. Y. Yang, and J. Wang, “Effect of Powder Reuse Times on Additive Manufacturing of Ti-6Al-4V by Selective Electron Beam Melting”, JOM, Vol. 67, pp. 555~563, 2015.

[65] V. V. Popov, A. Katz-Demyanetz, A. Garkun, and M. Bamberger, “The effect of powder recycling on the mechanical properties and microstructure of electron

beam melted Ti-6Al-4 V specimens", Additive Manufacturing, Vol. 22, pp. 834~843, 2018.

[66] Arcam AB, "Arcam-Ti6Al4V-Titanium-Alloy".

[67] S. Ghods, E. Schultz, C. Wisdom, R. Schur, R. Pahuja, A. Montelione, D. Arola, M. Ramulu, "Electron beam additive manufacturing of Ti6Al4V: Evolution of powder morphology and part microstructure with powder reuse", Materialia, Vol. 9, 2020.

[68] ASTM Int'l, "E8M - 16a: Standard Test Methods for Tension Testing of Metalic Materials", pp. 1~30, 2018.

[69] Reid Schur, "Effects of powder reuse on the mechanical properties of electron beam additively manufactured Ti-6Al-4V", Thesis (M.S.), University of Washington, 2019.

[70] A. Ducato, L. Fratini,M. La Cascia, G. Mazzola, "An Automated Visual Inspection System for the Classification of the Phases of Ti-6Al-4V Titanium Alloy", Springer , pp.362~369, 2013.

[71] T. Ahmed, H.J. Rack, "Phase transformations during cooling in α+β titanium alloys", Materials Science and Engineering A, Vol. 243, pp. 206–211, 1998.

[72] T. Searles, J. Tiley, A. Tanner, R. Williams, B. Rollins, E. Lee, S. Kar, R. Baner-jee, H.L. Fraser, "Rapid characterization of titanium microstructural features for specific modelling of mechanical properties", Measurement Science and Technology, Vol. 16, pp.60~69, 2005.

[73] AP&C, "Brochure of plasma atomization".

[74] American Society for Metals, “Metals Handbook”, 1998

[75] G. Lütjering, J.C.Williams, ″Titanium-Second Edition″, Springer, 2007.

[76] Welsch, G., R. Boyer, and E.W. Collings, ″Materilas Properties Handbook: Titanium Alloys″. Metals Park, OH: ASM International, 1994.

[77] Rack, H.J. and J.I. Qazi, “Titanium Alloys for Biomedical Applications”. Materials Science and Engineering C, Vol.26, pp. 1269~1277, 2006.

[78] G.Lütjering, J.Albrecht, O.M.Ivasishin, “Titanium 95”, Proceedings of the 8th World Titanium Conference, 1995.

[79] B. J. Hayes et al., “Predicting tensile properties of Ti-6Al-4V produced via directed energy deposition”, Acta Materiala, Vol. 133, pp. 120~133, 2017.

[80] Mohsen Attaran, “The rise of 3-D printing: The advantages of additive manufacturing over traditional manufacturing, Business Horizons”, Vol. 60, pp. 677~688, 2017.

[81] Gary Kardys, “Factors to Consider When 3D Printing or Additive Manufacturing Metal Parts”, Engineering, Vol. 360, 2017.

[82] Dignesh Thesiya, Jay Dave, Avadhoot Rajurkar, Vaishali Prajapati, “Study on influence of edm process parameters during machining of Ti-6Al-4V”, Journal of manufacturing technology research, pp. 53~64, 2015.

[83] M. Armendia, A. Graray, “Comparison of machinability and TIMETAL 54M using uncoated WC-Co tools”, Journal of Materials Processing Technology, Vol. 210, pp.

197~203, 2010.

[84] ASTM Int'l, “E112–13 Standard Test Methods for Determining Average Grain Size”, 2013.

[85] Conall Wisdom, “Effects of powder reuse on the microstructure of electron beam additively manufactured Ti-6Al-4V”, Project paper University of Washington, 2020.

[86] G. Lütjering, J.C. Williams, “Titanium”, Springer, 2003.